MECHANICAL ENERGY HARVESTING AND CONVERSION BASED ON UTILIZATION OF LUMINESCENCE MATERIALS AND TRIBOELECTRIC NANOGENERATOR

WONG MAN CHUNG

PhD

The Hong Kong Polytechnic University

2020

The Hong Kong Polytechnic University

Department of Applied Physics

Mechanical Energy Harvesting and Conversion Based on Utilization of Luminescence Materials and Triboelectric Nanogenerator

Wong Man Chung

A thesis submitted in partial fulfillment of the requirements for

the degree of Doctor of Philosophy

July 2019

CERTIFICATE OF ORIGINALITY

I hereby declare that this thesis is my own work and that, to the best of my knowledge and belief, it reproduces no material previously published or written, nor material that has been accepted for the award of any other degree or diploma, except where due acknowledgement has been made in the text.

_____(Sign)

_____ Wong Man Chung _____(Name of student)

Wong Man Chung

THE HONG KONG POLYTECHNIC UNIVERSITY

Abstract

Mechanical energy is the most ubiquitous energy source in an ambient environment, which exists in various forms such as vibration, shocks or stress, with frequency ranging from few Hz to kHz. With the recent surge of technological advancements in low power devices, the escalating costs of power storage device and the ongoing energy crisis. A significant amount of extensive investigations has been conducted in the field of effectively harvest and converse these mechanical energies through smart materials. On one hand, harvesting and utilization of these mechanical energy could be an efficient strategy to reduce the dependence on the traditional energy source. On the other hand, smart material does not only harvest mechanical energy into electricity, the multi-functional property of various smart materials enables its output to be employed in a wide variety of applications. The study concerning harvesting and conversion of mechanical energy via smart material technology has been attracting wide attention and therefore deserves more attempts. In this thesis, three novel strategies based on utilizing piezophotonic material, aggregation induced luminescence (AIE) materials and triboelectric generator (TENG) to convert and harvest mechanical energy is developed and illustrated.

Firstly, a novel strategy is developed to realize the reversible tuning of the emission wavelengths of the piezophotonic material through variation of mechanical excitation frequency. Here, a non-conventional physical approach of temporal and remote tuning of light-emitting wavelength and color of piezoluminescence is demonstrated. It is shown that by modulating the frequency of the mechanical excitation, luminescence wavelength from the flexible composites of piezophosphors induced by the piezophotonic effect can be tuned in *in-situ*. Further investigation

Wong Man Chung

suggests that the observed tunable piezophotonic emission can be ascribed to the tilting band structure of the piezophosphor induced by a high frequency of mechanical excitation. Experiments were performed to verify this real-time and reversible piezoluminescence emission color tuning. Moreover, some proof of concept devices, including red-green-blue full-color displays and tunable white-light sources are been demonstrated simply by modulating the mechanical excitation frequency. This work has provided a new understanding of the fundamentals of piezoluminescence.

Secondly, in our society, the process of binding nitrogen with hydrogen under high pressure and temperature that produces fertilizer consumed 1-2 % of the world's energy production. Therefore, the development of green energy-based nitrogen fixation technology is realistically significant for the fertilizer industry and agriculture. Herein, an environmentally friendly microplasma discharge-based nitrogen fixation system driven by harvesting ambient or ignored mechanical energy with a novel triboelectric nanogenerator is conceived. This novel TENG has the capability to generate a high voltage of about 1300 V without additional auxiliary and it was integrated with a discharge reactor. The generated voltage can be utilized to induce microplasma discharge under an atmospheric environment in the discharge reactor. Thereby, this voltage is directly applied between electrodes of the discharge reactor to induce an atmospheric microplasma discharge and nitrogen fixation. It is observed that through this discharge nitrogen gas in the air had been successfully converted into nitrogen compound, including nitrogen dioxide and nitric acid solution, via the TENG-driven microplasma discharge process to finally realize the nitrogen fixation. The NO_3^- concentration of 250 ppm can be arrived after continuously operating the TENG for 400 min. Further, the effect of the magnitude of the separation between the discharge electrode on discharge process, including discharge voltage, discharge current and average

discharge energy per TENG operation cycle, had been systematically investigated. The TENG-driven microplasma discharge-based nitrogen fixation system was demonstrated its ability to serve as a nitrogenous fertilizer supplier, and correspondingly, $NaNO_3$ fertilizer was produced via driving the system by human walking stimuli for crop cultivation. After driving the system by human walking stimuli, the $NaNO_3$ fertilizer was produced to benefit the growth of the green bean. This work provides feasibility to develop an energy-saving, environmental-friendly, cost-efficient and safe nitrogen fixation route. This study offers a promising atmospheric nitrogen fixation strategy with energy-saving, environmental friendliness, flexible operation, and high safety.

Thirdly, a novel strategy to realized mechanical energy modulation of the AIE emission is purposed. Previously, the majority of switching of AIE luminogen between its on and off states reported were achieved by multiple forms of energy input, namely, mechanical energy preceded by heat or vapor fuming. This significantly hinders the development of a real-time, AIE regulating mechanism based solely on mechanical energy input. Hence, by fabricating a composite by incorporating the AIE luminogen into a polymer matrix. Mechanical stress was applied to the composite to control the free volume around these AIE luminogen, such that restricting the molecular motion of AIE luminogen and these nonradiative decay. Thereby, the emission intensity can be enhanced.

These researches investigated mechanical energy harvesting and converting utilizing luminescence materials and triboelectric nanogenerator. The novel findings provide valuable insight and demonstrated promising application in harvesting mechanical energy, such findings shall aid further research on various mechanical energy harvesting and conversion materials.

Wong Man Chung

THE HONG KONG POLYTECHNIC UNIVERSITY

List of Publications

Peer-reviewed Journals

1. **Man-Chung Wong**, Li Chen, Gongxun Bai, Long-Biao Huang, Jianhua Hao*. "Temporal and Remote Tuning of Piezophotonic-Effect-Induced Luminescence and Color Gamut via Modulating Magnetic Field." *Advanced Materials*, 2017, 29, 1701945. (Featured in Frontispiece) (Highlighted by the video abstract on YouTube at https://youtu.be/6KReKP4WXrA).

2. **Man-Chung Wong**, Wei Xu, Jianhua Hao*. "Microplasma discharge-based nitrogen fixation driven by triboelectric nanogenerator towards self-powered mechano-nitrogenous fertilizer supplier." *Advanced functional Materials*, 2019, 29, 1904090.

3. Wei Xu, **Man-Chung Wong**, Jianhua Hao*. "Strategies and progress on improving robustness and reliability of triboelectric nanogenerators." *Nano Energy*, 2019, 55, 203-215.

4. Wei Xu, **Man-Chung Wong**, Qiongyu Guo, Tiezheng Jia, Jianhua Hao*. "Healable and shape-memory dual functional polymers for reliable and multipurpose mechanical energy harvesting devices." *Journal of Materials Chemistry A*, 2019, 7, 16267-16276.

5. Wei Xu, Long-Biao Huang, **Man-Chung Wong**, Li Chen, Gongxun Bai, Jianhua Hao*. "Environmentally Friendly Hydrogel-Based Triboelectric Nanogenerators for Versatile Energy Harvesting and Self-Powered Sensors." *Advanced Energy Materials*, 2017, 7(1), 1614-6832.

6. Long-Biao Huang#, Wei Xu#, Gongxun Bai, **Man-Chung Wong**, Zhibin Yang, and Jianhua Hao*. "Wind energy and blue energy harvesting based on magnetic-assisted noncontact triboelectric nanogenerator." *Nano Energy*, 2016, 30, 36-42.

7. Long-Biao Huang, Gongxun Bai, **Man-Chung Wong**, Zhibin Yang, Wei Xu, and Jianhua Hao*. "Magnetic-Assisted Noncontact Triboelectric Nanogenerator Converting Mechanical Energy into Electricity and Light Emissions." *Advanced Materials*, 2016, 28, 2744-2751.

8. Tsz Hin Choy, Ying Ying O, Feichi Zhou, Wei Xu, **Man Chung Wong**, Tao Ye, Jianhua Hao, and Yang Chai*. "Enhanced output power of freestanding ball-based triboelectric generator through electrophorus effect", *Journal of Materials Chemistry A*, 2018, 6, 18518–18524.

Wong Man Chung

Presentations in international conferences

1. **Man-Chung Wong**, Li Chen, Gongxun Bai, Long-Biao Huang, Jianhua Hao*. "Temporal and remote tuning of piezoluminescence and color gamut via modulating magnetic Field." The 3rd International Conference on Mechanoluminescence and Novel Structural Health Diagnosis, **Conference poster**, December 15-17,2017, Hong Kong, China. (Best poster awards)

2. **Man-Chung Wong**, Wei Xu, and Jianhua Hao*. " High Voltage Output Contact-Separation Mode Triboelectric Nanogenerators Based on Commercial-Available Polymers", The 2019 MRS Spring Meeting & Exhibit, **Conference poster**, April 22-26, 2019, Phoenix, USA.

Wong Man Chung

THE HONG KONG POLYTECHNIC UNIVERSITY

Acknowledgements

I would like to express my sincere appreciation to my chief supervisor Prof. J.H. Hao for his patience, advice, constant caring throughout my years of research work, and in recognition of his worth for the dedication, support, and encouragement for starting me on my path and believing in my future. With his broad knowledge, academic insight, enthusiastic and painstaking guidance, I can finish my PhD study effectively, smoothly and successfully.

I also need to thank Dr. W. Xu for the triboelectric measurements and support, without his help, I can't smoothly finish my research. I would also like to thank Dr. R. Ding for the UV-vis measurements, and Miss S.Y. Pang for the Raman measurements. I would also like to thank all members in Prof. Hao group, especially Dr. L. Chen, Dr. M.K. Tsang, Dr. L. Huang, Dr. G. Bai, for their friendship, help and valuable discussions on my experiments. In addition, I would like to give my sincere thanks to my colleagues in our department, Dr. H. Sun, Dr. M. Li, Dr. Q. Chen, and Dr. Vincent Chan, for their great help and assistance.

Last but not the least, I am deeply indebted to my parents and friends for their warm understanding, support and encouragement.

Wong Man Chung

THE HONG KONG POLYTECHNIC UNIVERSITY

Table of Contents

Wong Man Chung

Wong Man Chung

Wong Man Chung

THE HONG KONG POLYTECHNIC UNIVERSITY

List of Figures

Wong Man Chung

THE HONG KONG POLYTECHNIC UNIVERSITY

Wong Man Chung

THE HONG KONG POLYTECHNIC UNIVERSITY

Wong Man Chung

THE HONG KONG POLYTECHNIC UNIVERSITY

Wong Man Chung

THE HONG KONG POLYTECHNIC UNIVERSITY

Wong Man Chung

THE HONG KONG POLYTECHNIC UNIVERSITY

Wong Man Chung

THE HONG KONG POLYTECHNIC UNIVERSITY

Chapter 1   Introduction

Mechanical energy is the most ubiquitous energy source in an ambient environment.[1-4] They exist in various forms such as vibration, shocks or stress, with frequency ranging from few Hz to kHz. With the recent surge of technological advancements in low power devices, the escalating costs of power storage device and the energy crisis.[5-9] Thereby, there has been a significant amount of extensive investigation on the harvesting and conversion of mechanical energy.

In this thesis, *in-situ* tuning piezoluminescence emission wavelength through modulating the temporal of mechanical excitation is briefly described first, serval novel applications based on this intriguing tuning of piezoluminescence emission wavelength which is described in subsequent sections. After that, a novel microplasma-based nitrogen fixation system driven by harvesting ambient mechanical energy though a novel triboelectric nanogenerator is presented, the fundamentals and characterization of this novel high voltage triboelectric nanogenerator and the nitrogen fixation system are discussed, providing a new strategy to realize environmentally friendly in- situ nitrogen fertilizer supply. The possibility of an alternative route for the realization of mechanical tuning of AIE was also discussed. Finally, the thesis concludes with perspectives in mechanical energy harvesting based on the current development.

Wong Man Chung

1.1. Background of mechanical energy harvesting and conversion

Currently, the most familiar mechanical energy harvesting and conversion techniques can be divided into four main types. They are electromagnetisms, electroactivity / flexoelectricity, piezoelectricity and electrostatics.[10-19]
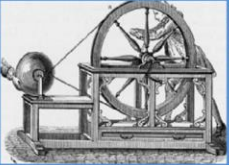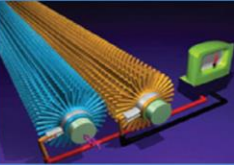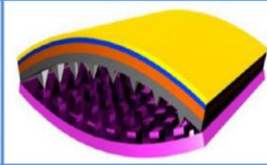
Mechanical energy harvesting	Electromagnetic	Electrostatic	Piezoelectric	Triboelectric
Harvesting principle	Electromagnetic induction	Electrostatic induction	Piezoelectric effect & Electrostatic induction	Contact electrification & Electrostatic induction
Impedance type	Resistive	Capacitive	Capacitive	Capacitive
Pros	High efficiency, easy to scale up	Light weight	Easy to scale down to nanoscale	Large output power, high efficiency, low weight, cost effective materials, simple fabrication
Cons	Heavy magnet required, low output for small-scale devices	Precharge required, low output, high matched impedance	Low output & low efficiency, pulsed output, high matched impedance	Pulsed output, high matched impedance

Figure 1-1 Comparison about the harvesting of mechanical energy using electromagnetic, electrostatic, piezoelectric and triboelectric effect for illustrating their merits and possible practical limitations.[19]

Based on Faraday's law of electromagnetic induction, electromotive force was generated by relative displacement of magnetic field lines and a conductor.[19] Conventionally, electromagnetic induction is most suitable for large-scale power generation owning to its gigantic

Wong Man Chung

sizes and operation condition. This technique harvest mechanism energy with maximum efficiency in the high frequencies' regime and macroscopic scale. Although electromagnetic induction is normally most effective to harvest mechanical energy, however, its unique operation characteristic limited the possible harvesting circumstances and only electric output. [20-25]

Furthermore, the recent development of multifunctional and on-wafer devices generally only require a relatively low power consumption, while the number of these devices can be numerous.[26-31] This puts forward severs challenges for electromagnetic induction based mechanical energy harvesting and conversion. For instances, it is almost impossible to integrate an induction motor on to microdevices due to their sizes, this results an *in-situ* mechanical energy harvesting unfeasible. Various power storage devices such as battery can transfer the harvested mechanical energy into each microdevice.[2, 32-37] However, monitoring and maintaining such innumerable devices routinely and frequently will be an enormous task and may results in a catastrophic environmental issue.[38-40] In this regard, developing smart material that can efficiently harvest and converse mechanical energy into various useable forms of energy could be an ideal strategy.

Smart materials are definite as intelligent materials that have a single or multiple properties that can be significantly changed upon external stimuli, such as moisture, pH, or stress.[41-44] Utilizing smart material to harvest mechanical energy may process various benefices. On one hand, the sizes of smart materials can be miniaturized to adapted various harvesting circumstances. Therefore, harvesting and utilization towards mechanical energy could be an efficient strategy and may be able to reduce the dependence on a traditional energy source. On the other hand, smart

material not only harvests mechanical energy into electricity, the multi-functional property of various smart materials enables its output to be employed in a wide variety of applications. Therefore, the study concerning harvesting and conversion of mechanical energy via smart material technology has been attracting extensive attention and deserves more attempts.

1.2. Luminescence and mechanoluminescence

Luminescence is defined as the light emission from a luminescent material whereas the electronic state of the substance is excited by external energy (photon, electron, etc. except heat) and the excitation is released as photon emission.[45-51] It is a cold body radiation. Luminescence from luminescent material can be provoked by photon excitation, the passage of a strong electric field, electron beam excitation, or stress inducing light emission.[52-54]

Phosphor is a substance that exhibits the trend of luminescence under various stimuli.[45, 55-61] The types of stimulus that cause luminescent from phosphor depended on the phosphor's crystal structure and its electronic configuration. Luminescent and phosphor have been extensively investigated, such as understanding the kinetic process of the luminescence changes with structural symmetry, crystal field, or band energy.[62-69] It is also necessary to develop an alternative approach to vary the phosphor's energy-level structure where tunable luminescence can be achieved.

THE HONG KONG POLYTECHNIC UNIVERSITY
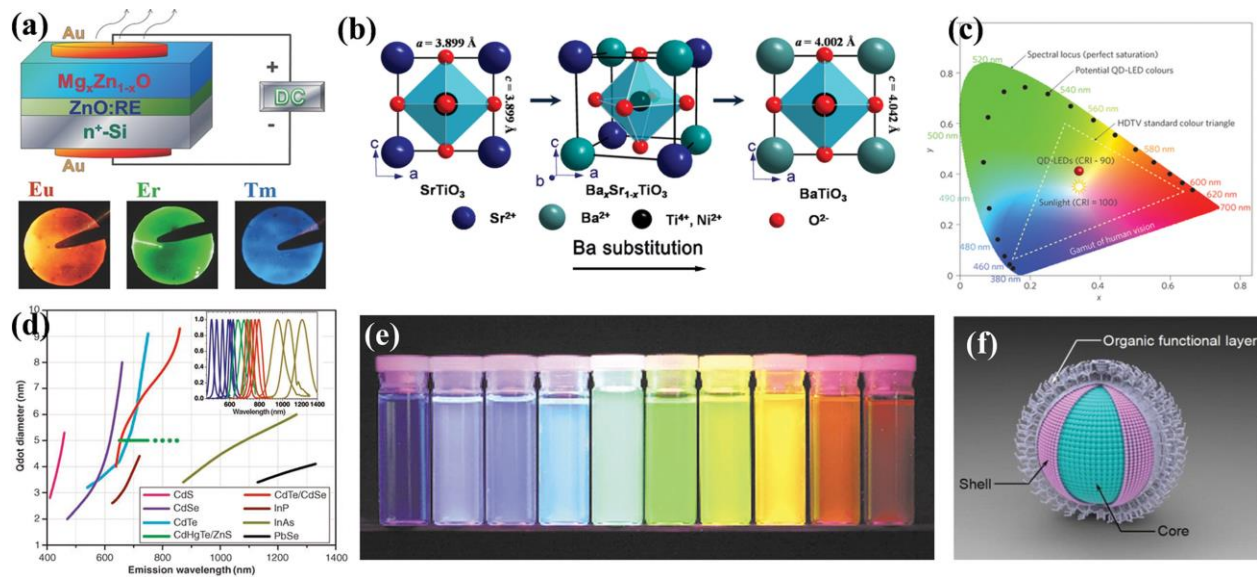
Figure 1-2 Various luminescence tuning methodology from different phosphors.[45]

Currently, the most familiar luminescence emissions include photoluminescence, electroluminescence, bioluminescence, chemiluminescence, etc.,[70-72] with each luminescence emission form possesses its own potentials and uniqueness. Compared to its counterparts, mechanoluminescence, by harvesting and converting mechanical energy to luminescence emission, have several applicational advantages. Firstly, due to the abundant availability of ambient mechanical energy and low cost in engineering. Further, its enormous potential in various applications situation, namely application in sensing, actuation, energy conversion, and sourcing, already attractive approach to achieve a sustainable energy source and self-sufficient systems, which deserves more attention.

Wong Man Chung

THE HONG KONG POLYTECHNIC UNIVERSITY

1.2.1.   Definition and basic principle of piezoluminescence

Mechanoluminescence (ML) is defined as luminescence induced under any mechanical stimuli.[73-78] Various form of mechanical action such as grinding, rubbing, stress, fracture, vibration can induce ML. In some case, a sudden change of temperature or photon induced deformation are also capable of inducing ML. There are numerous materials or compounds capable of inducing ML. Although the physical mechanism for ML emission from different materials varies from one another. They can be categorized into two major types: tribo-ML, and deformation-ML.

Tribo-ML is produced during the contact or separation of two dissimilar materials.[79] Whereas deformation ML is produced due to mechanical energy induced during deformation of solids, it may further be divided into three types. The first one is Fracto-ML, the luminescence produced at the instance new surfaces are created due to fracture of solids. The other type of Tribo-ML is regarded as Plastic-ML, which is the luminescence emission during plastic deformation of solids. The third is Elastic-ML is the luminescence during the elastic deformation of solid. Both Fracto-ML and Plastic-ML may not be reproducible once emission occurs.[80] However, as the definition suggested, Elastic-ML is highly reproducible and deserved more study in a mechanical energy harvesting and conversion context.

Despite its great potential, the understanding behind the mechanism governing Elastic-ML is still limited. It is generally accepted that the Elastic-ML emission originates from the transition of electrons from the excited state to the ground state during dynamic loading of the ML

phosphor.[81, 82] However, how these electrons overcome barriers from charges traps are facilitated to be released during elastic deformation of an ML phosphor remains a mystery. One proposition is that the piezoelectricity of host compounds generated an electric field which aided the carriers to be excited into an excited state.[83-86] This is regarded as the piezoelectrically stimulated electron detrapping model.

The model can be briefly described in **Figure** 1-3, and it can be intercepted as follow. When mechanical energy is applied onto a piezophosphor, phosphor processes of the piezoelectrical properties, the phosphor is subjected to deformation. The non-symmetric structure of the phosphor crystalline will produces an inner piezoelectric field inside the phosphor lattice. This piezoelectric field thereby would decrease the trap depth of these charge trap arise from doping ions into the phosphor or the phosphor special phases. Electrons may, therefore, be de-trapped. The energy released from the subsequent recombination of these electrons with holes either directly induced a photon emission or transferred to doped ion and induced a characteristic emission from that ions acting as luminescent centers. This proposition combined piezoelectricity, luminescent centers, and charge carrier traps into ML. The process is thereby regarded as piezoluminescent. Based on this proposed mechanism of piezoluminescent, the phosphor itself are supposed to be able to maintain its crystalline structural integrity under stress. These charge traps inside the phosphor lattice must have a proclivity for the charging and discharging processes, and an *in-situ* reproducible emission from the phosphor under a dynamical variation in pressure distribution.
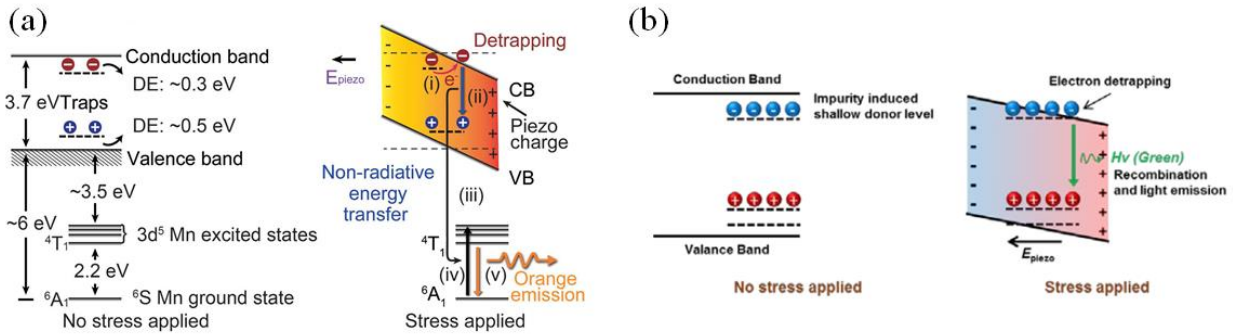
Figure 1-3 The mechanisms of the piezophotonic emission from (a) ZnS:Mn,[85] and (b) ZnS:Cu.[87]

Thereby, under these conditions mentioned, only a limited type of piezoluminescence phosphors have been reported. The most familiar host material included silicate, aluminate and phosphate systems. These materials were capable of acting as host material since they are relatively stable, and they are either doped with few types of transitional metal or lathanide. The doped ions not only create additional energy levels that prohibit the mechanical energy input converted excitation into non-radiative relaxations, but also able to act as additional charge traps for the enhancement of piezoluminescence. Take ZnS: Cu as an example, its piezoluminscence mechanism can be interpreted as follow. According to the lattice structure, a wurtzile structured ZnS crystal under deformation would produce a piezoelectric field inside. During sintering, the small sizes of Zn^{2+} ions may induce Frenkel defect inside the crystal lattice. In addition, the doping process of ZnS also induced Schottky defects that create various types of charge traps, namely, electron donors and holes acceptors. When this ZnS: Cu phosphor subjected to mechanical energy,

Wong Man Chung

the piezoelectric field induced inside the lattice structure results in an energy band bending. Simultaneously, the energy levels of these charge traps decrease due to this piezoelectric field. Thereby, electron trapped inside these charge trap may be able to reach the conduction band and recombined either with holes trapped in another defect center or back into its original trap. Energy is released in the form of photon or transferred to the ions respectively. Notice that the de-excitation of excited ions would give rise to the light emission characteristic of the doping ions, which can be regarded as luminescence center.
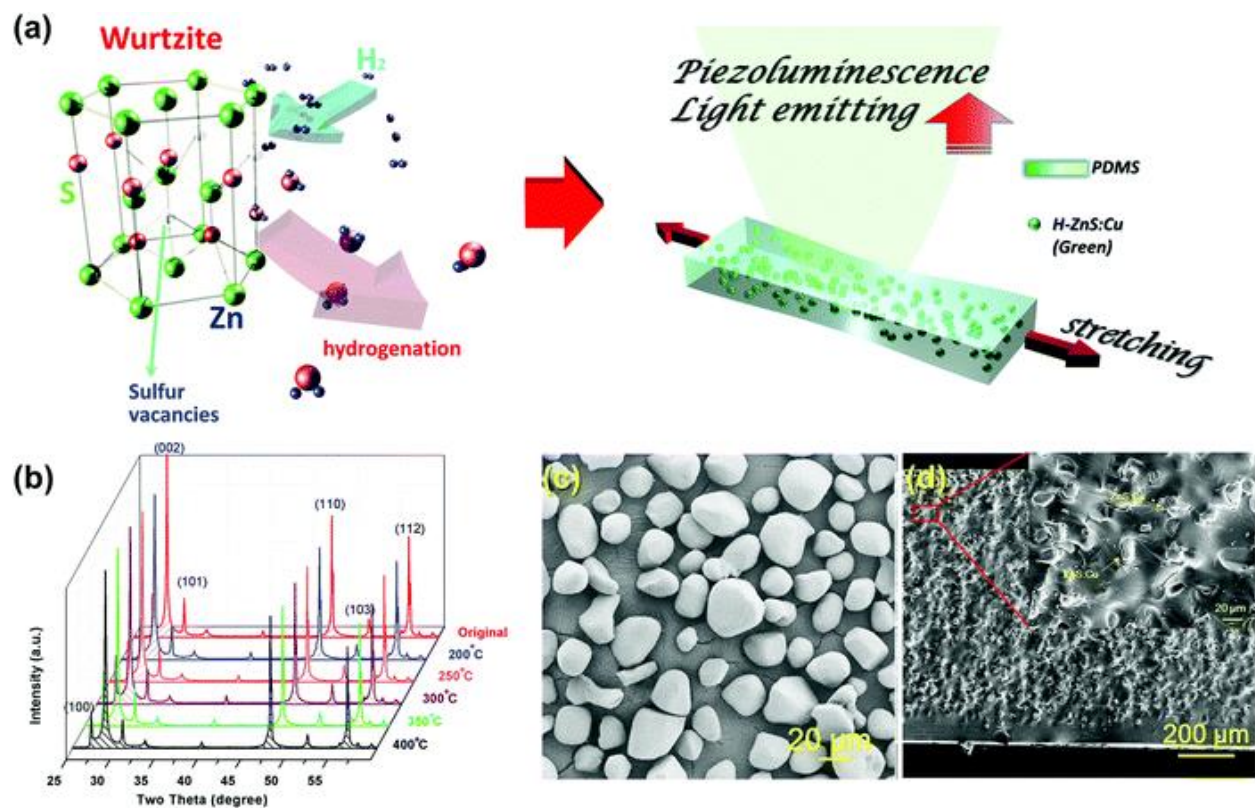
Figure 1-4 Crystal structure and piezoluminescence from ZnS:Cu phosphor. [87]

Traditionally, the representative piezoluminescence material that conducted ML based on the above mechanism include $SrAl_2O_4:Eu^{2+}$, $LiNbO_3:Pr^{3+}$, $mCaO \cdot Nb_2O_5:Pr^{3+}$ (m = 1, 2 and 3) and $ZnS:Mn^{2+}$.[68, 78, 88, 89] Among them, $ZnS:Mn^{2+}$ emit a strong 585 nm strong piezoluminescence as a relatively small mechanical energy applied to it. This intriguing phenomenon embarked further developing type II-VI doped ZnS based piezoluminecscent material. For instance, both Cu^+ and Cu^{2+} are doped into ZnS synthesize a green (510 nm) piezoluminescence phosphor. Later, co-doping of Cu^{2+} and Mn into ZnS produces a warm white piezoluminescence. This intriguing color mixing properties of ZnS piezoluminescence based on co-doping would have a significant impact in the field of ML. Since it would certainly broaden the scope of applications as well as deepen the understanding of piezoluminescence, therefore deserved more investigation.
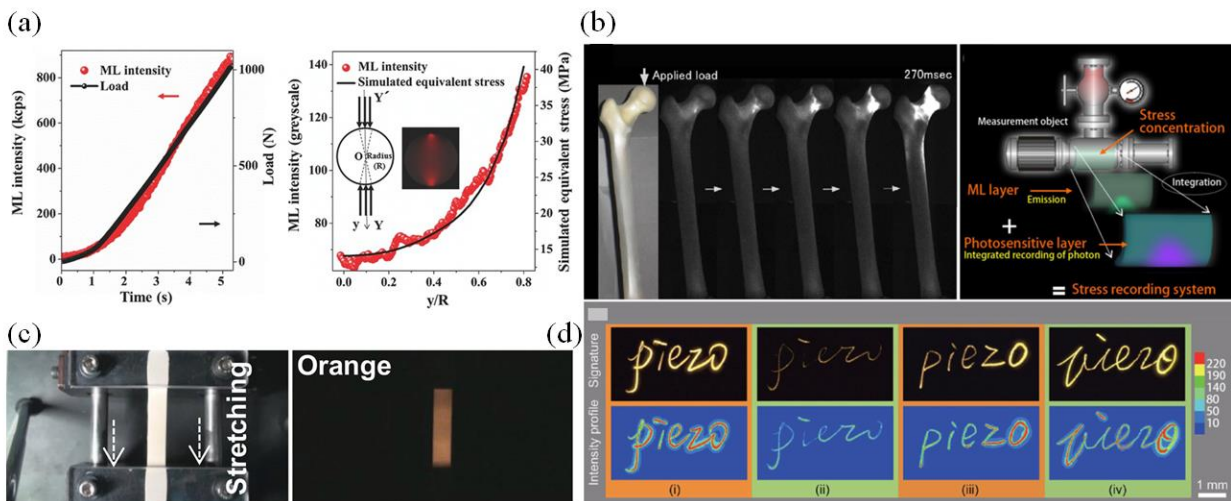
Figure 1-5 Summarized examples of recent development of piezoluminescent material and its applications. [68, 88-91]

Wong Man Chung

1.2.2. Mechanical stimulated and controlled aggregation induced emission

Mechano-responsive luminescence material is a type of material/composite demonstrates variation in photoluminescence (PL) emission in responses to a mechanical energy input.[92-94] The changes can be a completely switching on/off PL emission upon the application of various mechanical stimuli. These mechano-responsive luminescence materials have shown a steady increase of attention in recent years since their potential applications in various fields are indeed promising.

It is well established that the structural properties of a solid-state molecule dominate the luminescence properties of the particular molecule.[95-98] These structural properties include molecular packing, intermolecular interactions, mobility of various ligand.[99] Upon a mechanical stimulus applied to the molecules, the changes of the molecules physical factors can induce alternation of the properties of the subsequent luminescence. For instance, the changes in the energy levels of the highest occupied molecular orbital (HOMO) and the lowest unoccupied molecular orbital (LUMO) of molecules can be dynamically controlled results a shift in emission wavelength. [100-102] Although the majority of known mechano-responsive luminescence materials display fine reversibility under mild operation condition, but there are a few hindrances hindering the understanding mechano-responsive luminescence molecules, such as limitation of choices of material, luminescence quenching, a weak luminescence in solid state and aggregation caused quenching.[103]

Although aggregation generally is regarded as a destructive role and great obstacle in the field of development and limitation of luminescence. In recent years, scientists and researcher around the globe had put enormous effort developing aggregation-induced emission (AIE) since Tang et al first reported this intriguing AIE phenomenon in 2001.[104, 105] AIE have first observed in a silole based organic molecules. Afterward, a prolific number of molecules, organic luminophores capable of AIE have been developed.[106-109] Apart from this solvent exchange method, the magnitude of AIE emission can be modulated *in situ* via various physical means, this simple and effective phenomenon manifest numerous applications. However, there is a limited report based on solely and directly utilize local mechanical energy input to regulate the properties of AIE emission from any AIE molecules. Recently, incorporating AIE-type structural moieties into macromolecules have been investigated.[110-112] This integration provides an easy and effective strategy for the fabrication of various flexible AIE composite materials and mechano-responsive luminescence material. This not only provides a deeper mechanistic insight of AIE material but also enhanced the possibility for realizing a solely mechanical energy driven AIE emission modulation. Therefore, it is critical for fundamental research and practical applications.
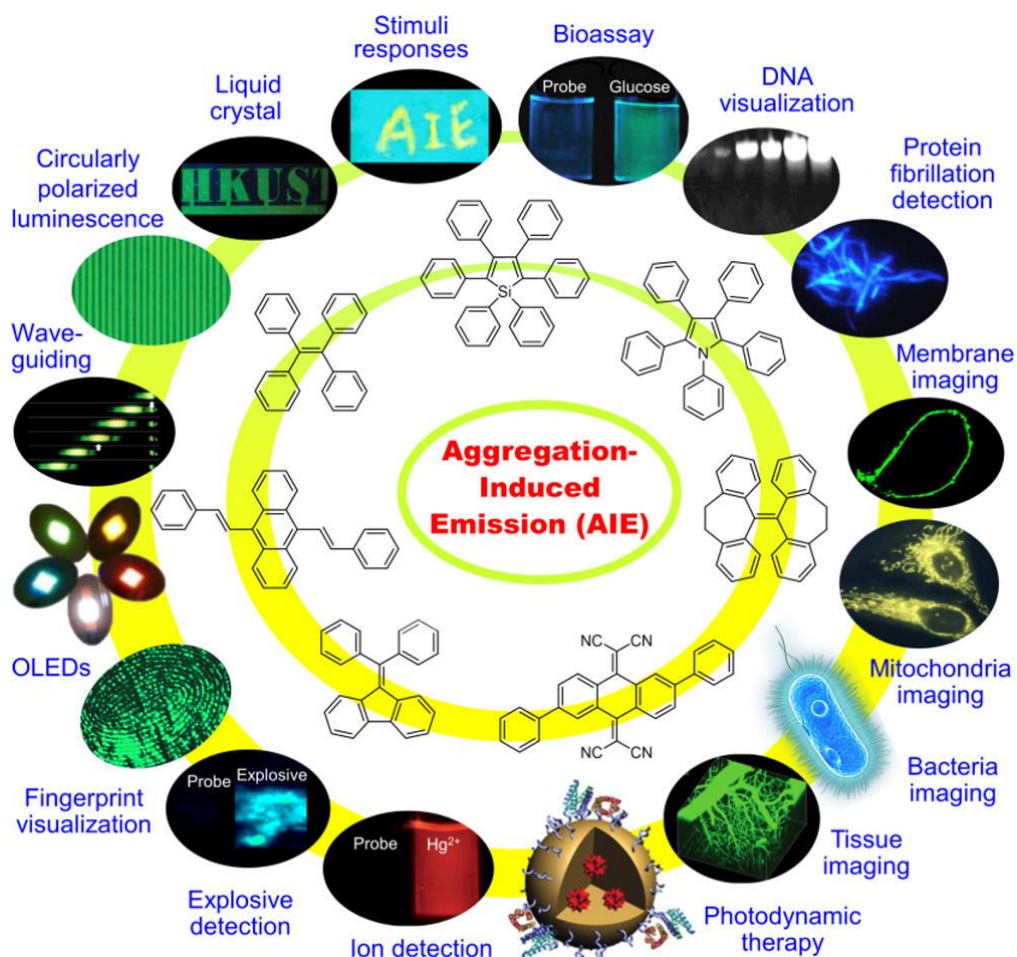
Figure 1-6 Example of AIE numerous applications. [113]

The AIE mechanism of silole based luminophoric molecules can be interpreted through the structural topology of these AIE molecules.[114, 115] Different from planar shaped conventional luminophores, such as perylene. An archetypical silole based luminophoric molecule has a shape resample the propeller of a container vessels. It consists of multiple phenyl as the rotors and silole in the center acting as a stator. When these silole based luminophoric molecules are in a good solvent, the rotors of the molecule undergo a dynamic intra-molecular rotation against its stator

upon photon-energy input. Since this dynamic intra-molecular rotation dissipated the incoming photon energy into kinetic energy of the rotor, renders the molecules non-luminescent. When the luminophoric molecule was situated in a poor solvent, the propeller-shaped molecules prohibit the packing of molecules through a π–π stacking process. Furthermore, a restriction of intramolecular rotations of these rotors arises from physical constraint in poor solvent results the radiative channel reopen. Once photon energy enters the system where the luminophorpric molecules are situated in, the molecules become emissive and AIE occur. There are a various of silole based luminophoric molecules exhibit AIE. As shown in **Figure** 1-7
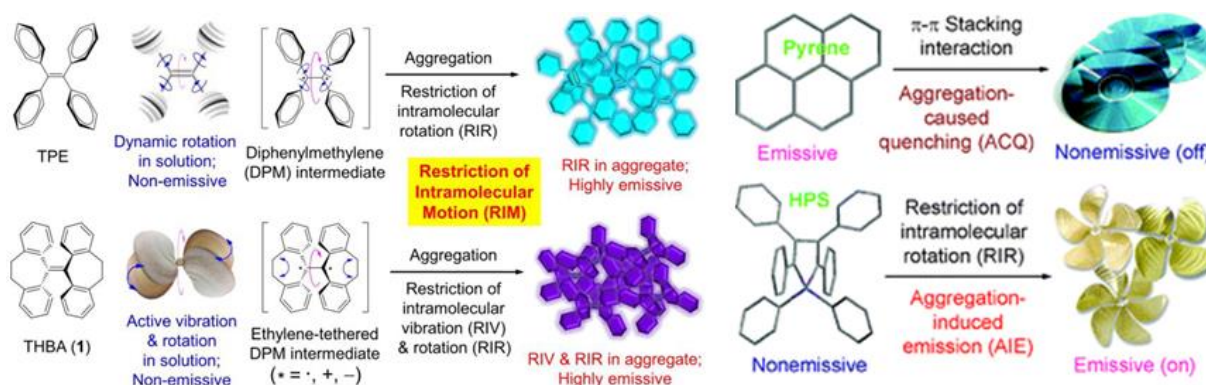
Figure 1-7 Example of archetypical AIE molecules and the AIE mechanism.[113, 116]

Among them, Hexaphenylsilole (HPS) molecule is a distinguish archetypal AIE luminogen.[117] It has a propeller-like configuration from the torsion between its six peripheral phenyl rings and the silole plane. In the silole core, six phenyl rings are decorated though single bonds. The carbons in the peripheral phenyl rings are all arranged either in a clockwise or anticlockwise manner It has high electron acceptability, fast electron mobility. It is non-emissive in its normal state. During aggregation, the increased molecular interactions cause restriction of

Wong Man Chung

HPS intramolecular rotations and also hamper its molecular motions. Aggregation-induced emission therefore occurs. Comparing with other fluorescent molecules, HPS has shown significant AIE property, their fluorescence emission intensity increased several hundred times upon aggregation. Tetraphenylethene (TPE) is another archetypal luminogen with a simple molecule structure but shows a splendid AIE effect.[118] In its crystalline lattice, it has four propeller-like phenyl rings. These rings are twisted out of the central alkene plane. Multiple intramolecular C–H···π hydrogen bonds are formed between the hydrogen atoms and the π electrons of the phenyl rings of an adjacent TPE molecule. This configuration inhibited nonradiative recombination by preventing the direct π–π stacking interactions, compile TPE a highly emissive luminophore in the aggregated state. TPE typically shows a deep blue electroluminescence emission peak at 445 nm, which is close to the PL of its crystals.

Aforementioned, AIE based mechano-responsive luminescence system that exhibit tunable emission generally require another types of stimuli to return to its original state.[119-122] Nonetheless, they can still be regarded as mechano-responsive material. Tang et al. reported that several luminophoric AIE molecule shown an emission switching between crystalline and amorphous states.[123] In the report, the AIE molecules were deposited onto a quartz substrate. Once these AIE molecules were annealed into its crystalline state, with 3-fold intensity enhancement occurs. The crystalline thereafter was transformed into an amorphous film via an application of mechanical stress. The subsequent emission from the molecules were diminished significantly. The observed phenomena were explained by crystallization enhanced emission, a form of morphology depended emission. Since these intramolecular interactions luminogens

molecules is restricted owning to steric effect from its crystalline state, which enabling these radiative interactions. On the other hand, when the luminogens molecules are not packed in a macroscopic framework or in its amorphous phase, these luminescence quenching criteria such as intramolecular rotation, p–p stacking or H/J-aggregation may occur, results in a significant reduction of the luminescence.

Additionally, a shift in emission wavelength can be observed in some AIE luminogens molecules under mechanical stimuli. The underneath mechanism of the shift has been reported. It is generally believed that a morphological change between the thermodynamically stable crystalline state of an AIE luminogen and its metastable amorphous state render the hyperchromic and bathochromic emissions respectively. This reversible modulation of morphology under mechanical stimuli combined with thermal or organic solvent fuming driven recrystallization medicate the peak emission wavelength of the AIE luminogen dynamically. For instance, Tang et al. reported that 1,1,2,2-tetrakis(4-ethynylphenyl) ethane, an archetypical AIE luminogen, exhibit a 477 nm emission during its crystalline phase.[116] Upon mechanical stimuli such as grinding the crystalline with a glass rod into amorphous powder, the emission red shifted to 505 nm. Thereafter, the peak emission reverts to 477 nm by fuming these amorphous powders with organic solvent to recrystallization.

However, as stated earlier, most of the cyclic (switch on/off) AIE modulation are achieved by multiple form of energies input, namely mechanical energy preceded by heat or vapor fuming driven recrystallization to realize a phase change of these AIE luminogen. This significantly hinder the development for a real time, simple AIE regulating mechanism based on mechanical

energy input solely. Although most of previous studies revealed that the restriction of intramolecular motion of the rotor of the in its amorphous phases is primarily responsible for the AIE phenomenon, though demonstrating AIE in a solvent exchange context. AIE luminescence amplified comparatively when it was dispersed into a poor solvent than in good solvent. But one can suspected that, based on the intramolecular motion of rotor, aggregation formation is not a necessary condition for AIE to occur. Rather, the aggregation may merely be a sufficient condition for AIE to happen. It implies there may be an alternative method to realize such an intriguing phenomenon. In recent year, Shinkai and coworker have been realizing an emission known as cyclization induced emission by utilizing supramolecular interaction to induced or suppress these rotor motion, in turn to trigger AIE emission, [112] as shown in **Figure** 1-8 (a). Compared with AIE luminogen, incorporation into macromolecule or polymerization of AIE materials provide several advantages. Among them, ease of functionalization and prominent processability are the two key factors that may promises a solely mechanical energy modulated AIE emission could be realized. Although AIE polymer matrix already demonstrated its great potential in practical applications, such as florescent chemosensors and the application scope had been expanded in relative potency. As a young field, AIE polymer research is experiencing exponential growth and tremendous progress have been made so far, studies in design, syntheses protocol, morphology, functionalities etc. have been conducted and significant progress have also been made.[102, 124] In the mechanical energy perspective, the major factor in realizing solely mechanical energy medicated AIE emission should be structural morphology and functionalities of the AIE-polymer matrix. Thereby, a brief overview of these three key factors will be introduced.

Wong Man Chung
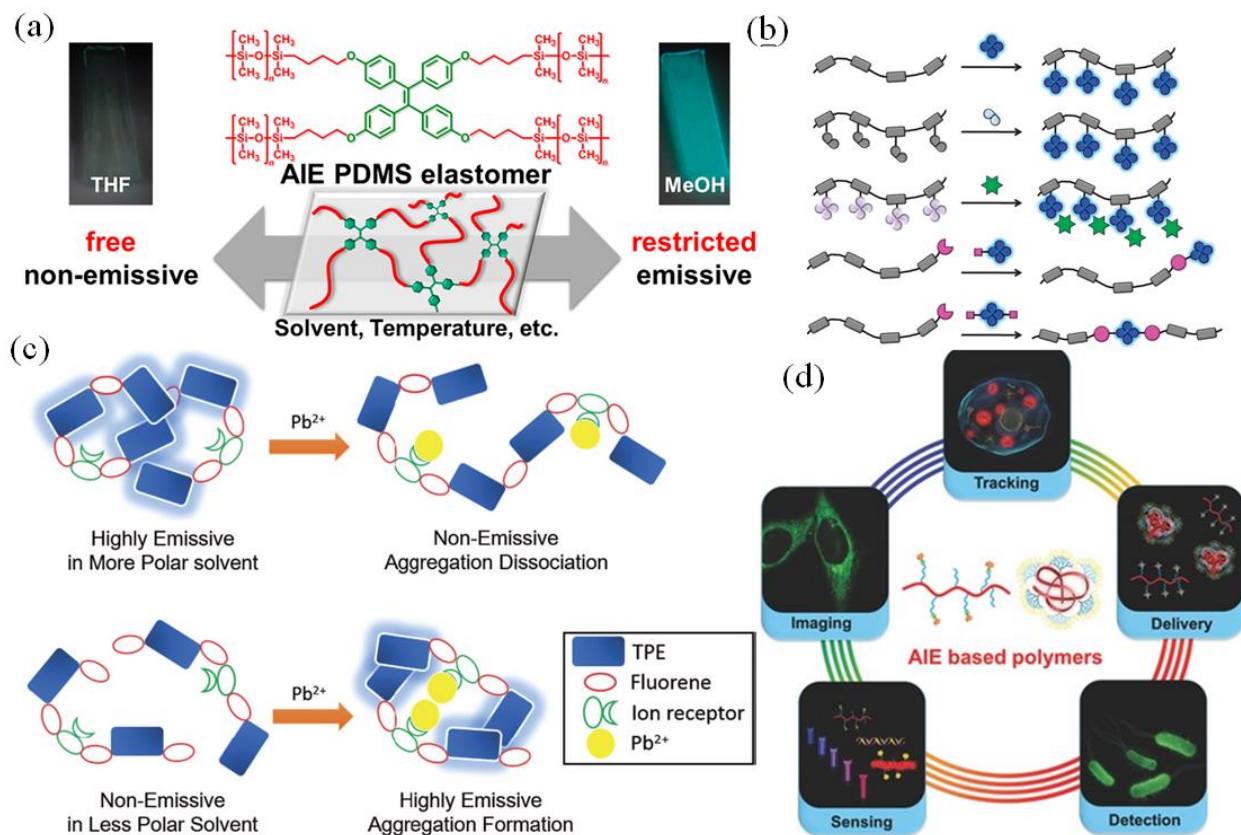
Figure 1-8 AIE macromolecules (a) Working principle of tuning of emission of AIE polymer (b) Examples of crosslinking AIE luminogen with polymer. (c) Working principle of tuning of emission of AIE polymer (d) Numerous applications utilizing AIE polymer. [110, 112, 124, 125]

AIE macromolecules and the sequent polymerizate polymer can be constructed through numerous synthetic strategies. These strategies generally aimed either at integrate archetypical AIE luminogens into monomer or empowered these AIE luminogens as a crosslinker and directly

polymerized another monomer, some examples are demonstrated in figure 1-8 (b). For integration of archetypical AIE into monomer, typical methods include direct linkages of AIE into monomers or copolymerization AIE luminogens with other monomers. These two basic strategies can be further modified with an AIE luminogens act as a side chain of the monomer or as a terminator.

Besides direct polymerization via modulation of monomer, various polymerization strategies have deviated to polymerized various types of monomer discussed previously. [102, 124] They can be categorized into two main schemes, chain polymerization and step polymerization. These two schemes can furnish both nonconjugated, and conjugated AIE-polymer. For example, acetyl or alkyne have been used to synthesize conjugated AIE-polyacetylenes, while homopolymerization or copolymerization form vinyl polymerizations have been utilized to synthesize nonconjugated AIE-vinyl polymers. Furthermore, step polymerization have also be employed. Free radical is utilized to initiate polymerization of nonconjugated AIE-polymers. This method received wide attention as they added additional and various functionalities in the polymers, such as, enhanced mechanical properties, biocompatibility and temperature or solvent based stimuli responsive properties.

Though incorporating AIE lumingens into a polymer matrix, the fabricated composite equipped with both the advantages of AIE small molecules and polymer. For instance, the performance of AIE-polymer may be comparable or even enhanced when compared to its small molecule counterpart.[126, 127] Further, many intrinsic properties of the polymer matrix are inherited by AIE-polymer, such that, the scope of applications and functionalities could be expanded, especially for conjugated polymer. Since they have shown facile processability and

Wong Man Chung

superior sensitivity to various environmental factors, therefore, it opens the possibility for the conjugated polymer to be applied in the applications such as chem and bio sensors, non-linear, electroluminescence device cell imaging and stimuli-responsive polymer, as shown in **Figure** 1-8 (d).

1.3. Harvesting ambient mechanical energy for electricity generation

Electricity and energy are key factors governing the future of society and quality of life. Traditional fossil energy sources namely coal, natural gas or petroleum fuel are all limited in there and leave a significant carbon footprint.[128-132] Thereby, energy crises and catastrophic climate changes have become aware and concern by the general public.[133-135] The urgency to develop novel renewable and green electrical source to substitute or replace fossil fuel have become prominent.

In the field of portable and wearable electronics, an unprecedented pace of development has been observed in the past two decades.[132, 136, 137] These portable and wearable electronic entered various sectors of life, such as healthcare, fabrication, security, and sensing. The current trends of miniaturization of electronic technology have not only expanded the knowledge in material and electronic science but also the revolutionized the concept of energy supply and sources.

Wong Man Chung

The miniaturization of these electronic devices required moderate power to operate, in the range of milli and micro watt, when the number of these devices can be numerous, furthermore, as the buck-boast technique has become more mature and low cost in recent years.[8, 138-140] The possibility to harvest and convert the local ambient environmental energy to match and supply the devices electrical requirement become significantly realistic. Moreover, in a traditional power supply sources context, a severe challenge was imposed to traditional energy storage or energy source. For instance, battery-powered electronic devices are a common practice in modern society.[141-143] However, to routinely and frequently monitor, replace, and recharge such a vast number of electronic devices are not practical. Especially for electric or electronic devices that are in a rural area, not only replacing the battery for these devices impractical, the limited voltage available from a battery causes the operation cost uneconomical.

In this regard, developing new technology that not only can harvest ambient energy such as wind, temperature gradient or mechanical energy, in order to satisfy rural area energy needs but also can supply enough voltage for various application in these areas is likely to be an ideal choice. Since these ambient energies usually have been ignored and they generally are renewable. Thereby, harvesting and conversion of such ambient energies could reduce the dependence on traditional energy significantly. Further, by generating a large voltage, a variety of electrical application can be operated independently. Therefore, the study concerning harvesting ambient energy has been attracting extensive attention.

Among substantial energy harvesting, traditionally ambient mechanical energy has been harvested based on electrostatic, electromagnetic and piezoelectric effects.[13] For instance, the

Wong Man Chung

piezoelectric generator is used to converse mechanical stimuli to an electrical signal or directly to electricity for micro-electronics and IoT system. The limited frequency range for piezoelectric generator limited optimum performance utilization and a piezo generator usually required a strenuous effort to fabricate these problems still pose a challenge for its application as a power source.

Electromagnetic generator is the most sophisticated mechanical energy harvest and conversion technology.[144] Its advantage included its conversion efficiency, while its conversion is independent of environmental factors. In addition, a stable high current output can be obtained as long as the input mechanical energy is above a threshold value the electromagnetic generator required. However, ironically, this threshold value required a relatively high frequency. Moreover, the torque to start an electromagnetic generator is generally unfeasible in an ambient mechanical energy context, which significantly hindered the application of electromagnetic generator in harvesting ambient mechanical energy. Therefore, its ability to harvest ambient mechanical energy generally is regarded as limited. In recent years, triboelectric nanogenerator (TENG), a novel mechanical energy harvesting technology have attracted tremendous attention. Due to its advantage over piezoelectric generator and electromagnetic generator owning to its eases of fabrication and low threshold energy to operate, have attracted much attention. Furthermore, TENG shows advantages of wide range of operation frequency, flexible sizes, wide range of working modes and capable of generate a relative high voltage.
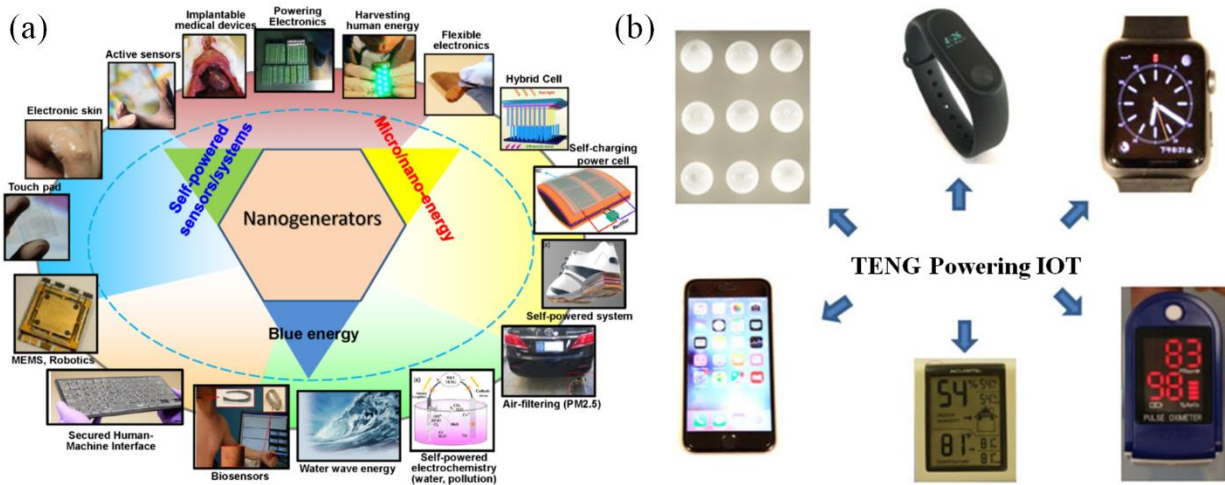
Figure 1-9 (a) Numerous fields of application of TENG (b) Examples of TENG powering IOT. *[19, 145]*

1.3.1. Triboelectric generator and its fundamental

TENG was invented in 2012, it has been attracted extensive attention in academia and rapid progress have been made. [19, 138, 146-149] Generally, it converted ambient mechanical energy to electricity. Its operation is based on triboelectrification and electrostatic induction.

By means of triboelectrification, it is the electrically charging of two dissimilar material as their surface during a rubbing action.[146, 150-152] Although the underneath mechanism is still uncertain, it is generally believed that the surface contacted exchange charges due to the electrochemical potential gradient between the two surfaces. From this potential difference, charges are migrated from a high potential surface to a low potential surface. As the two surfaces parted, each surface will be acquired or loss static charges. Afterward, a voltage is built up between these two surfaces due to these charges are generally prohibited to drain to the ground, a high

voltage is therefore subsequently built up and be utilized as the output of TENG. This mechanism is summarized in **Figure** 1-10 By harvesting various form of ambient mechanical energies and utilizing it for the aforementioned rubbing and separating action, TENG therefore converts the local ambient energy and acts as a sustainable electric source.
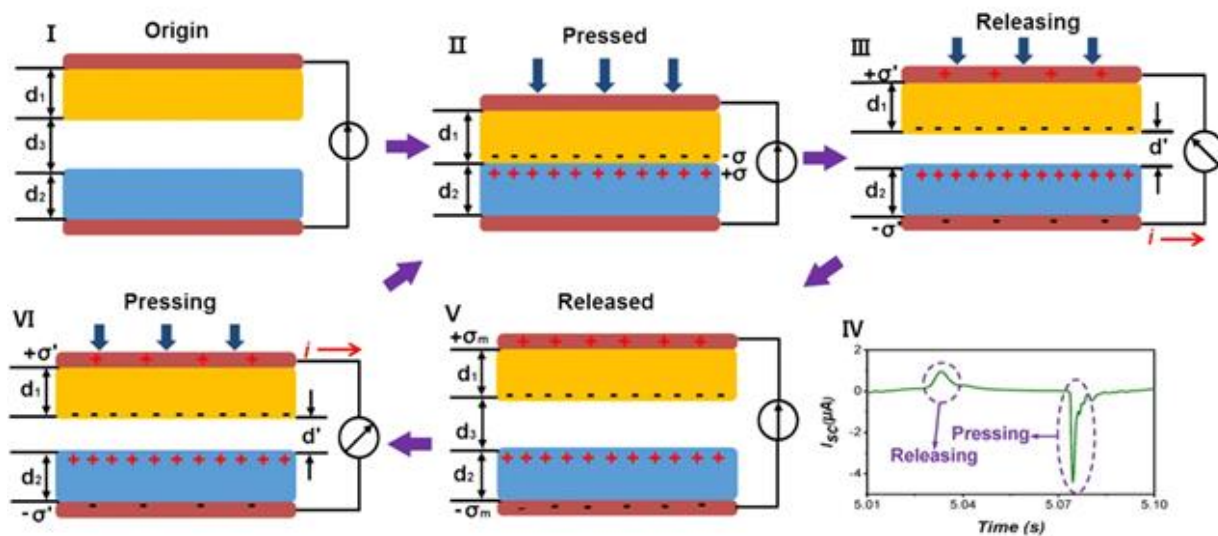
Figure 1-10 Work mechanism of a typical TENG. [153]

The operation of TENG is based on triboelectricity of material. Prior to numerous effort and research from the past few years, [8, 138] fundamentally, the operation mechanism of TENGs can be divided into four modes. Based on these four modes of operation, TENG could be utilized in a vast situation and/or circumstances for mechanical energy harvesting and conversion. Hence a brief discussion concerning four modes will be given in the following,

(1) Vertical contact-separation mode

The vertical contact-separation mode is considered as the most fundamental types of TENGs.[154-158] **Figure** 1-11 shows a typical dielectric-to-dielectric vertical contact-separation mode TENG.
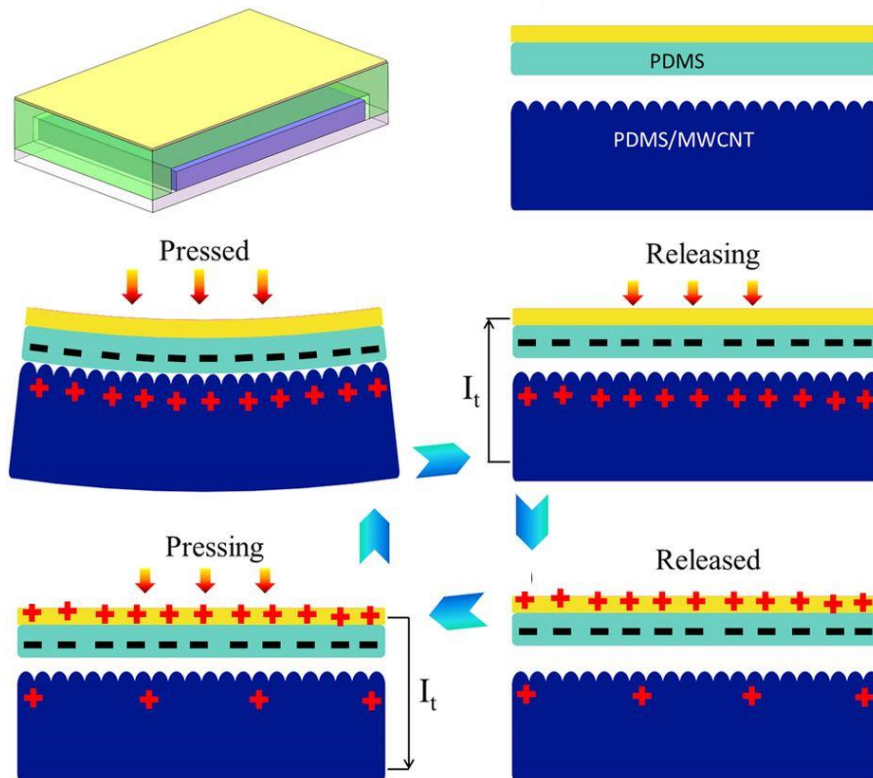
Figure 1-11 Typical dielectric-to-dielectric vertical contact-separation mode TENG.[159]

Two different materials regarded as frictional layers with electrodes coated on their top surface in contact with each other in the bottom surface, surface charges are built up due to contact electrification between these materials. The difference in electron affinity of two materials will

cause charge transferred between two surfaces. As electrodes are electrically connected to an external circuit, once the two oppositely charged surfaces are separated, an electric potential difference between the two electrodes is generated from coulomb interaction between the charged frictional layers. This potential different drives electrons in the connected external circuit to flow. Once the frictional layers separation decreases and were brought into contact by mechanical energy input. A potential different with revered polarity is induced and electrons thereby in the external circuit will flow in the opposite direction until the frictional layers contacted with each other. Upon a periodical application of mechanical energy onto TENG, electric energy is generated.

(2) In-plane sliding mode

Apart from vertical contact-separation mode TENG operator via the two contact materials as they separated in direction perpendicular. An alternative strategy TENG electricity generation from contact electrification of two frictional layers is separating these layers in the direction parallel to the length of the frictional layers. This contact separation mode is regarded as the lateral sliding mode TENG. **Figure** 1-12 shows the structure and working principle of a typical dielectric-to-dielectric lateral sliding mode TENG.[143, 160-163]
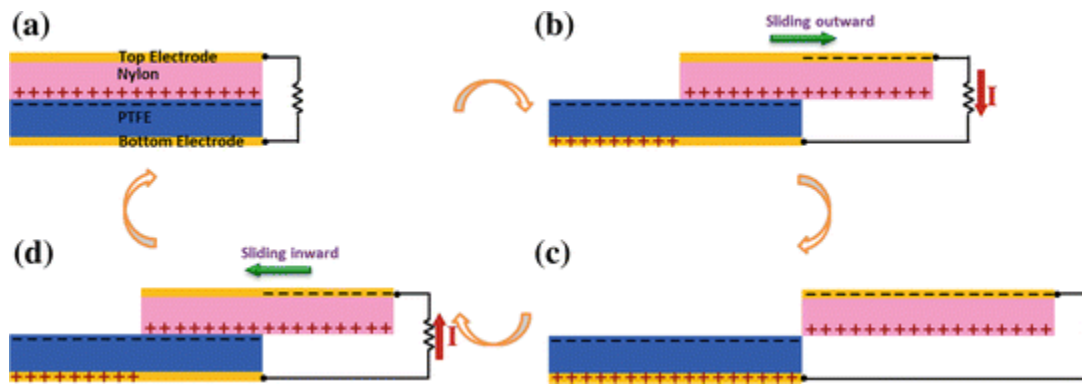
Figure 1-12 Working mechanism of a Sliding mode TENG. [164]

The working principle is similar that of vertical contact-separation mode TENG whereas frictional layers of TENG slide across each other. The triboelectrification causes the charge transfer between the interface, this direction and amount of transferred different charge carriers are also mainly depended on the variance of the electron affinity between frictional layers as in vertical contact-separation mode TENG. Furthermore, the two frictional layers as in contact-separation mode are deposited with electrodes and connected to the external circuit. Hence, a potential difference will be generated upon the separation of the frictional layers, and a current is thereby induced. Further, as mechanical energy brought the two frictional layers to contact again, via coulomb interaction a potential difference will generated to oppose the mechanical energy input, this potential difference also will induce a current across the external circuit in the opposite direction. However, unlike vertical-contact separation mode TENG, though the mechanical energy can drive the frictional layers of the sliding mode TENG to sliding back and forth. The structure of this mode TENG can also be modified such that a rotational mechanical force can also be harvested and conversed electricity. In a manner similar to an electromagnetic generator, this type

Wong Man Chung

of TENG not only can enhances its ability to harvest various form of mechanical energy, the low cost, simplicity and flexibility of the TENG can also provide an attractive alternation from tradition electromagnetic generator.

(3) Single-electrode mode

The reliability of operational output of both vertical contact-separation and lateral sliding mode TENG depended on whether the inputting mechanical energy is or not periodic.[165-168] However, most of the ambient mechanical energy available for harvesting is not practically predictable.[169] Therefore, a single-electrode mode TENG was devised based its operation on a single electrode and an electrical reference or grounded point. When mechanical energy was inputted into a single electrode mode TENG, it generally is through a surface. This surface is backed with an electrode as the primary electrode of the TENG. The surface itself can be a metal, polymer or any dielectric. Once this primary electrode contacts the secondary electrode, which usually is another surface with electrode beneath and connected to ground, charge carriers are transferred upon the two surfaces are in contact with one another. A potential difference is generated once these two surfaces were parted. Depending on the polarity of the generated potential differences, electrons will flow towards or from the ground and a current is generated. This single electrode mode TENG is flexible in terms of harvesting various form of mechanical energy.

THE HONG KONG POLYTECHNIC UNIVERSITY
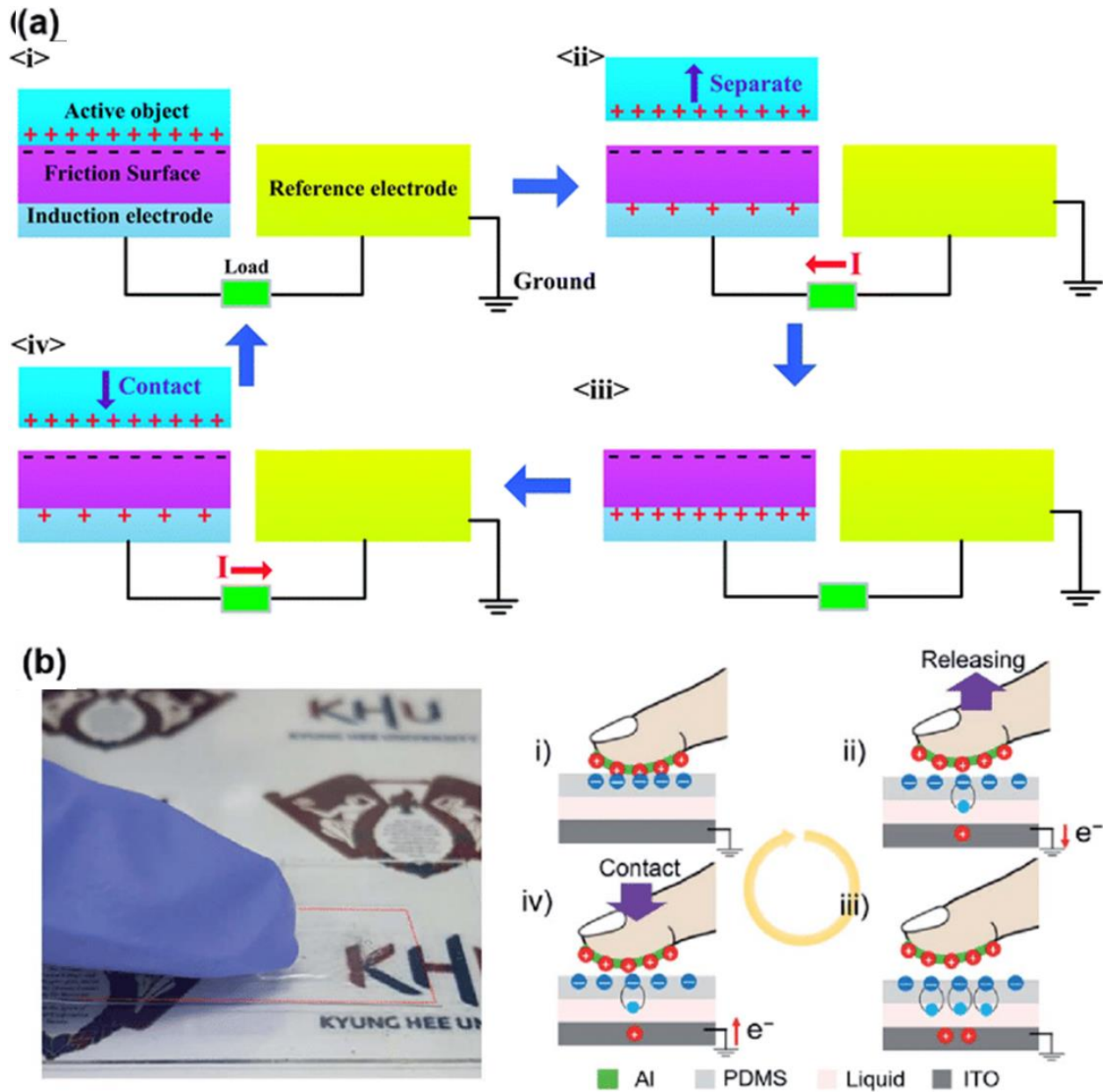
Figure 1-13 (a) Working principle of single electrode mode TENG (b) Example of a single electrode mode TENG. [170, 171]

Since it can harvest mechanical energy in parallel or perpendicular direction relative to the contact surfaces, moreover, the mechanical energy can be impulsive, long duration, or non-periodic, such that increases the circumstances that it can be employed.

(4) Free standing mode

Different form the previous discussed TENG, a free-standing triboelectric layer mode TENG operating based on two immovable frictional layers above electrodes connected across an electric load.[172, 173] When a third frictional layer, which is not connected to any electric circuit and regarded as freestanding layer are allowed contacted the two immovable frictional layers separately. Since, during each contact between the freestanding frictional layers and one of the immovable frictional layers, the contact electrification between them causes a charge carrier transfer. This charge transfer causes a differences in the amount of static charge between the two immovable frictional layers and induced a potential difference between them, a current will thereby flow though the electric load. As the freestanding electrode contact the other immoveable frictional layer, the current of opposite direction will flow across the electric load. This format of mechanical energy harvesting based displacement of various objects traveling along TENG with no moving part provide a durable TENG and expanding the scope of TENG applications.
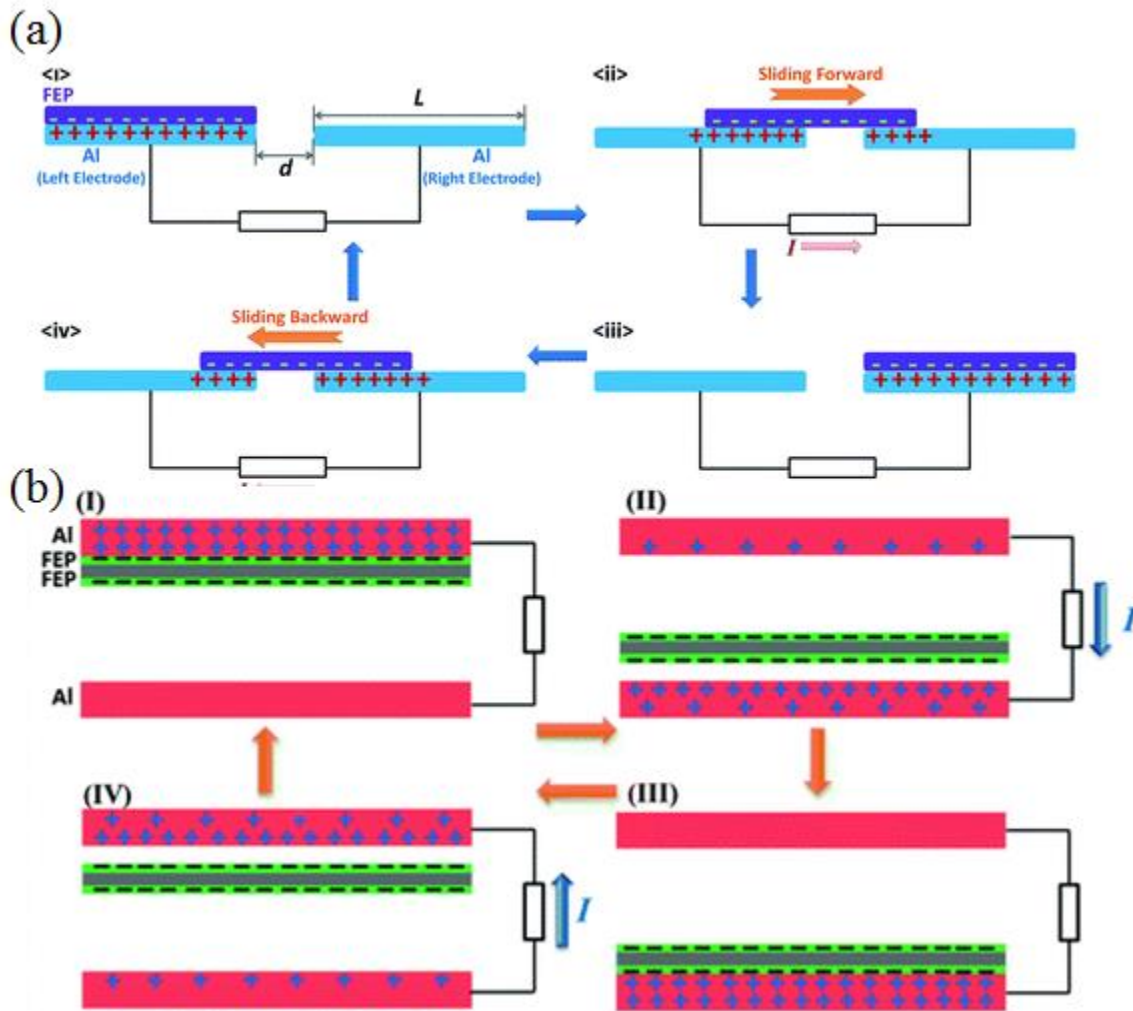
Figure 1-14 Working principle of two types of free standing mode TENG (a) Contact slicing mode

(b) Contact mode free standing triboelectric based nanogenerator. [174]

Technically, almost all materials can be the utilized to be a frictional layer in TENGs. Although contact electrification is a complicated process where both the magnitude and polarity of the developed charge is sensitive to the material composition, the contact process and the environmental conditions.[175-178] The critical criteria are for a TENG to be able to generate a

Wong Man Chung

voltage under same amount of mechanical energy could be regarded to be depending on the variances in tendencies of the two materials to gain or lose electrons during contact electrification. That is, with one material as frictional layers with the tendency to lose charge carriers, the other material that aimed to conduct contact electrification with the first material must have the tendency to gain charge carriers. The greater the variances, the high the output voltage.

For metallic materials, the charging process during contact electrification can be regarded to be govern by the work functions of individual metal or alloy. Contrary, a unified theory concerning the charging process of polymers material have yet to be developed. Since the charging behavior of polymer vary between different polymer although several charging pattern could be observed consistently. For instance, Polytetrafluoroethylene (PTFE) is generally regarded as the most negatively charged material after contact electrification while Polyurethane foam is known to be an apex positively charged material.

Therefore, various material can be arranged in a "triboelectric series" which enlists these materials in the order of the relative polarity after contact electrification charging, from those that capable of charged to most positive, like sorbothane, to those that charge most negative, such as halogenated polymers. In the triboelectric series the higher positioned materials will acquire a positive charge when contacted with a material at a lower position along the series. Thus, the triboelectric series can be used to estimate the relative charge polarity of the materials.

Table 1 Triboelectric series of various typical materials

Material	Affinity (nC/J)
Polyurethane foam	60
Sorbothane	58
Solid polyurethane, filled	40
Nylon, dry skin	30
Nylatron (nylon filled with MoS2)	28
Glass (soda)	25
Wood (pine)	7
Cotton	5
Nitrile rubber	3
Polycarbonate	-5
ABS	-5
Acrylic (polymethyl methacrylate)	-10
Styrene-butadiene rubber (SBR, Buna S)	-35
PET (mylar) cloth	-40
EVA rubber for gaskets, filled	-55

Wong Man Chung

Polystyrene	-70
Polyimide	-70
Vinyl: flexible (clear tubing)	-75
Olefins (alkenes): LDPE, HDPE, PP	-90
Neoprene (polychloroprene, not SBR)	-98
PVC (rigid vinyl)	-100
Latex (natural) rubber	-105
Viton, filled	-117
Epichlorohydrin rubber, filled	-118
Santoprene rubber	-120
Hypalon rubber, filled	-130
Butyl rubber, filled	-135
EDPM rubber, filled	-140
Teflon	-190

1.3.3 Application of triboelectric generator

Aforementioned, TENG of various working mode and structural design have been fabricated and developed for a variety of applications. Currently, TENG is mainly functioned its function as power sources and self-powered active sensor.

(1) TENGs as sustainable power sources

The ability of TENG in harvesting and converting ambient mechanical energy have attracted great attention.[179] The most prominent is its ability to acted as a sustainable power source to driven electronic devices.[136, 180-182] Moreover, the inherent high voltage output of TENG provide a unsurpassed simplicity in those circumstances that required high voltage output, such as mass spectrometer (**Figure** 1-15 (a)),[183] dielectric elastomer (figure 1-15 (b)),[184] ferroelectric polymer,[185] field emission devices,[186], (figure 1-15 (c)) electrospinning[187] etc. Moreover, various types of ambient mechanical energies, such as vibration, wind, blue energy and human body motion energy have been harvested via TENG owning to the dismal design constraint of TENG that can suit various occasions.
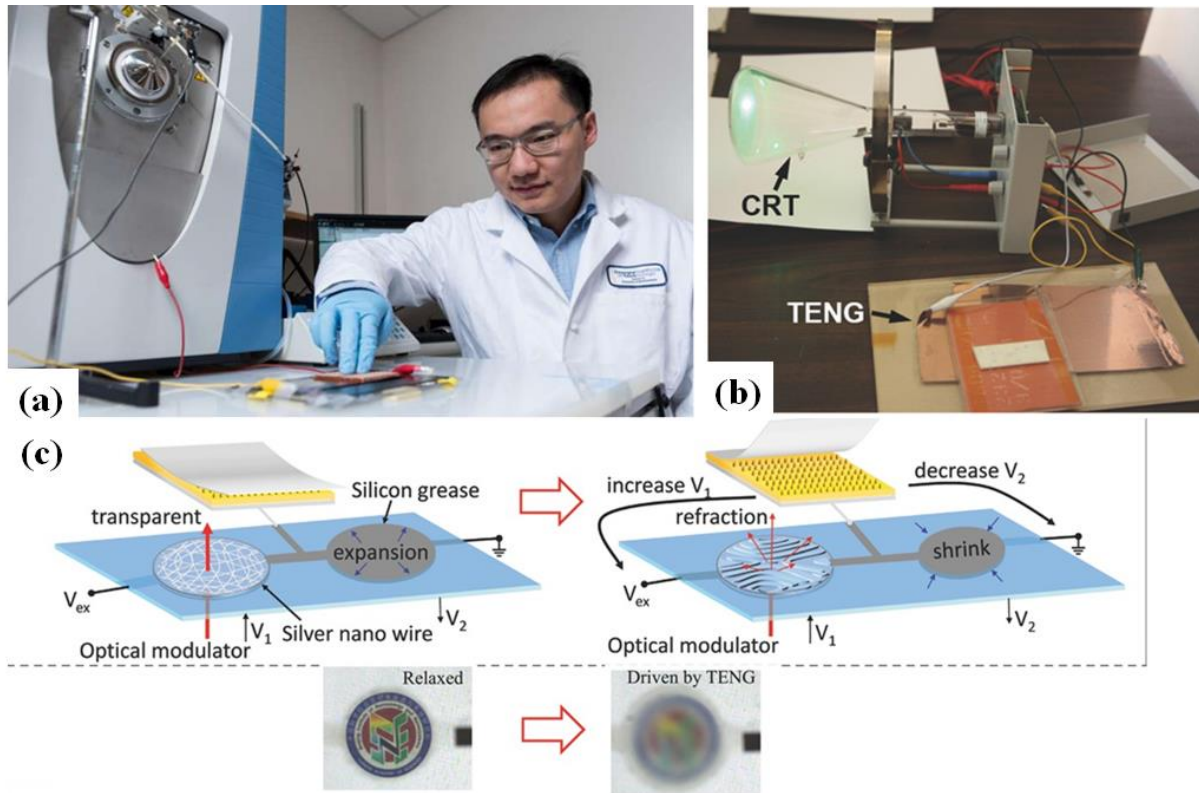
Figure 1-15 Examples demonstrating various TENG applications.[183, 186, 187]

(2) TENGs as self-powered active sensor

By its nature, TENG convert mechanical energy into an electric signal output, it is obvious that TENG can be utilized as a self-powered direct mechanical stimulus sensing device.[188-191] Though analyzing the feature of output signals, such as amplitude and frequency, the time portfolio of the applied mechanical stimuli, and the environmental parameter can be interpreted through careful analysis affecting the charge density of these surfaces of frictional layers. As shown in **Figure** 1-16 (a). This provides the TENG with the ability as a self-powered mechanical or

Wong Man Chung

chemical/environmental sensor to obtain the information about the mechanical input and the working environment. Moreover, various range of sensing types have been developed such as wind, force,[192] acceleration,[193] MEMS fine displacement and rotational sensors etc.
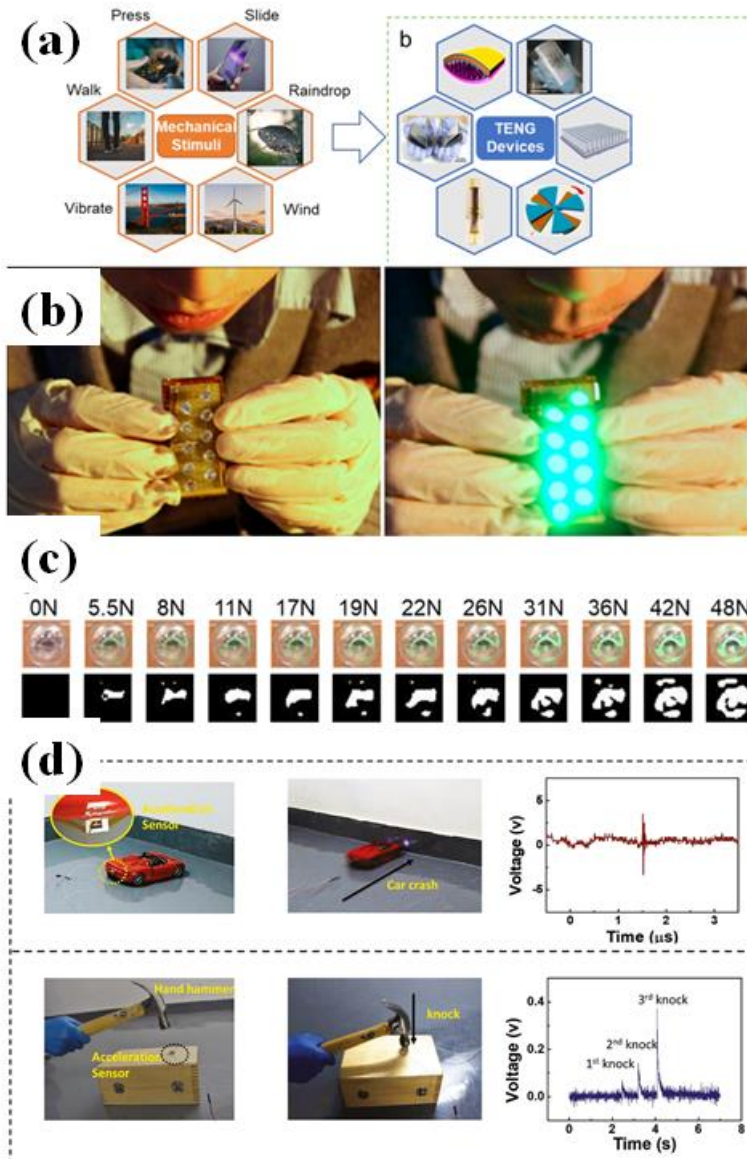
Figure 1-16 TENGs as self-powered active sensor. [192, 193]

(3) Power storage and management of TENGs

The inherent output characteristic of TENG leaded to the utilization of TENG output directly hindered a number of obstacles. Such as the impedance matching of different forms of TENGs with various electric devices, power mismatch between TENG output and devices. Therefore, numerous power management schemes have been deviated.[27, 28, 194, 195] In a usual strategy is to incorporate TENGs with a power management circuit, rectifier, or buck boast convertor. In some occasions mechanical energy would be converted to another form of energy though TENG.
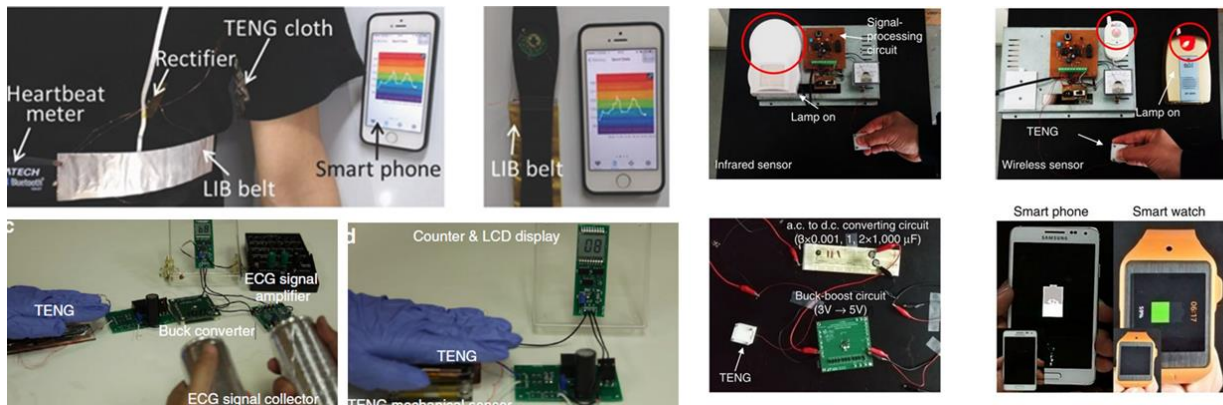
Figure 1-17 Examples of TENG applications ultizing power managment circuit.[22, 26, 182]

Chapter 2   Experimental techniques

The utilized experiment methods, and the equipment employed in this thesis will illustrated in this chapter. Crosslinking of polymer and various fabrication strategy will be discussed. Structural characterization, luminescence emission, electrical characterization, nitrogen sensing and concentration of solution measurement are conducted various instrument will also presented.

2.1 Device preparation

2.1.1.   Crosslinking of polymer chains

Crosslinking of polymer can be defined as binding of originally separate molecules permanently by chemical bonds. These chemical bonds either directly from one polymer chain to another such as C-C bonds, or indirectly through a short chemical chain as in S bonds in rubber vulcanization.[196]

Long chained polymer inherently resembles liquid regarding their viscosity. Generally, the viscoelastic properties they exhibited are based on their chemical structure, entanglement of polymer chains (chain mobility). However, once cross-linked, they will behave like solids and maintaining their shape against deformation. Thus, the mechanical behavior of cross-linked polymeric materials has been investigated by many researchers.

For instance, when cross-linked polymer is immersed in a particular solvent, the polymer absorb the liquid solvent until the swelling force associated with the mixing entropy between the

Wong Man Chung

chains and the solvent balances the elastic force of the chains between junction points. These cross-linked polymeric systems containing the solvent are called chemical gels.

2.1.2.   Spin coating

Spin coating is one of many standard procedures for fabricating thin film or micro-fabrication with thickness from few nanometers to micrometer thick film.[197] Generally, this fabrication method is relativity simple and the duration of the actual coating processing usually are not time consuming.

The fabrication process of spin coating basically required a fixed amount of coating material placed at the center of a substrate. Once the substrate started spinning, centripetal acceleration will cause these coating materials to spread out across the surfaces of the substrate. Although the majority of the coating material will eventually fall off from the substrate, on the other, a thin film will be coated relativity uniform on the surface of the substrate. This thickness of this film will be depended on a few factors, namely, spinning speed, viscosity of the coating material, surface tension between the coating surface and the coating material etc.
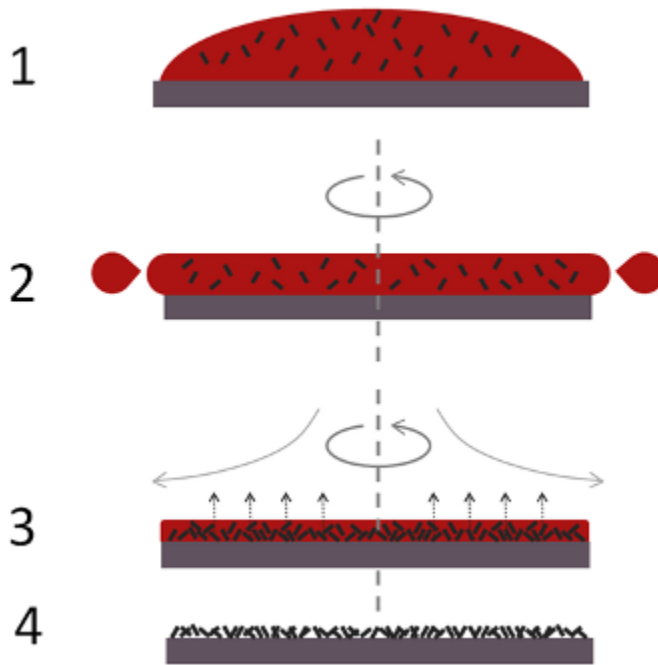
Figure 2-1 A typical spin coating process

Typical spin coating process, as depicted in **Figure** 2-1, consists of a few key steps. Firstly, after cleaning, wetting or plasma treatment of a substrate. The coating materials were dispensed onto the substrate. There are two typically ways to dispenses these coating materials, either a static dispenses, or dynamic dispense. A static dispense is the deposition of coating materials in the center of the substrate. Whereas a dynamic dispense is the dispensing the coating material when the substrate is turning at low speed. The coating material spread out over the surface uniformly then the spin speed ramped up. The optimal spin speed for the dynamic dispense spin coating is relatively high as compared with static spin coating. Also, the solvent containing the coating material have less time to evaporate before the actual spinning, furthermore, the ramp speed and

Wong Man Chung

the time of dispersion are less critical then their counterpart in during static dispersion. In both cases, a higher spin speeds and prolonged spin duration tend to fibrate a film with smaller thickness.

In case of a patterned substrate coating, the acceleration rate adapted a critical role.[197] The time to evaporate the solvent that aid the coating process can be determined by this rate. Moreover, the acceleration rate also governs the magnitude of twisting forces acted on the coating material, this twisting force aids the uniformity of the dispersion of the coating material onto the substrate surface.

2.1.3. 3-D printing

Additive manufacturing technique for fabricating structures with a wide range of complex geometries from 3-dimensional (3D) model data is known as 3D printing.[198]

The process of 3D printing generally based on printing succession layers of materials stacking on one other. Although powder bed fusion and fused deposition modeling can be regarded as a bottom up process, generally they are regarded as a variation of 3D printing. Currently, 3-D printing has been widely applied in different aspect of society, from hobbyists to industrial application. Although numerous research and business have been employing this novel technique. New applications are kept on emerging, such as the utilization of novel materials and additive manufacturing method are continuously being developed and exploited. In addition, the resolution and aspect ratio of the 3D printing reaches an unprecedented level, whereas the cost of 3D printer

has been significantly reduced. Thereby 3D printing process has been widely utilized in numerous applications.

Typically, a 3D printing process involved melting the feedstock (powder or wire) by an energy source such as laser, electron beam or heat. These molten materials are deposited layer by layer to form a continuous structure, they subsequently fused or bonded together either through temperature gradient or various methods, such that a solid was formed. In some cases, materials in the form of paste, sheet or inks can also be used for 3D printing.
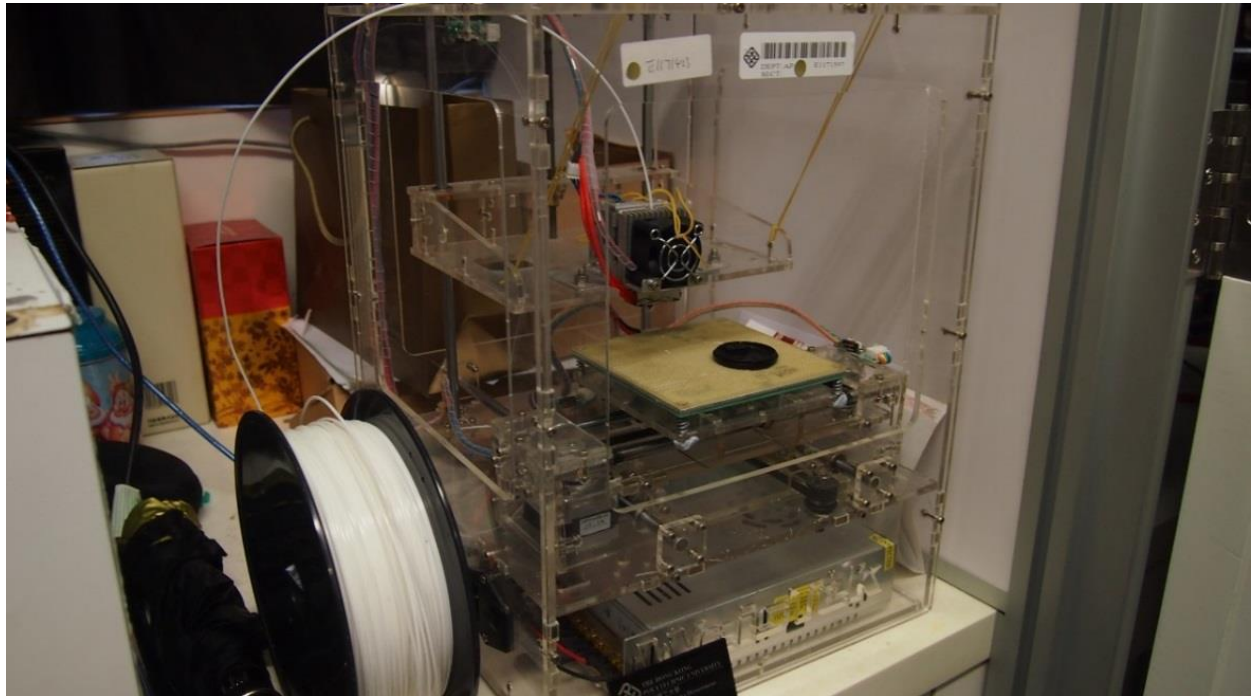
Figure 2-2 An in-house 3D printer used in this thesis

Recently, 3D printing had been applied to various fields, such as biomaterial for prototyping complex and customized tissues under patient -specific requirement. Although the

Wong Man Chung

number of choices of material available for the printing process are still limited.[199] On the other hand, aerospace industry utilized 3D printing for on-site application such as demand manufacturing or quick maintenance of aircraft. Although the precision of the part may still require refinement.[200] Nonetheless, the evolution of 3D printing in recent years has been phenomenal. The increased funding, research and development worldwide would result in a fast transition from traditional methods of manufacturing to 3D printing in the near future.

2.2. Characterization

2.2.1. Scanning electron microscopy

Scanning electron microscopy (SEM) is regarded as a standard tool to study the morphology of a sample. It focused a high energy electron beam onto the sample in order to gather a variety of information about the sample's such as, surface topography and composition.

Wong Man Chung

Figure 2-3 A typical scanning electron microscopy.

Electron gun (field emission guns or thermionic guns) produced electron beams upon the application of an ultra-high voltage, the produced electrons are further accelerated and directed towards the sample by a grid of anode. Before impacting with the sample, the electron beam will pass through a series of condensing lenses to focus and direct the beam into a more precious manner. As the high energy electrons impacted with the sample, various signals are generated though different kinds of interaction between electron and sample. These signals include but not limited to secondary electrons, backscattered electrons, characteristic X-ray, transmitted electrons

and photon, will be detected by the corresponding detectors to furnish image and information of the sample.

For instance, the generated secondary electron provides the morphology, while backscattered electrons generated from deeper penetration of these incident electron beams will provide chemical composition information of the sample. Atomic composition of the sample can be obtained through X-ray characteristic emission induced via inner shell electron bombardment with the canning samples.

It is generally difficult to analyze nonconductive material by SEM as SEM analyzation depend on electron interaction with the sample. However, layer of conducting material with thickness of 10 to 20 nm may be deposited onto the surface of these non-conducting material to enhance the emission of secondary electron and eliminating the surface of charging effect while the incident electron beam bombarding the non-conducting surface, results a more stable and refined morphology image.

2.2.2. Raman spectroscopy

Raman spectra is an analytical method to study molecular structure. It aims to obtain information concerning molecular vibration, rotation change via analyzing the variance between the incident light spectra and the scattering spectra.

Wong Man Chung

Its operation principle is based on quantum mechanics theory. As presented in **Figure** 2-4. It was based on the interaction between the electron cloud of a sample and the external electric field of the monochromatic light, which can create an induced dipole moment within the molecule based on its polarizability. Since the incident light does not excite the molecule itself, such that there can be no real transition between energy levels. The Raman effect therefore is not a photoluminescence emission, in many cases to a vibrationally excited state on the ground electronic state potential energy surface. According to the theory, elastic and inelastic collision may take place when a photon collided with molecules. When some of these collisions may be elastic such that there is no energy exchange during the collision, while during the inelastic collision, frequency of the scattered photon varies such that a shift in emission spectra of the excited light can be registered. This scattering is known as Raman scattering. If the frequency of the scattered photon increases, the scattering is called Stokes Raman scattering. If the corresponding frequency decreases, the scattering otherwise is known as anti-Stokes Raman scattering. The molecules, in accordance to the magnitude of energy change, also adopted a new rovibronic state. Thereby, by measuring the shift in this energy change. The characteristic value of the vibrational energy of the molecules can be obtained.

Wong Man Chung
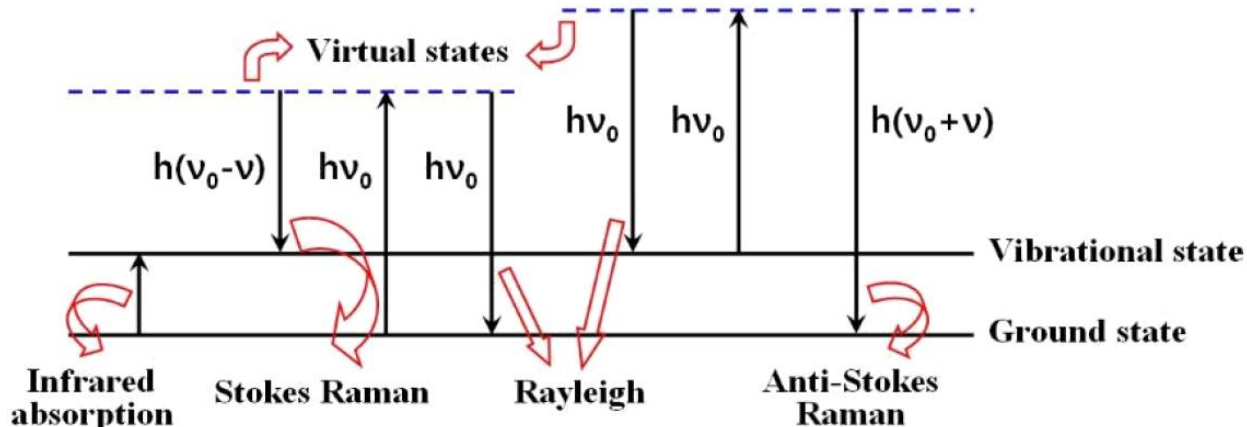
Figure 2-4 Raman scattering effect during Raman spectroscopy.

During the Raman spectroscopy measurement, a laser was irradiated onto the sample, energy exchange occurred, then a Raman spectrum is recorded with a grating spectrometer. The shift in energy and the recorded spectrum provide characteristic information concerning the vibration of the molecules.

2.2.3. Fourier transform infrared spectroscopy (FTIR)

FTIR is a technique generally for identification of molecular components, structure of various material. Its working principle is based on characteristic absorption of infrared radiation of different materials vary from one to other. Contrasts with Raman scattering, FTIR is the energy measurement based on molecules absorption on infrared light rather than the changes in the material electronic rovibronic state. During measurement, infrared light sources generates a specific part of the spectrum. The generated light beam was separated by beam splitter. A path

difference between these two beams is manifested after the beams through Michelson interferometer. The two separated beams were recombined again such that the intensity of the new beam change periodically. After the beam passes through a sample, the resultant signal is registered by a detector and the signal was analyzed by a common algorithm of the Fourier transform to obtain an infrared spectrum. Since each absorbed wavelength represents unique molecular or chemical structure, making FTIR become a great tool for chemical identification.
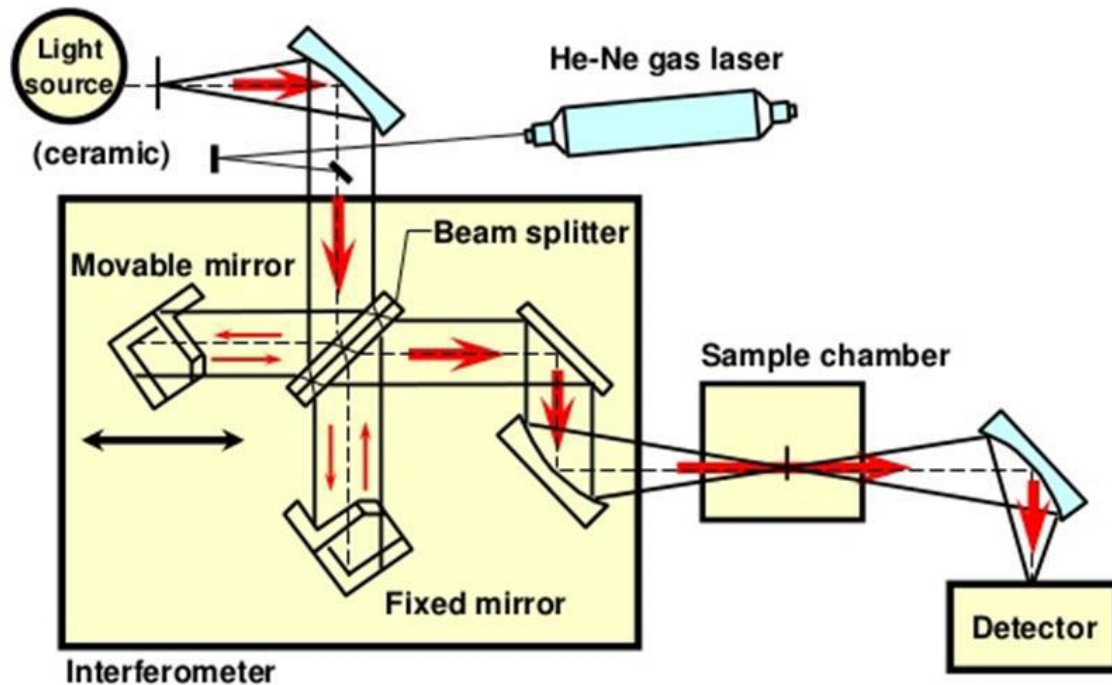
Figure 2-5 A schematic of a typical FTIR

Wong Man Chung

2.2.4. AC mechanical energy input system

In order to provide controllable and stable mechanical stimuli, two self-designed mechanical stimuli system were fabricated and applied during measurement.

The first one is a magnetic field inducted stress system which can generate a magnetic field strength of 3.5 kOe with 400 Hz. Through magnetic attraction, sample which is magneto-responsive will be under stress. Such that, high frequency sinusoidal mechanical energy can be applied to a sample.

(ii)

PWM based modulator

(i)

Power source

(iii)
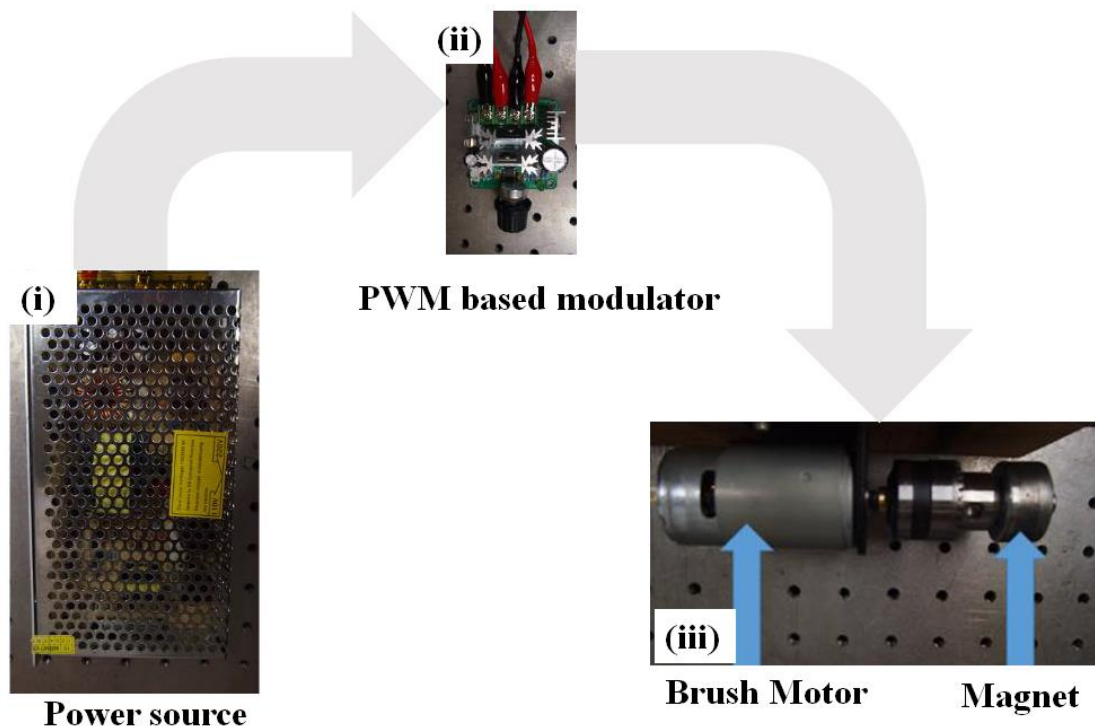
Brush Motor   **Magnet**

Figure 2-6 Homemade stress application system with various temporal of mechanical excitation.

The stress system consists of 4 main parts: (i) a high speed brush motor, which is used to rotation of a magnet; (ii) a NdFeB axial magnetized magnet with the remanence of 0.6 T; (iii) a PWM modulator to control the RPM of the motor from 0 to 22000 and a couple of carjacks to adjust the distance of the composites from the magnet which determine the magnitude of stress.

The second system for providing mechanical stimuli on a sample perpendicular to the sample surface is compose of a linear motor.

2.2.5.　Electric output characterization

Mechanical energy conversion through TENG is mainly measured by an oscilloscope. Oscilloscope is an irreplaceable tool utilized by researchers, engineers, technicians, students and hobbyists to design, debug, deploy and repair electronic designs. The most basic level oscilloscope allows users to visualize the behavior of a signal by displaying its voltage over a time period. Oscilloscopes are also commonly used to detect glitches and noise in a signal.

A digital storage oscilloscope read a voltage on an input channel, and then amplify the signal, after various mathematics modulation based on measurement requirement. The signal will finally covert with an Analog-to-Digital Converter (ADC). The ADC samples the voltage into an n-bit (n depends on the memory of each scope) sample taken every t s. These samples are stored in the scopes memory and then displayed on the screen.

Wong Man Chung
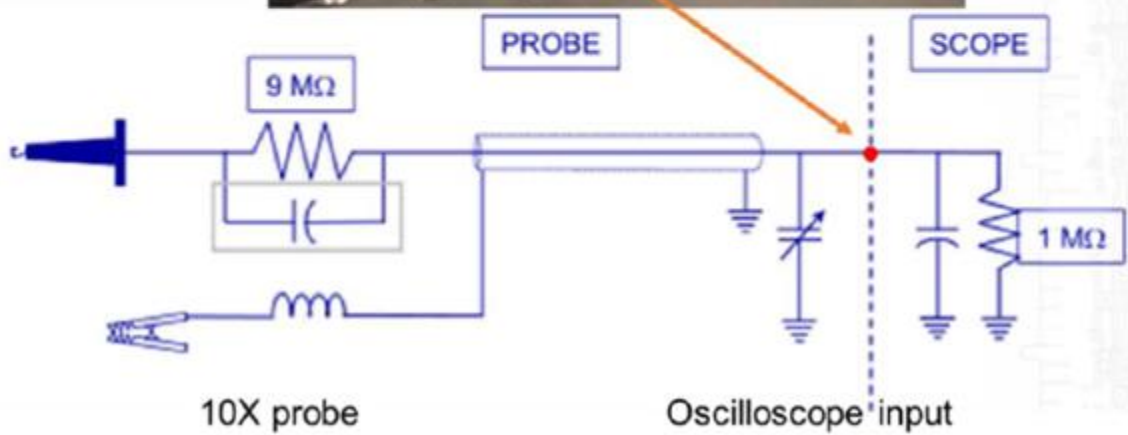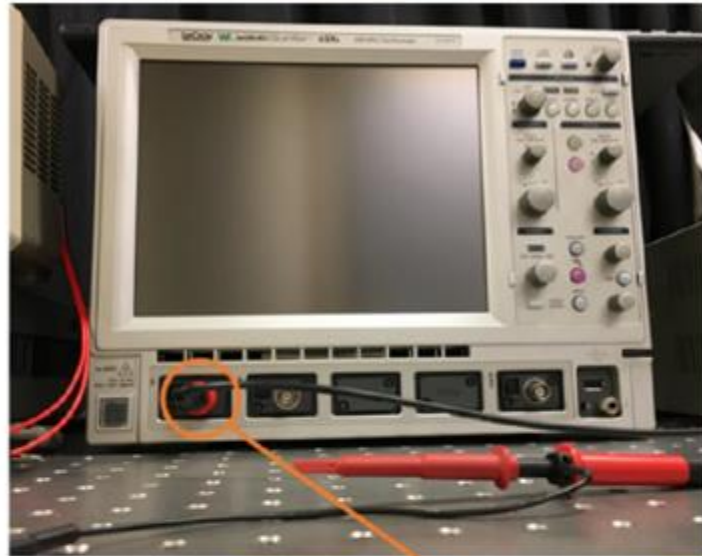
Figure 2-7 DSO and high impedance probe employed in this study.

Although more functions were imported to these digital storage oscilloscopes, there are few key performance characteristics that determine what types of signals can be captured by the scope and the associated probes. Firstly, the Bandwidth of a digital storage oscilloscope describes the frequency range of the oscilloscope (in Megahertz MHz) where the sampled signal's amplitude

will be attenuated to -3 dB of its original value. Signal attenuation describes a reduction in the strength of a signal during transmission. Thus, a signal that was transmitted with 1V peak-to-peak amplitude at 100MHz would be received at 0.7V peak-to-peak amplitude on a 100MHz scope. The other key factor is risetime, if the rise time of a scope is slower than the signal rise time, the scope will show a false positive that cause device under test. The sample rate of a digital scopes also adapted a key role in performance characteristic. Between each sample taken by the scope, an interpolated data is not actually present, it is a mathematical make up. Therefore, the higher the sampling rate, the more samples are recorded, and the fewer points are interpolated, and the more faithful the signal will be to its original.

2.3. Optical spectroscopy

Various instruments in this study had been utilized to investigate the luminescence properties, here a brief introduction discussing these apparatuses.

2.3.1. Spectrometer

A charge coupled device spectrometer from Ocean optics with fixed well depth associated with each photodetector. Generally, a spectrometer is an apparatus to measure an optical emission spectrum. The spectrum is recorded through the following steps, firstly, the detection process is to guiding light through a fiber optic cable into the spectrometer through a narrow aperture known as an entrance slit. The slit vignettes the light to enter the spectrometer. In most spectrometers, the

divergent light is then collimated by a concave mirror and directed onto a grating. The grating disperses the spectral components of the light at slightly varying angles, which is then focused by a second concave mirror onto the detector.
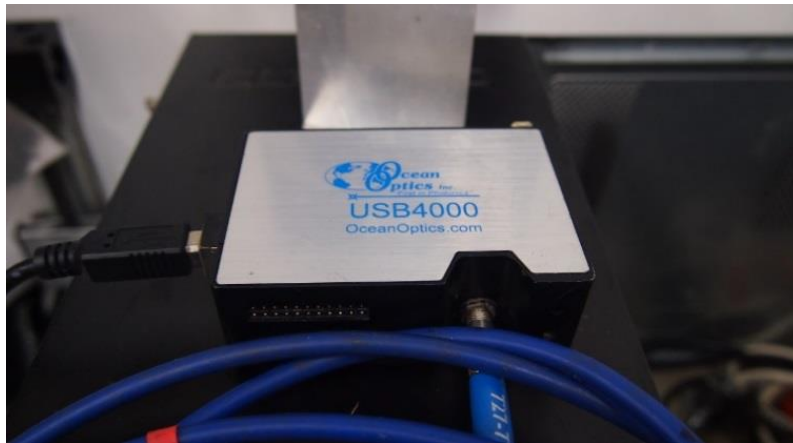
Figure 2-8 A typical spectrometer, Ocean optics USB 4000, for recording emission spectrum.

Photon is then coupled and electron are generated by a CCD, the electrons which are digitized and through the software in the then interpolates the signal based on the number of pixels in the detector and the linear dispersion of the diffraction grating to create a calibration that enables the data to be demonstrated as a function of wavelength over the given spectral range.

2.3.2. Spectroradiometer

A spectroradiometer is designed to includes photometric and calorimetric measurements. However, other measurement such as source spectral power distribution, dominant wavelength

and correlated color temperature can also be registered. The essential components of a spectroradiometer consists of input optics, a monochromator and a detector. Firstly, input optics gather electromagnetic radiation from the luminescence sources. Then the monochromator separating light into its component wavelengths, the detector then converts the incoming photon into electric signal and transfer to a control and logging system to define data.

The design of Spectroradiometer includes spectrally based photometric and calorimetric measurements, source spectral power distribution, dominant wavelength and correlated color temperature quick and simple. The measurement can be a cosine receptor for irradiance/ illuminance. Spectroradiometer consist input optics that gather the electromagnetic radiation from the source, a monochromator separating light into its component wavelengths and a detector, and a control and logging system to define data and store it.

Figure 2-9 A spectroradiometer for color temperature and CIE coordinates measurement.

Wong Man Chung

Chapter 3   Tuning of piezophotonic emission spectrum via modulation of mechanical stimuli frequency

3.1. Introduction

Phosphors have been extensively investigated because of their wide range of applications in display, solid state lighting, sensor, and bioimaging.[45, 78, 85, 201-206] For these applications, it is desirable for the luminescence to be tunable in terms of the luminescent intensity and wavelength. Tuning of luminescence properties previously had been focused on modification of the phosphor, such as changing the phosphors chemical composition, crystal structure, phases, lattice morphology or surface group, etc.[45, 86, 207, 208] However, these changes are essentially ex-situ and irreversible. An *in situ* and dynamic modification of emission wavelength or color gamut has rarely been reported. Recently, a full color tuning through non-steady state upconversion photoluminescence was realized. This tuning is based on the modulation of pulse width between the laser interaction and the samples.[209] The emission properties from a multiphase core shell nanocrystal is controlled by varying the photo-excitation frequency and excitation wavelengths. However, the nanocrystal processed a core shell structures that posed a relative challenge in fabrication of these nanocrystal. The specific excitation wavelength and excitation duration also limited the spectrum of applications. Furthermore, there had been a limited work that demonstrated both luminescence intensity and color gamut can be remotely modified. which hinder the development and understanding of various phosphor's properties. Therefore, in

recent decade, numerous pioneering works have manifested development of piezophosphors.[76, 78, 83, 85, 201]. For instance, a metal-ions doped ZnS wurtzite phosphors, as one of the archetypical piezophosphors, has been investigate extensively. Based on these studies, the origin of its piezoluminescence can be attributed to the doped ZnS wurtzite phosphors crystal structure. Upon a mechanical energy stimulus, a piezoelectric potential will be generated within the crystal lattice of the phosphor. This piezoelectric potential will excite these charge carriers in the piezophosphors, thereafter, the relaxation of these charge carriers generates photon. Previously, magnetic-induced luminescence (MIL) based on piezoluminescence was realized.[58] It is a piezophotonic luminescence emission remotely triggered by a weak magnetic field excitation. The corresponding emission intensity can be modulated by magnitude and frequency of magnetic stimuli in a non-contact, reversible and dynamical manner. Based on this interesting work, a novel strategy is devised to realize an *in-situ* exquisite control over the emission wavelength of the piezophosphors. Generally, this strategy is based on modulating the frequency of mechanical excitation exerted onto the piezophosphors, incorporating the properties of mechanical responses' piezophosphor such that, charge traps at a shallower trap levels were excited, thereby the emission peak of the luminescence was shifted. After the realization of such intriguing tuning of piezoluminescence, an investigation concerning the mechanism of this real time tuning of the piezoluminescence was conducted. It is ascribed to the properties of tilting energy band of the piezophosphors under high frequency of mechanical energy stimulation. Furthermore, some proof

Wong Man Chung

Tuning of piezophotonic emission spectrum via modulation
of mechanical stimuli frequency
THE HONG KONG POLYTECHNIC UNIVERSITY

of concept devices, for instance red green blue full-color displays and tunable white-light sources are demonstrated simply by frequency modulation.

3.2. Sample fabrication

(1) The preparation of color-tunable piezoluminescence composites:

Metals-ion-doped ZnS microparticles with average size of 23 μm (Global Tungsten & Powders) were homogeneously mixed into a PDMS matrix. With the ratio of phosphor material to PDMS was maintained at 7:3. The cured PDMS composites (5 mm in length and 1 mm in diameter) were embedded into magnetic elastomer (2 mm in length and 1 mm in diameter) consisted of soft ferromagnetic microparticle (Fe–Co–Ni alloy particles of average size of 100 μm) uncured PDMS in weight ratio 2.5:1. The samples were cured at 120 °C for 45 min.

(2) Fabrication of the Phosphor Possessing RGB emission ability and tunable White piezoluminescence composite: The red-colored Hong Kong Polytechnic University logo was patterned by screen printing (thickness 200 μm) the (SrS, CaS):Eu phosphor paste onto the top of a ZnS:Cu-based piezoluminescence composite. The other format, namely rod based RGB piezoluminescence emission consists of the a ZnS: Cu , SrS,CaS :Eu phosphor coated ZnS: Cu as red element composite rods, and ZnS: Al,Cu as blue composite elements. each with a diameter of 1 mm and a depth of 5 mm. Such that the piezoluminescence red green blue composite consisted of 16 composite rods, all of them is capped with the magnetic elastomer. For the element of white

Wong Man Chung

tunable white MIL composite was fabricated via homogenous mixing of YAG:Ce phosphor with ZnS:Al, Cu piezophosphor. Inside a PDMS matrix to form the tunable white MIL composite.

3.3. Mechanism of *in-situ* tuning of piezophotonic emission spectrum

In order to formulate the mechanism beneath the *in-situ* modulation of piezoluminescence emission wavelength, a brief discussion of the piezophosphors doping will be introduced as follows.

Generally, specific metal ions such as aluminum and copper were doped into the host lattice of the ZnS piezophosphor. A nonequivalent charges substitution will thereby occur, such that various kinds of defects will present inside the phosphor lattices. These defects will generate different types of luminescent centers and based on the types of luminescent centers; different wavelengths were therefore emitted. Typically, for sulfide ions in the ZnS, Frenkel type defect will generate sulfide vacancies. an additional shallow donor state will exist below the conduction band. In the meantime, the metal ions doped into the ZnS host will create different types of charge traps inside the band gap of ZnS. For instance, for aluminum ions (Al^{3+}) related defect, Al^{3+}ions will occupied a zinc (Zn^{2+}) site, regarded as Al_{Zn}. These nonequivalent charges substitution will create a trapping centers for electrons. On the other hand, when copper ion (Cu^+) occupied a zinc site, $Cu_{Zn,}$ the site will carry a negative charge, thereby created an additional hole trap below the valence band of the ZnS host. These charge traps in different energy levels are bounded together by

Wong Man Chung

Coulomb interaction to form various luminescent centers in the form of donor–acceptor (D–A) pairs with discrete spatial intrapair separation (r). The separation between a Sulphur vacancy and the copper ion occupied zinc site, and that of between aluminum occupied zinc and copper occupied zinc site is depended solely on the radius of the dopant ions and the lattice structure of the host crystalline. According to literature, the spatial intra-separation r of Vs-Cu_{Zn} and Al_{Zn}-Cu_{Zn} pairs can be expressed as r_1 and r_2 respectively, with $r_1 < r_2$.[210] Therefore, from coulomb laws of attraction, the emitted photon energy and the intra-pair separation can be expressed as:

$$E(r) = E_g - (E_A + E_D) + \frac{q^2}{4\pi\varepsilon_r r} \tag{1}$$

where E_g is the energy bandgap, E_A and E_D represent the trap depth of acceptor and donor, respectively, q is the electron charge, and ε_r is the permittivity of phosphors.

To trigger luminescence, mechanical energy was applied into the piezophosphors in the form of an induced magnetostrictive strain. The general formula relating the magnetic field (H) applied to the piezophosphors, with the magnetostrictive coefficient (λ) and the induced magnetostrictive strain (ε) generated are related to each other can be as,

$$\lambda = \frac{\partial\varepsilon}{\partial H} \tag{2}$$

This strain will induce a piezoelectric potential inside the phosphor crystal, the electrostatic energy of an electron inside a charge trap of the crystal is increased and can be expressed as

Wong Man Chung

$$\Delta E = \frac{1}{k} \left(\frac{\lambda q H d_0}{\varepsilon_r} \right)^2 \tag{3}$$

where d_0 is the local piezoelectric constant, k is the force constant of host lattice.

The piezophotonic emission is essentially required the piezophosphors to be under a dynamic mechanical energy changes rather than a static mechanical stimuli, therefore, the relationship between the change rate of the electrostatic energy of an electron inside a charge trap and the applied mechanical excitation, (in this case magnetic excitation) is written as:

$$\frac{\partial E}{\partial t} = \frac{2H\dot{H}}{k} \left(\frac{\lambda q H d_0}{\varepsilon_r} \right)^2 \tag{4}$$

where $\dot{H} = \frac{\partial H}{\partial t}$ is the change rate of magnetic field, which is related to the strain change rate acting on to the sample.

Moreover, arise from the piezoelectric properties of the phosphor, the induced strain would change the trap depth of the charge trap inside the crystalline,

$$E_D = E_{Di} - \frac{2H\dot{H}}{k} \left(\frac{\lambda q H d_0}{\varepsilon_r} \right)^2 t \tag{5}$$

E_{Di} is the initial trap depth.

Based on the above equation, the tuning of piezophotonic emission spectrum via modulating the frequency of mechanical energy input can be interpreted as the followings. When a mechanical stress was applied onto the ZnS piezophosphors, the energy band of the ZnS was

Wong Man Chung

tilted and the detrapping of electrons in the donor states takes places. Photon is emitted upon these electrons are recombined with holes in various types of charge trap afterwards. Under low frequency mechanical stimulus, owning to the titling of the energy band is limited under a fixed amount of induced strain, thereby only the deep charge traps in Al_{Zn} site are excited. The charge carriers in the deeper charge traps can therefore be excited and reaches the conduction band, emission in this case is peaked at 503 nm, which is the characteristic emission of the Al_{Zn}-Vs recombination. Upon the frequency of the mechanical energy stimuli increases further. Although the magnitude of the mechanical energy stimuli remain the same, the mechanical hysteresis of the piezophosphors in such a high frequency of stimulation will results a remnant strain in the crystal lattice, such that the slope of the energy band titling steepens and the charge carrier inside these shallower charge traps are excited. The emission intensity of this shallow charge traps therefore increases, aforementioned, the intra-spatial separation between a deep charge traps are relatively larger than that of shallow charge traps. Therefore, for a deep charge traps pairs, the corresponding wave functions describing this charge trap have a relatively small overlapping, results in a saturation of emission intensity under high frequency mechanical energy excitation. On the contrary, as shallow charge traps have a smaller intra-spatial separation, implicates a high electron hole recombination rate. Therefore, the green emission intensity saturates as the excitation frequency increases, while blue emission will subsequently dominate in the luminescence spectrum, as shown in **Figure** 3-1. It should be notice that the assignment of the 503 nm emission to the Al_{Zn}-V$_S$ recombination arises from the following. Firstly, in literatures reported earlier

Wong Man Chung

concerning the electroluminescence of this phosphor. [89, 211-213] The emission of various luminescence center/pair have been well classified and documented. It is well known that electroluminescence is closely related to the emission properties of mechanoluminescence. Therefore, it is reasonable to assign the emissions to Al_{Zn}- Cu_{Zn} luminescence pair. Secondly, the dependent of various emission wavelengths from Zinc Sulphur phosphor can be examined through the doping of different dopants into the same host material. Investigation results suggested that a green emission generally arises from copper ions related defects. And a Sulphur vacancy related defect will emit a blueish photon.
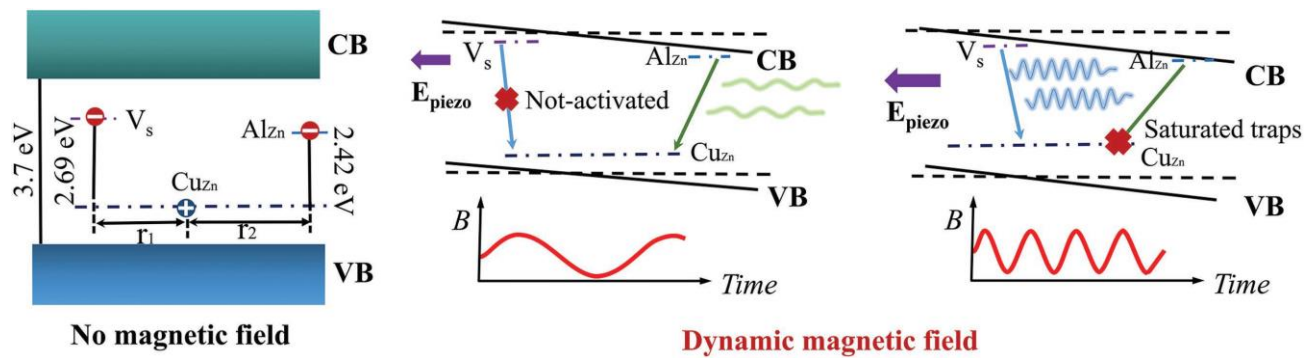
Figure 3-1 Schematic illustration of the mechanism responsible for temporal color tuning of piezoluminescence emission in ZnS: Al, Cu piezophosphor by modulation of mechanical excitation frequencies.

3.4. Demonstration of the tuning of piezophotonic spectrum emission

To realize the temporal and remote tuning of piezophotonic luminescence wavelength and color gamut, a composite capable of the tuning were fabricated and various experiments were conducted to examine, and the mechanism discussed in the previous sections.
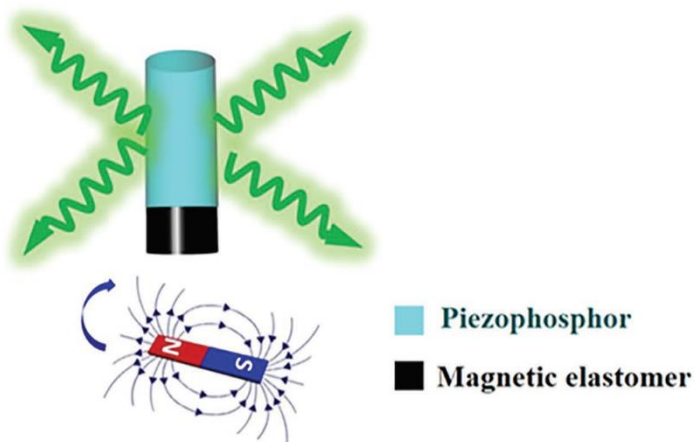
Figure 3-2 Schematic illustration of ZnS composite doped with metal ions (e.g., Al, Cu) when excited by a modulated mechanical energy via magnetic field.

The composite was designed as a laminated structure with two phases with two phases connected with poly(dimethylsiloxane) (PDMS). PDMS was also chosen as polymer matrix for its optimized Youngs modulus such that the strain induced in the magneto-responsive phase can effectivity induced a strain upon piezophosphor to stimulate piezophotonic emission. To be precise, The magneto-responsive phase was composed of a micro-sized ferromagnetic particles embedded

into PDMS, such that it will generate magnetostrictive strain when it is stimulated by an external magnetic field. The generated strain was transferred to the other phases of the composite, where mico-sized piezophosphors are embedded inside PDMS, as shown in **Figure** 3-2.

3.4.1. Shifting of emission wavelength under different frequency of mechanical stimuli

During the measurement process, mechanical stimuli in the form of magnetic field was acted on to the composite. Such that mechanical strain generated from the magneto-responsive phase was applied to the piezophosphors. Based on experiment conducted, the strain generated from the magneto-responsive phase changes monotonically with the magnetic field strength. The magnetic phase of the composite has a low coercive field (9 Oe), therefore, it is reasonable to assumed that the strain rate induced on to the piezophosphors various in accordance with the frequency of the mechanical stimuli. The emission spectra of the piezophosphors under different frequency of mechanical excitation are shown in **Figure** 3-3,
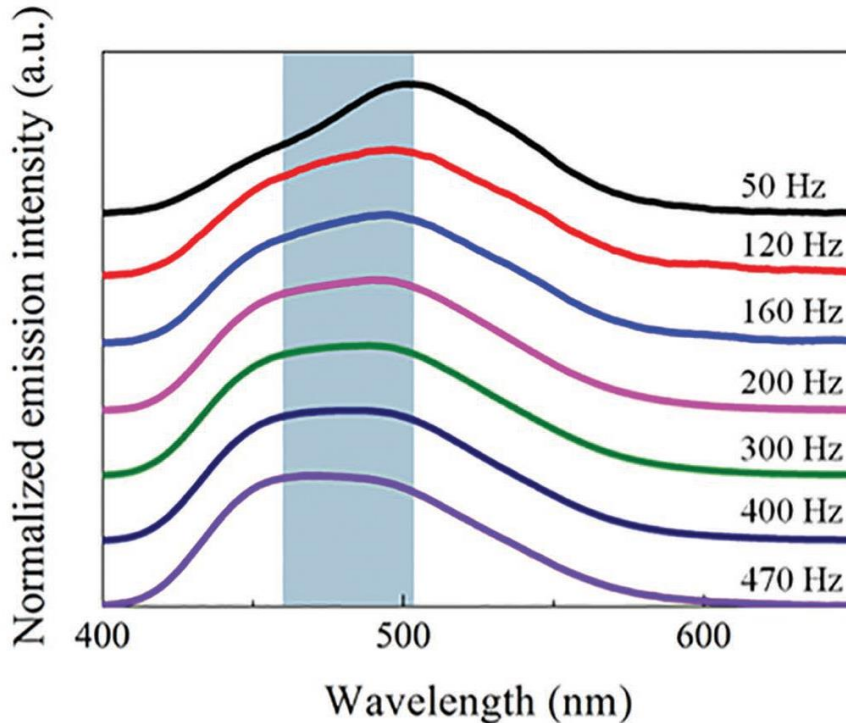
Figure 3-3 Normalized emission intensity of the composite under various frequencies of mechanical excitation, showing the emission wavelength tuning

In figure 3-3, the piezophotonic emission spectrums from the same composite under different frequencies of mechanical excitation were shown. From the figure, it can be observed as the mechanical excitation frequencies were set at no higher than of 50 Hz, the composite produces a dominant green emission band peaked at around 503 nm. As the excitation frequencies increases when maintaining the magnitude of excitation constant. The emission spectrum shown a relative increase in intensity at the shoulder peak of 460 to 472 nm, when the 503 nm emission intensity started to decline simultaneously. Upon further increased the excitation frequencies, the emission

Wong Man Chung

from the composites shown a trend of intensity increase in the shoulder peak at a range from 460 to 472 nm of blue emission band. The emission intensity of 460 to 472 nm become dominant as the frequency of excitation increased further when the suppression of emission intensity at 503 nm continued. Hence, a dynamic and *in situ* control over the piezophotonic emission wavelength by adjusting the excitation frequency of the mechanical energy stimuli alone was therefore achieved.

In addition, the change of emission intensity of the piezophosphor was in accordance with mechanical excitation frequency. **Figure** 3-4 shows the integrated intensities of the emission as the function of the mechanical excitation frequency. It can be observed that, initially the emission intensity increases with the frequency of mechanical stimuli. The intensity of the emission increases monotonically up to around 300 Hz, where the emission intensity reaches its maximum. Afterwards, the intensity of the piezoluminescence emission from the composite declined readily as the frequency increased further.

Wong Man Chung

Tuning of piezophotonic emission spectrum via modulation
of mechanical stimuli frequency
THE HONG KONG POLYTECHNIC UNIVERSITY
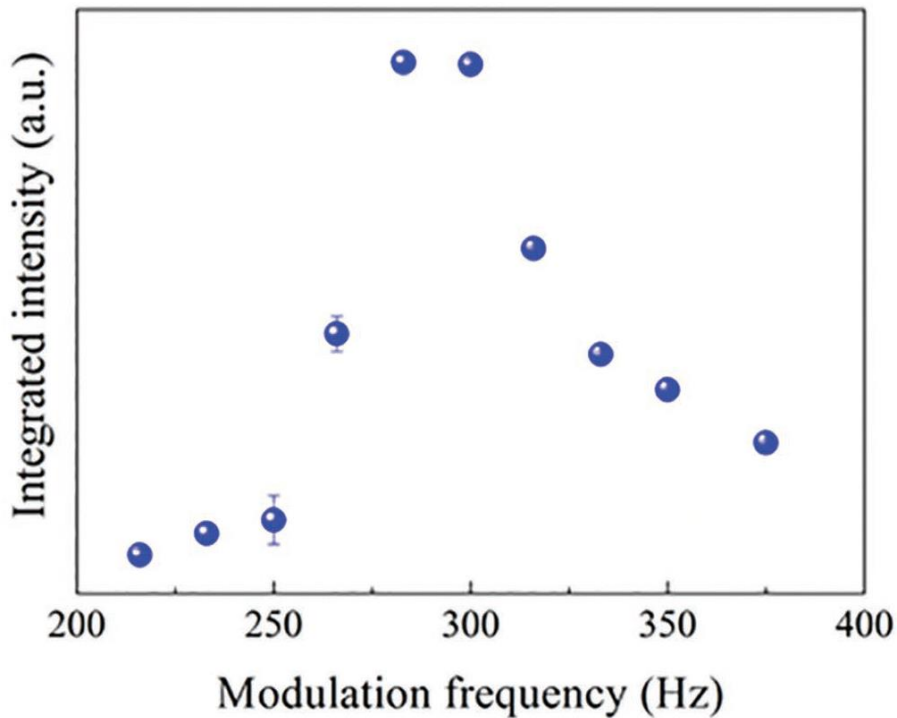
Figure 3-4 Integrated emission intensity as a function of the modulation frequency of the mechanical excitation at a fixed strength.

To visualize the excitation frequency-modulated color and intensity from the piezophotonic emission. **Figure** 3-5 illustrates the photographs presenting the emission color varied with the frequency changes. It can be observed the change in color from the composite from green to blue. The intensity from the composite also varies with mechanical excitation frequencies. The change in intensities were suspected to be arises from the mechanical hysteresis from the

Wong Man Chung

composite. During high frequency excitation (> 300 Hz), the emission from a portion of the piezophosphors in the piezophotonic phase of the composite reduced significantly, the phenomena may be attributed to the mechanical hysteresis from the composites. Since the portion of the piezophotonic phase that the emission became diminished remained identical and independent of the frequencies, while the shift of color coordinates from composites was n the The color coordinates, peak wavelength and luminance of the emission of the composite as it is under different mechanical excitation frequency are summarized as shown in **Table** 2.
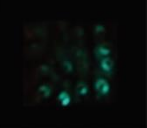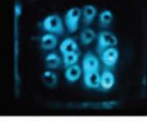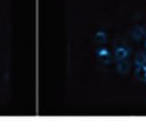
Frequency	50 Hz	80 Hz	120 Hz	160 Hz
MIL peak	503 nm	499 nm	498 nm	496 nm

200 Hz	250 Hz	300 Hz	400 Hz	470 Hz
490 nm	488 nm	479 nm	475 nm	472 nm

Figure 3-5 Photographs showing from green to blue color variation of the sample by changing the modulation frequency of the mechanical excitation.

Wong Man Chung

Frequency of excitation [Hz]	CIE (x,y)	Peak wavelength [nm]	Luminance [cd m^{-2}]
80	(0.2129,0.3470)	503	24
120	(0.1975,0.2996)	496	30
160	(0.2216,0.2679)	494	59
200	(0.2252,0.2279)	489	82
300	(0.1841,0.2239)	488	166
400	(0.1802,0.2266)	479	64
470	(0.1627,0.2108)	472	47

Table 2 CIE coordinates, emission peak wavelength, and corresponding light intensity of ZnS: Al, Cu under different modulating frequency of mechanical excitation.

3.4.2. Time dependent luminescence profile of the tunable piezophotonic emission

To investigate the blue and green components of the piezophotonic emission, the two characteristic emission wavelengths (472 and 503 nm) of the two luminescence center (Vs-Cu$_{Zn}$ and Al$_{Zn}$-Cu$_{Zn}$ respectively) in the ZnS:Al, Cu piezophosphor were studied. In the experiment, a sinusoidal mechanical excitation with constant root mean squared magnitude were applied to these

Wong Man Chung

piezophosphors. The transient characteristic emission from of the two wavelengths under different excitation frequencies is shown in the **Figure** 3-6.
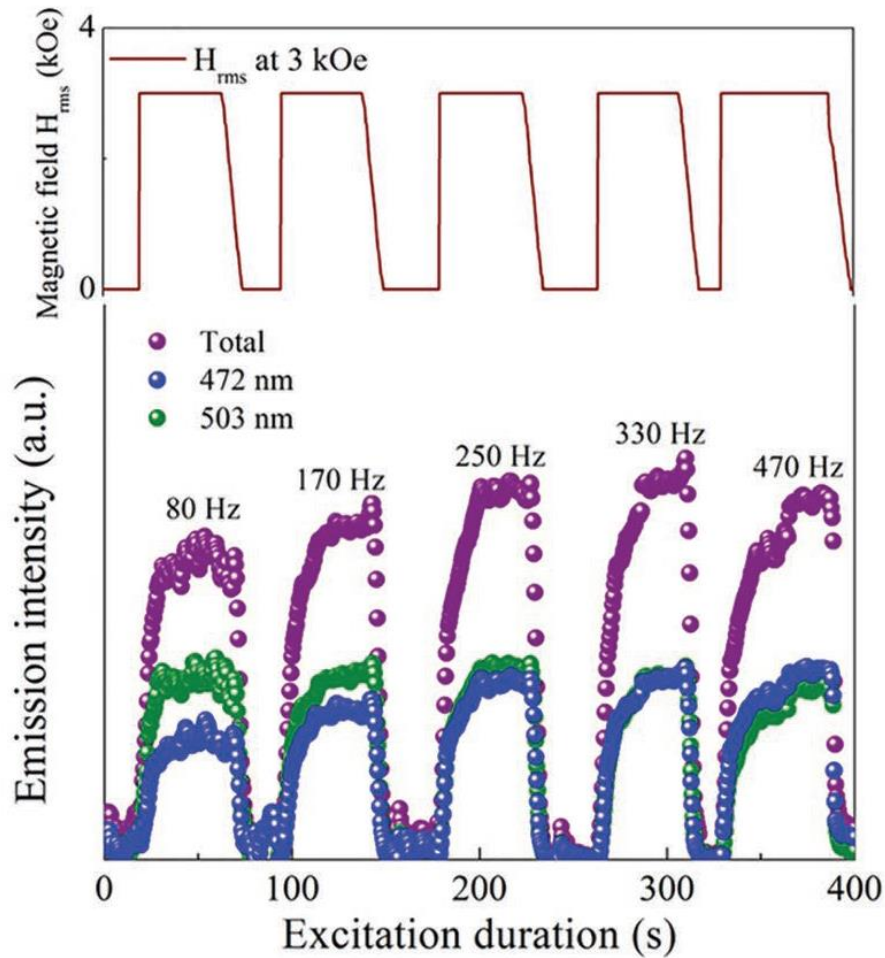
Figure 3-6 Time dependent luminescence profiles of ZnS:Al, Cu emitting at 472 and 503 nm under a sinusoidal mechanical excitation with various frequencies.

Wong Man Chung

During the investigation, the excitation frequencies were remained constant until the two wavelengths increased into saturated values. The summation of the intensities of each wavelength under various frequency were attributed to the total intensity. These three intensities then begin to fall toward zero as the mechanical excitation switch off. From the figure, it can be observed that the magnitude of the saturation value for each wavelength under different excitation frequency changes. the emission from the $Vs-Cu_{Zn}$ is more intense at low modulation frequency, while the emission in blue color region (the $Al_{Zn}-Cu_{Zn}$ pair) is gradually enhanced under a high modulation frequency.
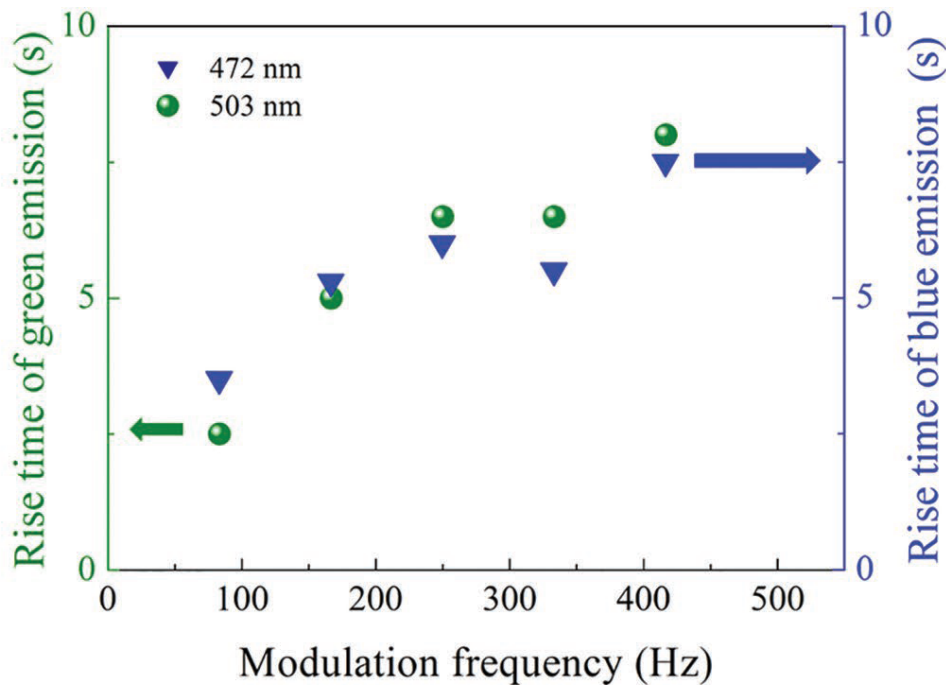
Figure 3-7 The rise time of 472 and 503 nm emission under different excitation modulating frequency.

In **Figure** 3-7, the changes in rise times for these two-characteristic wavelengths under different mechanical excitation frequency were demonstrated. In this context, the rise time is defined as the time duration for the emission intensity reaches its saturation magnitude in response to certain excitation frequency. **Figure** 3-8 shown that the rise time for both characteristic emission prolonged with the accretion of excitation frequency. That may imply the mechanical responsiveness of the piezophosphors under relative high frequency of excitation played a hemogenic role for the shift of spectrum of the piezoluminescence emission.
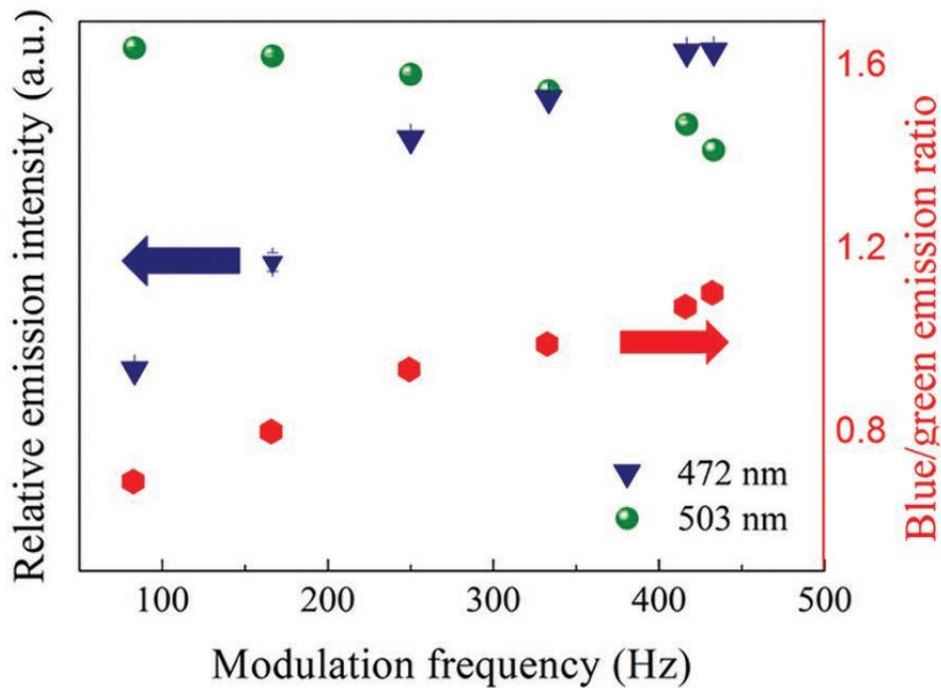
Figure 3-8 The relative emission intensity at 472 and 503 nm as a function of excitation frequency.

Figure 3-8 illustrate this change in emission intensity from the composite, it can be solely adjusted by excitation frequency. Moreover, the 472 nm emission intensity increases while 503 nm decreases with the increment of the mechanical excitation. Initially, the 503 nm emission is relativity more intense than the 472 nm in low excitation frequency regime. As this frequency increase further, 472 nm emission intensity eventually overtakes the declining emission intensity of 503 nm. The ratio of the two emissions intensity thereby also increase homogenously, implicating the color of the ZnS: Al, Cu piezophosphors can be solely, reversely modulate by changing the mechanical excitation frequency. It can be observed that the emission intensities of

Wong Man Chung

472 nm and 503 nm respectively increases and decreases with the increasing frequency. The reason behind the rise times of different emission wavelength changes is attributed to the frequency of the mechanical stimuli. Firstly, at a low-frequency regime, only deep charge traps inside the energy band gap can be excited. With a limited shallow charge trap being exited, and the probability of their excitation is relatively low. Therefore, the rise times for both 472 nm and 503 nm were limited. As the stimulation frequency increases, the energy band titled at a slope that it is more favorable for these shallow charge traps to be excited and excited simultaneously, the emission from these shallow charge traps become dominated. Therefore, it results a decrease in the rise time related to that deep charge trap as compared with the 503 nm emission.

Wong Man Chung

Traditionally, the emission intensity can be controlled via the magnitude of the mechanical stimuli. In a piezoluminescence context, there is a quadratic relationship between the intensity of emission, and the magnitude of the mechanical stimuli, as shown in **Figure** 3-9.
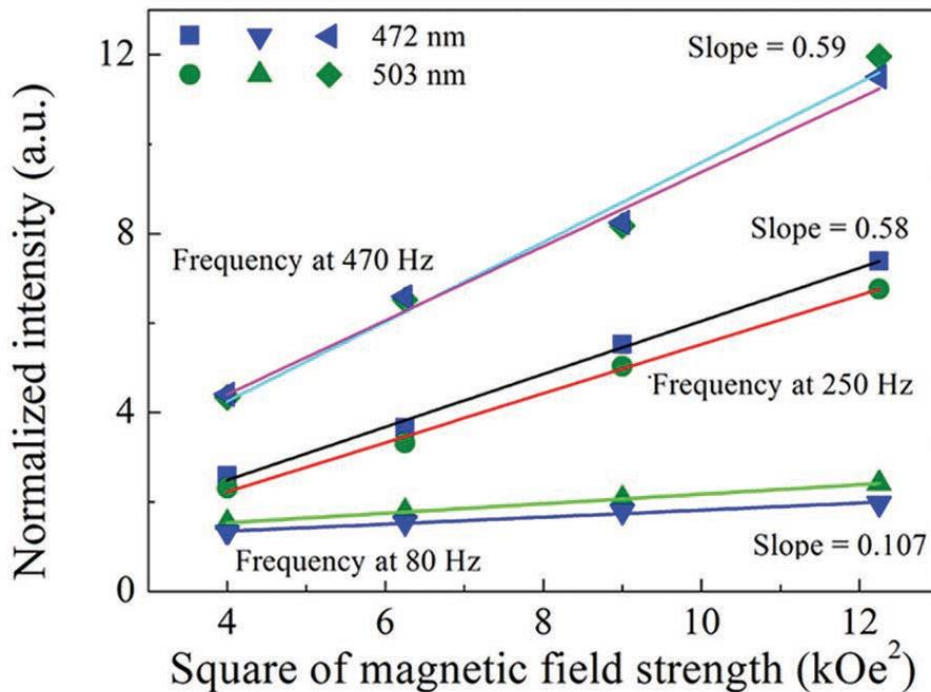
Figure 3-9 Emission intensity at 472 and 503 nm as a function of the square of the strength of mechanical excitation and the corresponding linear fittings.

In this measurement, the generated magnetostrictive strain from the magnetic elastomer phase of the composite varies linearly with the applied magnetic field. Therefore, the

piezoluminescence intensities of the two wavelengths change linearly with the square of the magnetic field applied to the composite. Moreover, the emission intensities of both blue and green components enhanced linearly with the increases of magnetic field in the same rate. This implicate there are no hypochromic shift with and only with enhancing mechanical stimuli. The shift can only be realized with changing the mechanical excitation frequency. Furthermore, a reliable linear relationship between the excitation strength and the output intensity can be observed as shown in **Figure** 3-9. Such reliable relationship is pragmatic for sensing application. These obtained results demonstrated the composite have a prominence potential to be utilized in mechanical-optical sensors which are capable of detecting a magnetic field with a wide range of frequency.

3.5. Piezophotonic emission full-color display

The *in-situ* color tunability though changing the excitation frequency provides a convenient approach to implement a full-color display. In addition, achieving a real-time modulation of color temperature of white color emission via reversible real-time physical approach has been attracting much attention for both fundamental research and numerous applications in recent year. Therefore, as a proof of concept, the piezophosphors based composite combined with other fluorescence phosphors to achieve a real-time tunable white light and a multicolor display. The mechanism is that through modulating the temporal of the mechanical excitation via changing the frequency of the magnetic field, such that the emission wavelength of the piezoluminescence can be modulated. Through this change in emission wavelength, the fluorescence emissions from various fluorescence phosphor excited by the piezoluminescence can also be controlled, thereby an RGB display and white color with tunable color temperature were materialized (summarized in **Figure 3-10**).
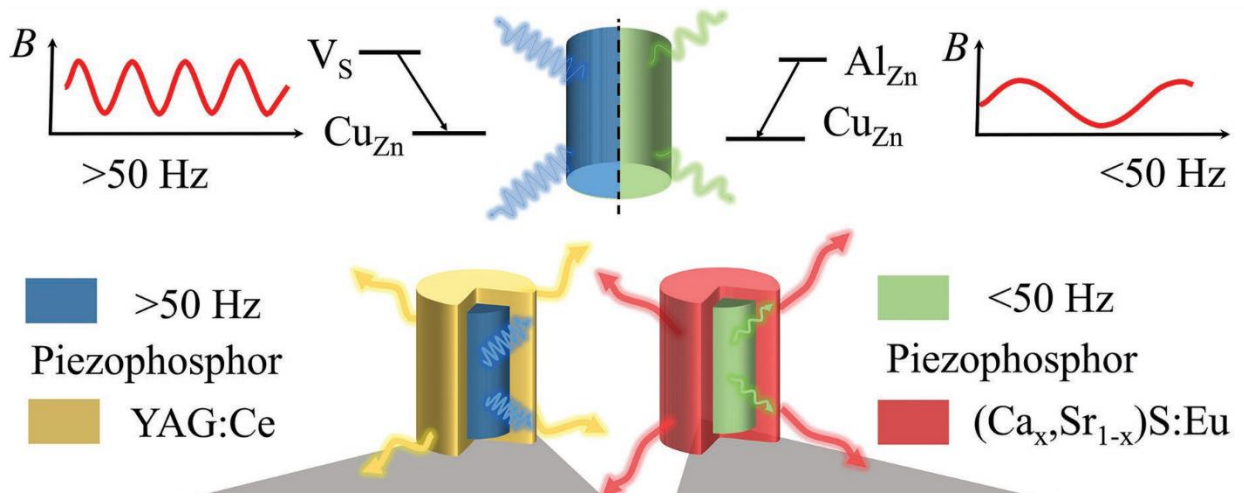
Figure 3-10 Schematic of MIL full-color display realized by coupling piezophotonic composite with different fluorescent materials.

To construct the real-time tunable color temperature white emission, Ce doped $Y_3Al_5O_{12}$ (YAG: Ce) phosphor was chosen. It is based on considering that this phosphor have yellow color emission and its high conversion efficiency when this phosphor is excited by a blue color irradiation. This high efficiency can be demonstrated with the fact that the corresponding yellow emission from YAG:Ce upon the blue color excitation is able to accompany the original blue excitation light. The combination thereby produces a white colored emission. Hence, by combining ZnS:Al, Cu piezoluminescence composite with YAG:Ce fluorescence phosphor, white emission color temperature modulation from 3700 to 5700 k has been achieved. This achievement is based on the mechanical excitation frequency induced spectrum shift from the piezophosphor, such that

Wong Man Chung

the final emission color changes from saturated yellow and warm-white to deep blue through cold-white owning to the blueshift of the piezoluminescence emission, as shown in **Figure** 3-11.
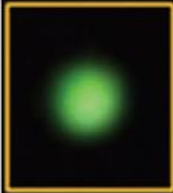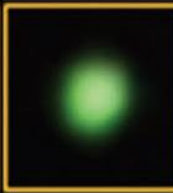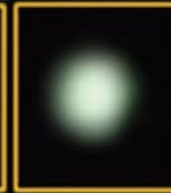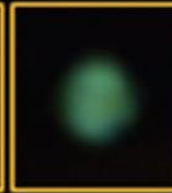
Frequency (Hz)	80	150	200	300	400
CCT (K)	N/A	3732	4832	5369	N/A
Luminescence Photograph					

Figure 3-11 Photographs of white emission with tunable color temperature from piezophotonic composite mixed with YAG:Ce phosphor.

The mixing of YAG:Ce fluorescence phosphors with tunable piezophosphors produces white color possessing a wide range of specific color temperature, allowing a reliable and continuous tuning of the emission color that can be perceived with naked eye.

Wong Man Chung

**Tuning of piezophotonic emission spectrum via modulation
of mechanical stimuli frequency**
THE HONG KONG POLYTECHNIC UNIVERSITY
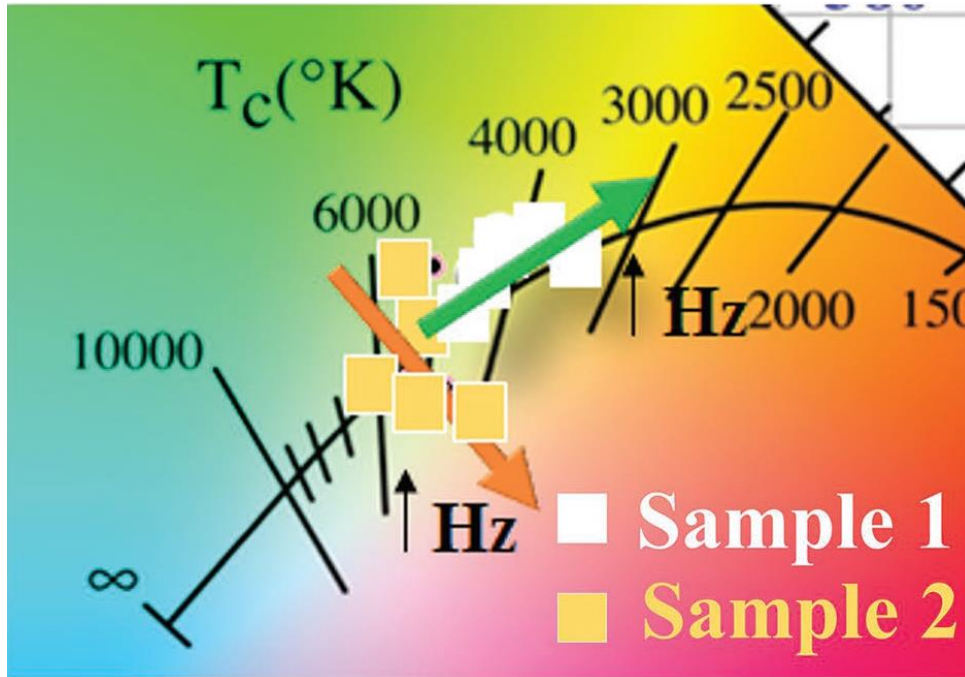
*Figure 3-12 Enlarged CIE coordinates of adjustable white emissions modulated by varying the frequency of mechanical excitation.*

Figure 3-12 shows the trends in Commission Internationale de L'Eclairage (CIE) coordinates of the white emissions, from the two composite samples with different ratio of YAG:Ce phosphor embedded inside of the piezophosphors composite. These coordinates were all situated within the area adjacent to the Planckian locus. Furthermore, as the mechanical excitation frequency changes, the corresponding color coordinates of the YAG:Ce phosphor coated piezophosphors composite migrated in accordance to the mixing ratio of the composites. For example, if the weight ratio in the piezophosphor and the YAG:Ce phosphor is 1:1 (piezophosphor composite: YAG:Ce), a shift of the CIE coordinate with increasing blue component under a high

frequency of the mechanical excitation is observed. Such that an approximate standard white color emission with CIE (x, y) = (0.3352, 0.3354) was observed with the mechanical excitation frequency at about 300 Hz, with an mechanical to illuminance efficiency η of about 0.0018 lm Oe^{-1} (η ~ light-emission output/magnetic-field input strength). From the above results, mechanical energy driven white emission with an appealing feature of tunable emission color in reversible and *in situ* route has been realized. This provides ground for a more diverse application opportunity.
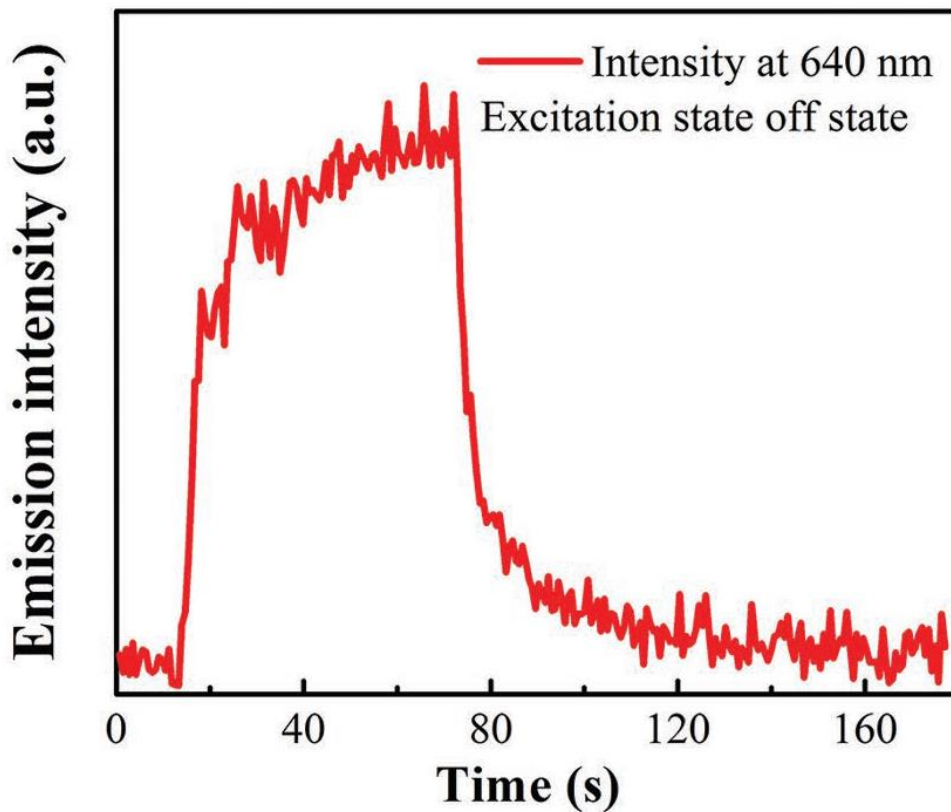
Figure 3-13 The excitation and afterglow of red emission intensity at 640 nm as a function of time.

Wong Man Chung

**Tuning of piezophotonic emission spectrum via modulation
of mechanical stimuli frequency**
THE HONG KONG POLYTECHNIC UNIVERSITY

It has long been criticized the duration of piezoluminescence is relatively short and the limited emission color. In order to extend this duration and provide more color for various applications, **Figure** 3-13 shows the transient characteristic of the red emission from the piezoluminescence composite coated with (Ca1−xSrx)S:Eu persistence phosphor. In this measurement, mechanical excitation frequency of 250 Hz was initially switched on and the magnitude of the mechanical excitation retained at a constant root mean square value. After one min, the excitation is switched off. From figure 3-13, it can be observed that the 640 nm emission rises almost instantaneously when the mechanical excited emission occurs and then begins to decay exponentially once the mechanical excitation ceases, resulting in a prolonged reddish persistence luminescence as expected. It is interesting to notice that this color conversion not only broadens the color expression of piezoluminescence, but also prolonged the illumination of piezoluminescence composite after the stoppage of the excitation. It can be observed that that the luminescence rises very fast and then rises slower; as well as decaying rapidly and then slowly The two parts contained inside the emission of the persistent emission shown in the figure are suspected of containing two parts, one is a fluorescence. The other is phosphorescence. The rapid decay observed upon the ceases of excitation is suspected to be a decay of fluorescence. As the emission of radiation, usually visible light, caused by excitation of atoms in a material, which then terminated almost immediately. The exponential decay observed after the rapid decline of emission intensity can be attributed to the phosphorescence decay.

Wong Man Chung

It is well established that red green blue color emission is essential to achieve a full-color display. A full color display has been realized in the field of photoluminescence and electroluminescence, however, these full color display are seldom reported in the field of piezoluminescence, even less in a tunable emission condition. Thereby, the realization of a red green blue colored emission from a piezoluminescence composite with persistence luminescence property will prompt a various of applications. Therefore the ZnS: Al, Cu based piezoluminescence composite is coupled not only with a highly efficient red-emitting phosphorescence phosphor of (Ca1−xSrx)S:Eu, a tricolored *in situ* tunable mechanical energy driven luminescence display with simultaneous persistence luminescence. The fabrication of the composite were structed as a patterned array of ZnS:Al, Cu-based composite coated with the (Ca1−xSrx)S:Eu phosphor.As in **Figure** 3-14, the illumination of the display was triggered by a sinusoidal mechanical excitation in the form of magnetic-field excitation. The (Ca1−xSrx)S:Eu phosphorescence was utilized to convert the green piezophotonic emission and displays a red colored logo of Hong Kong Polytechnic University.
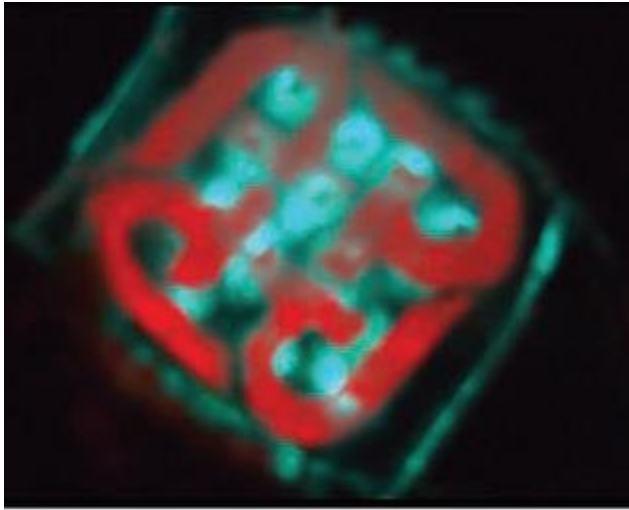
Figure 3-14 Multicolor MIL flexible composite combined with (Ca_x, Sr_{1-x}) S:Eu displaying the logo of the Hong Kong Polytechnic University.

Figure 3-15 shown a tricolor display elements which was fabricated by incorporating $(Ca_xSr_{1-x})S$:Eu phosphor with ZnS:Al, Cu-based piezophosphors composite(red) and ZnS:Cu based piezophosphors (green). These elements were incorporated into a single display with each element function as a pixel of the display. This display is capable of generate a simultaneous RGB emission via converting mechanical energy in the form of magnetic excitation.

Wong Man Chung
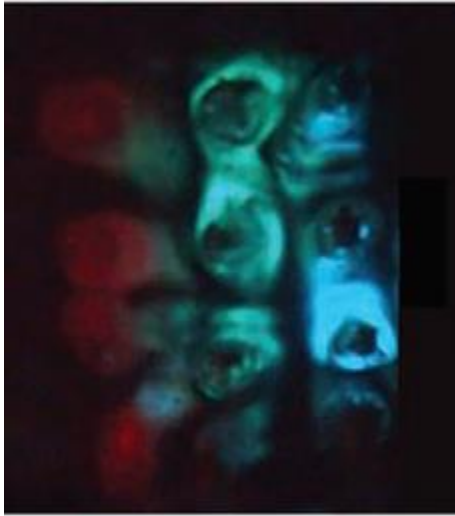
Figure 3-15 Display of piezophotonic medicated RGB emissions.

The RGB display emission can be seen by the naked eyes. This result implies the possibility of broadening up the range of energy harvesting and conversion applications based on the intriguing property of mechanical excitation frequency modulating piezoluminescence materials.

3.6. Conclusion

In summary, a novel strategy to realize an *in-situ* modulation the emission wavelength and color of piezoluminescence is developed. This strategy is based on varying the frequency of mechanical excitation upon the piezophosphors, induces a mechanical hysteresis of the piezophosphors. Such that the titled of the energy band structure under mechanical excitation is steepen without an increase of magnitude of mechanical excitation stimuli. The high frequency of

Wong Man Chung

mechanical excitation causes saturation of these deep charge traps and decreases the recombination rate of the charge carriers inside. The emission from the shallow charge trap become dominant, thereby the emission color changes. Experiment was performed to verify this real time and reversible piezoluminescence emission color tuning. A brief discussion on the mechanism of the temporal modulated tuning of piezophotonic-effect-induced luminescence and color Gamut via Modulating mechanical excitation was provided. Moreover, some proof of concept devices, including red–green–blue full-color displays and tunable white-light sources are demonstrated simply by frequency modulation. The study provides a new insight and understanding on the piezophotonic emission mechanism. These new finding of the luminescent materials with ability to be accessed and modulated remotely will offer opportunities for applications in the fields of mechanical energy harvesting and conversion, optical sensing, piezophotonics, nondestructive environmental surveillance, novel light sources, and displays.

Wong Man Chung

Chapter 4   Ultra-high voltage output triboelectric nanogenerator powered mechano-nitrogenous fertilizer supplier

4.1. Introduction

Nitrogen is an essential nutrient and indispensable building blocks for all organisms on earth. For example, nitrogenous bases is an indispensable building block of DNA and RNA. Although molecular nitrogen (N_2) is the most abundant element on the earth's surface (78.08 % of air is composed of N_2). The majority of organisms are incapable of exploiting this surplus.[214, 215] As nitrogen fixation, the convention of the gaseous forms of dinitrogen into biologically usable form, is very taxing for an organism in an energy perspective.[216] In our society, Haber-Bosch gas phase dinitrogen fixation process is the process of binding nitrogen with hydrogen under high pressure and temperature that produces ammonia. This process is essential for agriculture and the manufacture of fertilizer. However, its inherent harsh reaction conditions requirement results this energy intensive fixation processes consumed 1-2 % of the world's energy production. Considering the ever-escalating demand for fertilizers, the high energy intensity and environmental concerns triggered by the Haber-Bosch process, the urgency to develop and integrate a more sustainable nitrogen fixation processes becomes more imperative.

Several alternative fixation technologies are currently being investigated. Prominently, atmospheric-pressure microplasma discharge-based nitrogen fixation is considered as having great

potential as a supplementary or replacement of exists technology.[216, 217] Its most significant advantages are its insubstantial energy consumption and peripheral reaction criteria, which improve the fixation energy efficiency and reduce environmental impact. The microplasma discharge typically created by applying a high voltage across two electrodes under ambient condition. Whereas this high voltage established an electric field strength exceeded the dielectric strength of air, air molecules in the regions of this intense voltage gradients became ionized and conducting. Nitrogen fixation is therefore accomplished by producing nitric oxide via the subsequent recombination of these ionized nitrogen and oxygen molecules.[216, 218] Based on these insights, utilizing a renewable energy source capable of generating necessary voltage for an microplasma discharge under ambient conditions suggested a more sustainable nitrogen fixation route. However, existing environmental-friendly high voltage discharge sources all suffer several disadvantages, for example as the source usually required strenuous efforts to fabricate. In some cases, auxiliary apparatuses are mandatory during operation.[217] The operation condition is somewhat only finite to a few circumstances. Therefore, it is a prominent endeavor to create a simple, *in-situ* self-reliant sustainable direct microplamsa discharge sources in order to realize an environmentally friendly atmospheric-pressure nitrogen fixation.

Triboelectric nanogenerators (TENGs) is a novel mechanical energy harvester emanated on the contact electrification of two dissimilar materials. Since its invention in 2012, numerous self-powered applications had manifested TENG as an excellent sustainable power source.[19] It generates useful electrical energy by converting mechanical energy available in the surroundings.

Ultra-high voltage output triboelectric nanogenerator
powered mechano-nitrogenous fertilizer supplier
THE HONG KONG POLYTECHNIC UNIVERSITY

These ubiquitous mechanical energies usually either exist naturally or does not functionally participate in any given circumstance.[132, 219, 220] Therefore, scavenging these energies for recuperation is considered an ideal sustainable strategy. Moreover, these mechanical stimuli inherently exist in a low frequency regime. The versatility of TENG enables it to harvest these stimuli with various frequencies band because of its dismal design constraint. Though, its operation mechanism predetermines its paramount performance would be under a modest frequency range of mechanical stimuli. Hence, it is desirable for TENG to scavenge these mechanical energies.

Fundamentally, during each operation cycle, two insulating surfaces in a TENG are mandatorily contacted with each other. The contact surfaces will be acquired opposite static charges via triboelectric charging upon separation. These charges are prohibited from draining owing to the insulating nature of these insulators, high voltage is therefore subsequently built up and utilized as the output of TENG. This output principally capable of reaching several hundred or even thousand volts, depending on the variances in tendencies of the two insulating materials to gain or lose electrons. Quantitative properties of the inputting mechanical stimuli also play a hegemony role on the magnitude of the output voltage of TENG. Furthermore, TENG operational safety is inherently ensured by its intrinsic minuscule short-circuit current. These characteristics primed TENG as an excellent high-voltage source. In particular, TENG performs peculiarly upon powering a capacitive device.

Ever since this presupposition has been theorized, researcher have been striving to exploit this unique quantity in various circumstances, mass spectrometer, dielectric elastomer,

Wong Man Chung

Ultra-high voltage output triboelectric nanogenerator
powered mechano-nitrogenous fertilizer supplier
THE HONG KONG POLYTECHNIC UNIVERSITY

ferroelectric polymer, field emission devices, electrospinning, self-powered smart systems: these momentous applications have been pertinent to TENG. However, despite the prominence efforts have been applied in optimization, these illustrations have rarely manifest both reliability and autonomy properties of TENG simultaneously in a high voltage regime.[221-224] Researchers whom revealed in undeviating high voltage output generally required TENG to engage in operation under specific circumstances, such as high frequency of mechanical stimuli, unfeasible stress or a customized situation.[145, 183, 187, 225] Meanwhile, in order to maintain a steady high voltage output from TENG, complementary modification such as integrating TENG with another voltage sources or incorporating TENG with supplementary circuitry during TENG operation in an ambient environment generally disdain the autonomy of TENG.

Based on the evaluation of electron affinity of the different insulating materials at a during triboelectric charging. The involved charging process instantaneously converts human–TENG interactions into high voltage directly with an unpretentious mechanical energy input, without requisition supplementary nor magnification entity. Therefore, TENG inherent simplicity and high voltage output Based on the above discussion, a rudimentary structured TENG that remediate a consistent high voltage output was developed, the TENG with simple structure was designed based on our evaluation in contact electrification ability of materials, and was prepared using polyurethane (PU) foam and ebonite sheet as contact materials. It could provide a high voltage output of about 1300 V and a low current output of about 60 μA driven by mechanical stimuli. The generated voltage is directly applied on electrodes of the discharge reactor for atmospheric

Ultra-high voltage output triboelectric nanogenerator
powered mechano-nitrogenous fertilizer supplier
THE HONG KONG POLYTECHNIC UNIVERSITY

microplasma discharge, where the nitrogen gas in air is successfully converted into nitrogenous compound, including nitrogen dioxide and nitric acid solution. This TENG was further employed to power the TENG-microplasma driven nitrogen fixation system as a nitrogenous fertilizer supplier. Consequently, fertilizer ($NaNO_3$) is achieved via driving the system by human walking stimuli to benefit the plant cultivation. This work provides a feasibility to develop an energy-saving, environmental-friendly, flexible, and safe nitrogen fixation route.

4.2. Working principle of Ultra-high voltage output triboelectric nanogenerator

4.2.1. Fabrication of the high voltage output triboelectric nanogenerator

The structural design of the contact-separation mode TENG with high voltage output is illustrated in **Figure** 4-1.
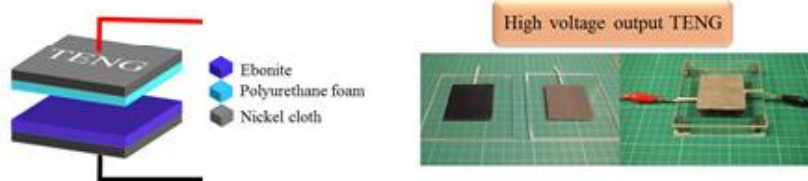
Figure 4-1 Schematic and Photograph high voltage TENG.

The structure of the TENG consists of a polyurethane (PU) foam and an ebonite sheet as top and bottom frictional layers, respectively. Two nickel (Ni) films were deposited on the surface of the two-contact layer and performed as electrodes for electric output of the TENG, and polycarbonate was used as the substrate of the device. The fabrication procedure is summarized as following: PU foam with the thickness of 2 mm and the Ebonite sheet of thickness 600 μm were employed as the friction layer of the TENG without further treatment. The contact-separation mode TENG was fabricated by confronting the two frictional layers (5 cm x 5 cm) against each other. Nickel fabric and polycarbonate were successively attached on the rear sides of the frictional layers as electrodes and supporting substrate, respectively. To ensure a strong bonding between the nickel cloth and Polyurethane foam, the nickel cloth and the Polyurethane foam was bonded by a layer of bi-oriented polypropylene (BOPP) adhesive thin film, which was deposited uniformly between the two layers. BOPP film is renowned for its excellent bonding ability such that the strength of the bonding between the two layers is guaranteed. During the entire course of operation of the TENG, the two layers haven't exhibited any detachment even the TENG is under moderate to strong compressive stress. Four springs with length of 10 mm and diameter of 8 mm were fixed on the four corners of polycarbonate substrates via epoxy adhesive and shafts to hold a gap between friction layers.

Wong Man Chung

**Ultra-high voltage output triboelectric nanogenerator
powered mechano-nitrogenous fertilizer supplier**
THE HONG KONG POLYTECHNIC UNIVERSITY

4.2.2. Working principle of the high voltage output triboelectric nanogenerator

As disused earlier, the contact separation mode TENG with a simple structure was designed based on the evaluation in contact electrification ability of materials. It was therefore prepared using PU foam and ebonite sheet as contact materials. During each TENG operating cycle, PU foam and ebonite are brought into physical contact by mechanical energy input. The amount of charge generated and transferred is based on the two materials electronic affinity. Herein, according to the triboelectric series of materials' tendency to gain or lose electrons, electrons are transferred from PU foam into ebonite at the interface, and these two surfaces are charged with opposite polarities. When they are parted, a difference in electric potential is generated between the two Ni electrodes. Subsequently, when the two separated charged frictional layers are gradually brought together again by external mechanical energy, a voltage output with reversed polarity is generated. By means of this process, the ambient mechanical energy is harvested to generate high voltage output.
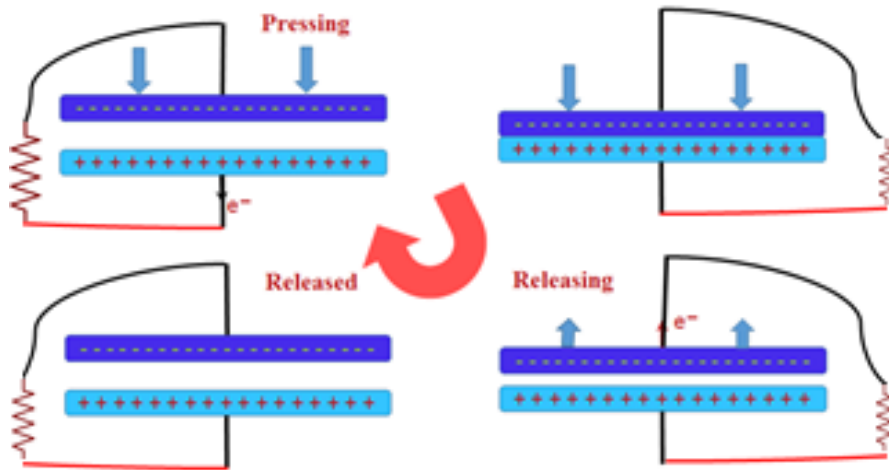
Figure 4-2 Schematic of the working mechanism of the TENG.

This high voltage output can mainly be attributed to the significant difference in electron affinity between the PU foam and ebonite, which increases the amount of separated charges generated during the TENG operation and results in a high voltage output. Additionally, compared with a flat structure, the porous structure of the utilized PU foam can lead to the enhanced effective contact area between frictional materials, which contributes to the high electric output of TENG as well. Moreover, PU foam generally is regarded as an excellent triboelectric charge donor. Previous studies suggested its output performance as a TENG frictional layer can be further refined.[226] It is suspected the pore sizes of foam adapted a critical role of triboelectric charging in a vertical contact-separation context. Therefore, experiment was conducted to verify the hypothesis, the results are shown in below,

Wong Man Chung

Ultra-high voltage output triboelectric nanogenerator
powered mechano-nitrogenous fertilizer supplier
THE HONG KONG POLYTECHNIC UNIVERSITY
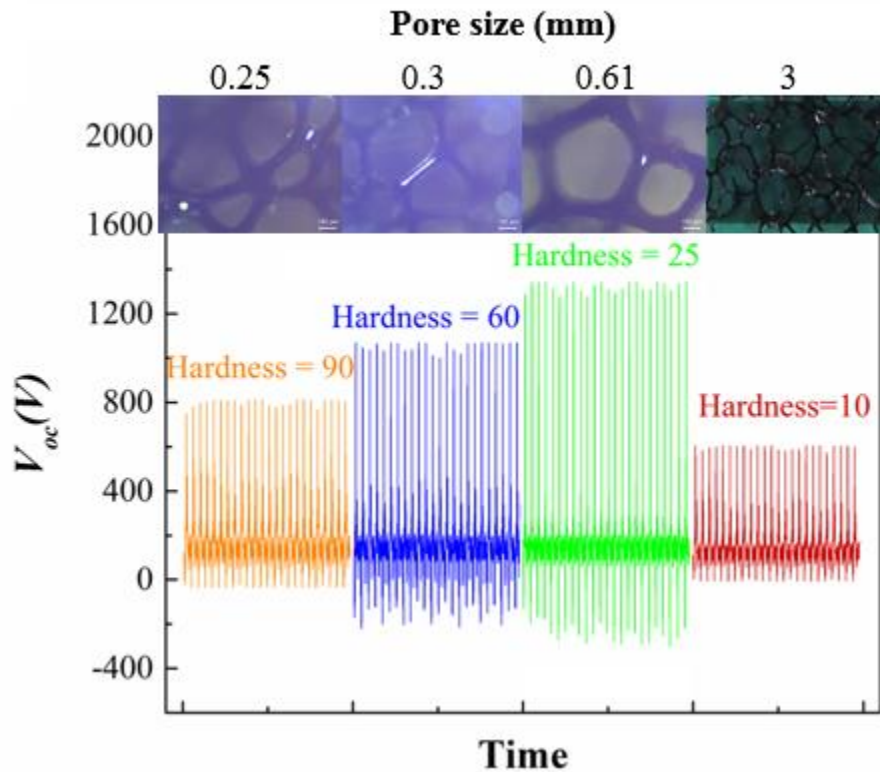
Figure 4-3 Open-circuit voltage of TENG versus the pore size of utilized PU foam friction material.

(Inserts are the optical images of the PU foams with different pore size).

It can be observed that porosity of polyurethane foam articulates the TENG output voltage eminently. This dictation via porosity variation were suspect to be aroused from two aspects. One is that elasticity of the PU foam is a variant of the porosity of PU foams. The other is the effective contact area (these areas actually commence contact electrification) of the two frictional layers during compression stage of TENG. For a low porosity polyurethane foam, its low elasticity prohibited an enhanced effective contact area from foam deformation during the

Wong Man Chung

compression stage of the TENG operation, which limited the chances of electrostatic charge exchange between the two frictional layers. Summarizing these two factors, the results shown in **Figure** 4-3 that the open circuit voltage obviously increases when the pore size increases from 0.25 mm to 0.61 mm. As aforementioned, during the operation of TENG, PU foam layer were periodically compressed and released with contact and separation of the two frictional layers. The larger pore size may be beneficial for forming an improved effective contact area between frictional materials accompanying with the compression of PU foam, leading to the enhancement of performance of the device. On the other hand, the hardness of PU foam will decrease with an increase of the pore size. It should be noticed that, in the field of polymeric material, hardness of a polymeric is the measurement of the ability of the polymer to recover after being indented through force. The major difference between hardness and Young's modulus is that, elastic modulus is a fundamentally related to the bonding of the materials atom or molecules. Hardness is an engineering property, it is closely related to elastic modulus and a "resistance to plastic deformation"., which depended on the loading rate and loading hold time. As the TENG system driven nitrogen fixation system can be operated in an ambient condition with various form of mechanical loading and of different loading dilation, such that it is more relative to consider the hardness of polyurethane instead of simply its elastic modulus. This reduces the resistance for device operation and may assists the contact area between frictional layers to become larger. Therefore, the V_{oc} obviously increases with the enlargement of the pore size of PU foam, and the peak V_{oc} of about 1300 V is obtained as the PU pore size is about 0.61 mm. Nevertheless, further

Wong Man Chung

Ultra-high voltage output triboelectric nanogenerator
powered mechano-nitrogenous fertilizer supplier
THE HONG KONG POLYTECHNIC UNIVERSITY

increase in the pore size to above 3 mm would result the proportion of PU in whole foam becoming too small as shown, such it will result a significant decrement of the effective contact area and the electric output of device. Therefore, PU foam with pore size of 0.61 mm was employed as an optimized friction layer for further device fabrication.

4.2.3. Performance of the high voltage output triboelectric nanogenerator

In order to evaluate the performance of the prepared TENG, a generator with the size of 25 cm^2 was fabricated for the performance characterization. The results demonstrate the TENG is capable of a high voltage output. As shown in **Figure** 4-4 and 4-5, triggered by an impulsive force of 70 N, the open-circuit voltage (V_{oc}) and the short-circuit current (I_{sc}) of TENG are capable of reaching up to about 1300 V and 60 µA, respectively.

Ultra-high voltage output triboelectric nanogenerator
powered mechano-nitrogenous fertilizer supplier
THE HONG KONG POLYTECHNIC UNIVERSITY
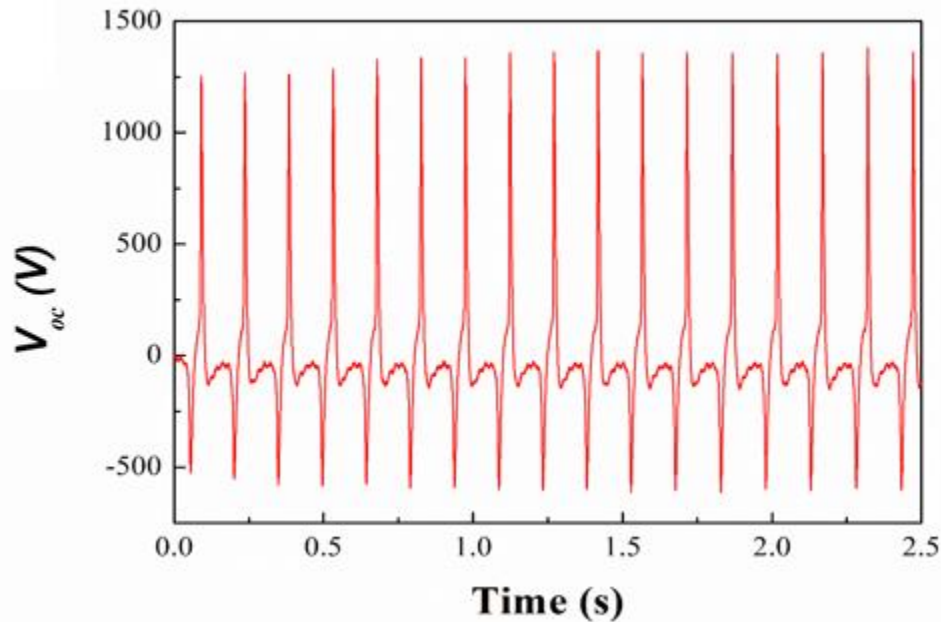
Figure 4-4 Open-circuit voltage generated by TENG.

It can be observed that the why the peak value of the voltage for the positive and negative part in the Figure 4-4 is difference. Theoretically, the response of the TENG is depended on the force applied onto the TENG during operation. In the cases of the mentioned TENG system, the TENG was applied with a compressive stress of 70 N while the releasing of the TENG is solely driven by a couple of spring inserted between these frictional layers. Since the force provided by these springs are considerably weaker than 70 N, therefore there is a different voltage output for the positive and negative part.

Wong Man Chung

Ultra-high voltage output triboelectric nanogenerator
powered mechano-nitrogenous fertilizer supplier
THE HONG KONG POLYTECHNIC UNIVERSITY
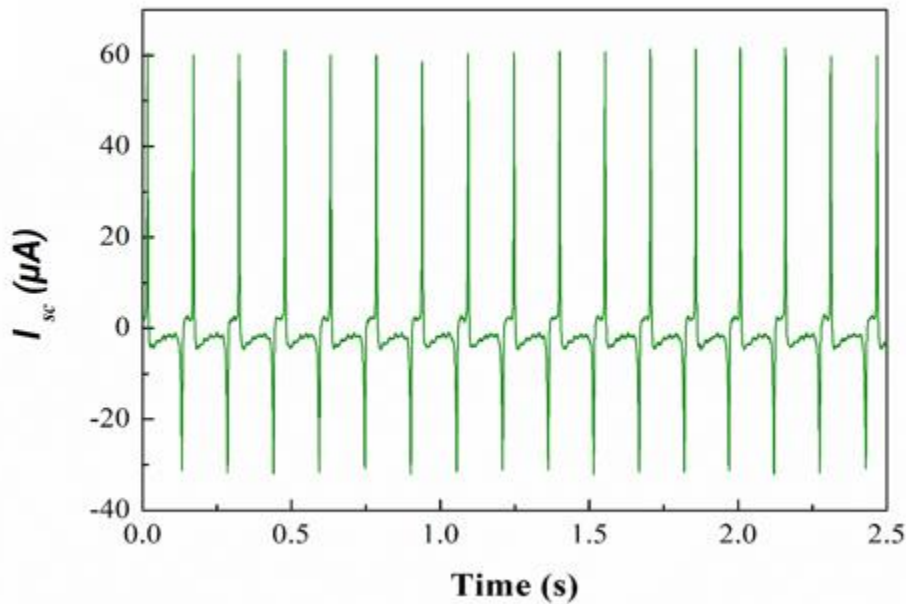
Figure 4-5 Short-circuit current generated by TENG

Meanwhile, the dependence of peak instantaneous output current and power on the external loads are also studied as shown in **Figure** 4-6. It is found that the increased load resistance leads to the instantaneous current drops, and correspondingly, TENG reaches the peak instantaneous power of the maximum of 27 mW at a load resistance of 100 MΩ. This implies the maximum instantaneous power density is 0.432 W/m².

Wong Man Chung

Ultra-high voltage output triboelectric nanogenerator
powered mechano-nitrogenous fertilizer supplier
**THE HONG KONG POLYTECHNIC UNIVERSITY**
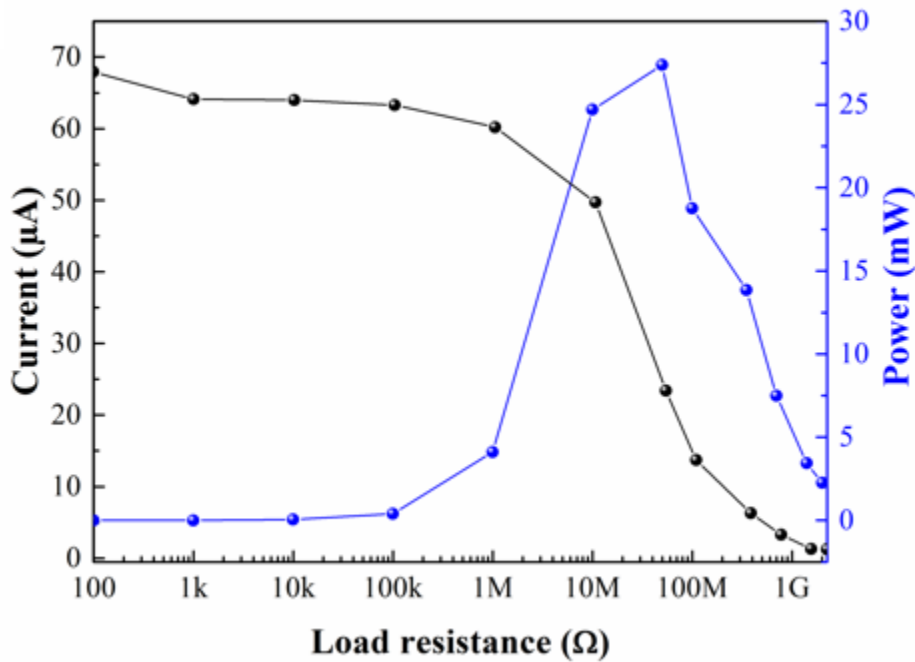
Figure 4-6 Dependence of the peak instantaneous current and peak instantaneous power of TENG on the external load resistance.

Moreover, a durability test of device was also conducted. The result was shown in **Figure 4-7**. The test result that after a continuous operation of 50000 cycles, no significant distortion or serious damage on the frictional layers is observed though comparing the morphologies of the two friction layers before and after operation. Further, the electrical output of device remains stable during the process and the fluctuation of V_{oc} is less than ±0.3% (with a fixed frequency of 7 Hz). The ultra-high electric output and great reliability of the prepared TENG enable itself to be capable of being a reliable and durable voltage supply.

Wong Man Chung
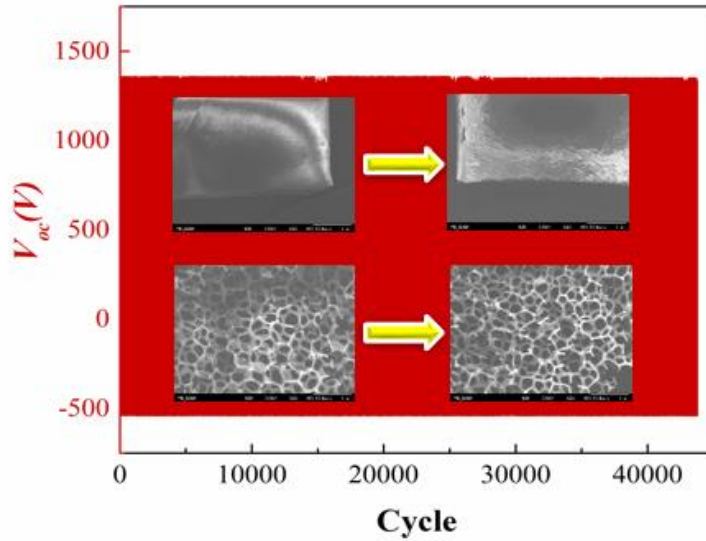
Figure 4-7 The open-circuit voltage of the TENG after continuous operation for 45000 cycles at 7

Hz. Inserts are the SEM images of the two frictional layers before and after the operating process.

Ultra-high voltage output triboelectric nanogenerator
powered mechano-nitrogenous fertilizer supplier
**THE HONG KONG POLYTECHNIC UNIVERSITY**

4.3. High voltage output triboelectric nanogenerator induced atmospheric microplasma discharge

4.3.1. Fabrication of high voltage output triboelectric nanogenerator

From these TENG unique electrical output performances demonstrated in the previous sections, implicated its competent in capacitive device applications. Thereby, facilitating from the TENGs inherent simplicity in fabrication and a high voltage output under ambient pressure, it is suitable for it to power a capacitor-type sustainable atmospheric-pressure microplamsa discharge system. Such an microplasma discharge will be beneficial for realizing a nitrogen fixation system. Thereby, through harvesting ambient or wasted mechanical energy, reconciling the TENG to an ever more environmentally friendly biologically consumable nitrate solution. To realizes such a system, an microplasma discharge reactor is furnished. Generally, it is considered as an air-filled miniature glass cylinder. Two stainless steel needles, acting as the discharge electrodes, are fixed at the interior of the glass cylinder as shown in **Figure** 4-8.

Ultra-high voltage output triboelectric nanogenerator
powered mechano-nitrogenous fertilizer supplier
THE HONG KONG POLYTECHNIC UNIVERSITY
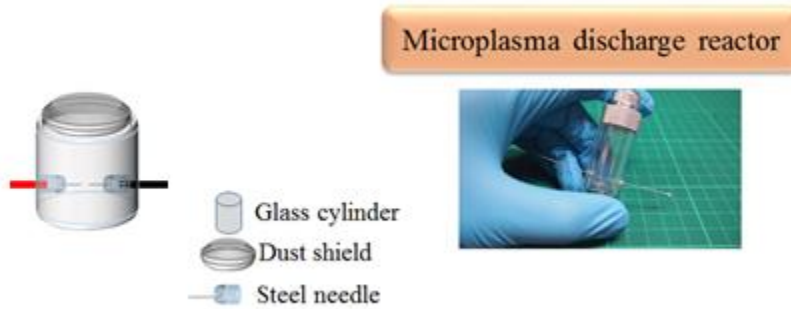
Figure 4-8 Schematic and Photograph of the microplasma discharge reactor.

Owing to the inherent high voltage from the TENG, the output voltage was directly applied to the needle electrodes directly connected to the TENG, and thus this voltage generated by TENG can be directly induced an microplasma discharge. Some DI water was placed at the bottom of glass cylinder to absorb generated nitrogen compounds during the process of microplasma discharge.

Ultra-high voltage output triboelectric nanogenerator
powered mechano-nitrogenous fertilizer supplier
THE HONG KONG POLYTECHNIC UNIVERSITY
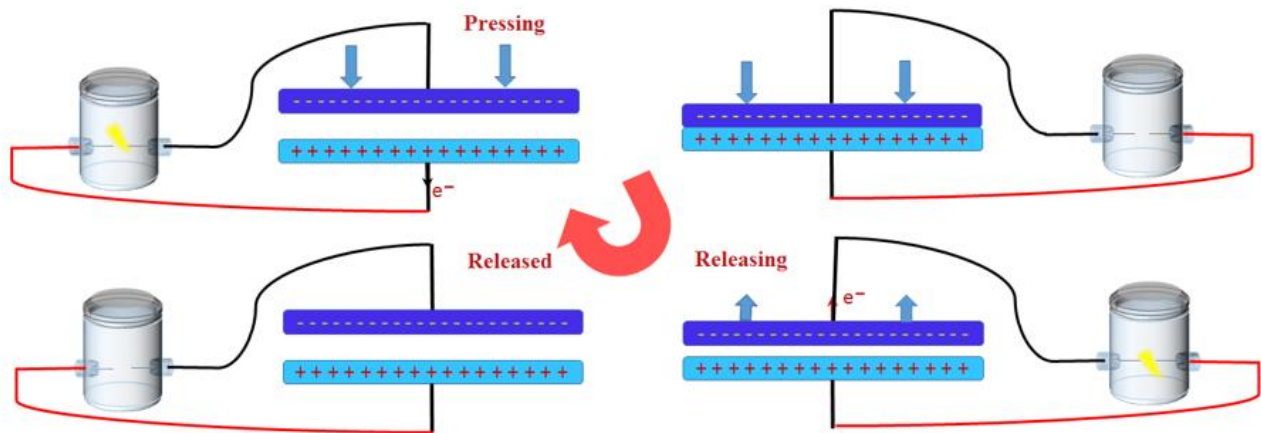
Figure 4-9 Schematic of the working mechanism of the TENG-microplamsa nitrogen fixation system.

The working mechanism of the TENG-microplasma discharge system is shown in **Figure 4-9**. For each operating cycle of TENG, PU foam and ebonite are brought into physical contact mechanical stimuli. According to the triboelectric series of materials' tendency to gain or lose electrons, charges are transferred from PU foam into ebonite at the interface, and these two surfaces are charged with opposite polarities. When they are parted, difference in an electric potential is produced between the two Ni electrodes. Subsequently, when the two separated charged frictional layers are gradually brought together again, a voltage output with reversed polarity is generated. The output voltages are applied between the two needle electrodes in the microplasma discharge reactor. The voltage across the needle thereby will change with the gradual contact or separation of the frictional layers. Once this voltage exceeds the dielectric strength of air, ionization of air molecules and microplasma discharge will happen in the regions between

Wong Man Chung

Ultra-high voltage output triboelectric nanogenerator
powered mechano-nitrogenous fertilizer supplier
# THE HONG KONG POLYTECHNIC UNIVERSITY

needle electrodes, which will enable nitrogen to be transformed into nitrogen compounds. By means of this process, the ambient mechanical energy is harvested to generate electricity for microplasma discharge-based nitrogen fixation.

The microplasma discharge reactor is a custom-made glass cylinder (Drummond Scientific, Φ outer 5 cm, Φ inner 4.6 cm) with two stainless steel needles located in the opposite side of the cylinder. The gap distance between the needles is adjustable. The top end of the reactor is caped with a helmet to avoid dust or dirt polluting the interior of the reactor. DI water or weak sodium bicarbonate solution was added into the reactor for absorbing generated nitrogen oxide.

4.3.2. Triboelectric nanogenerator driven plasma discharge characterization

Based on the aforementioned operation mechanism, the TENG-plasma discharge system, the output voltage generated by TENG will be directly applied to the needle electrodes in discharge reactor for plasma discharge was characterized as shown in **Figure** 4-10, the plasma discharge has been successfully observed during TENG operation.
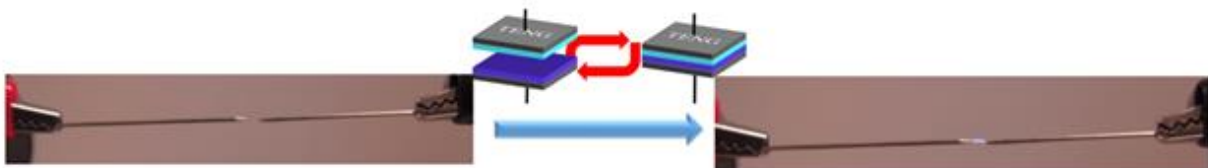
Figure 4-10 Photograph of the TENG-driven plasma discharge between needle electrodes.

Wong Man Chung

Ultra-high voltage output triboelectric nanogenerator
powered mechano-nitrogenous fertilizer supplier
# THE HONG KONG POLYTECHNIC UNIVERSITY

The detailed discharge process had been further analyzed by studying the change of voltage (V_c) and current (I_c) between needle electrodes. The output voltage and current of the TENG were measured by LeCroy WaveRunner Oscilloscope (44MXI) with the probe resistance value of 50 MΩ and low noise current amplifier (Stanford Research Systems, SR570), respectively.
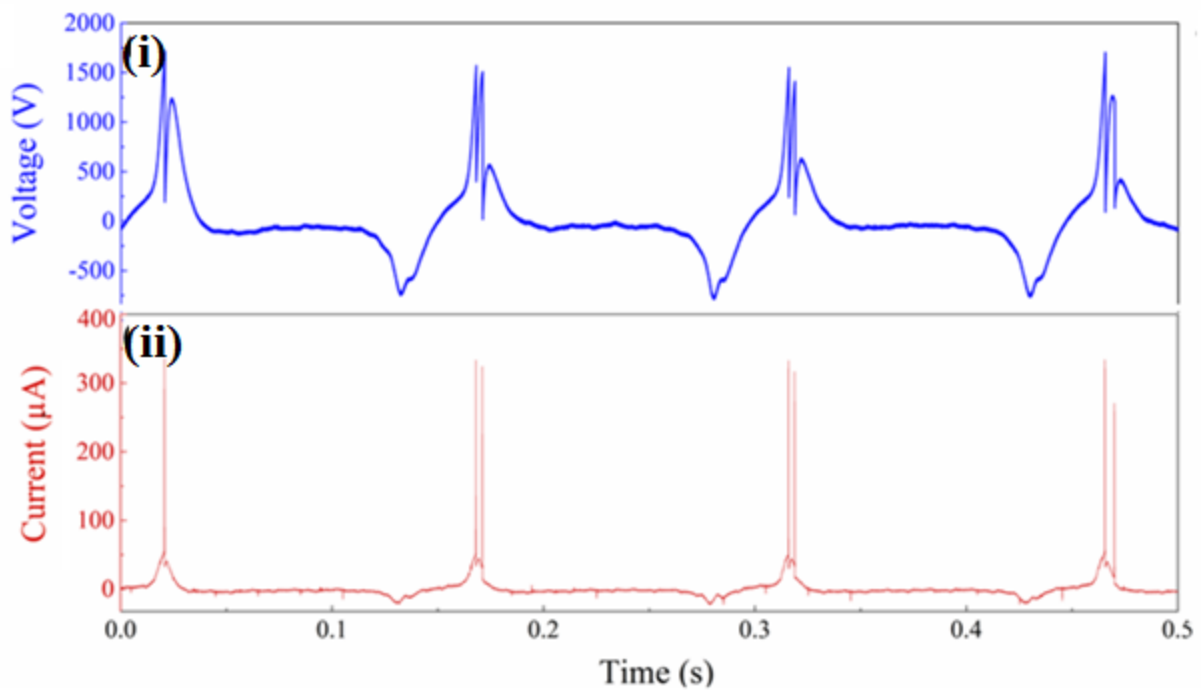
Figure 4-11 Change in voltage (i) and current (ii) between needle electrodes during four operation cycles of TENG. Gap distance between needle electrodes is 0.2 mm.

Figure 4-11 illustrates the V_c and I_c during 4 operation cycles of TENGs, and the gap distance between needle electrodes is 0.2 mm. Taking one cycle as an example, it can be observed that V_c first increases to discharge voltage of ~1500 V and suddenly decreases to 0 V, as in **Figure**

Ultra-high voltage output triboelectric nanogenerator
powered mechano-nitrogenous fertilizer supplier
### THE HONG KONG POLYTECHNIC UNIVERSITY

4-11(i). Simultaneously, Ic grows rapidly to discharge current of about 300 µA, as in figure 4-11 (ii). This implies that the applied electric field causes the air between the needle electrode electrical breakdown and induces immediate charges transfer through the air gap. Subsequently, the Ic decreases back to 50 nA within 0.002 s, and Vc started to gradually increase due to the continuous electric supply from the TENG as well as the remaining charges in needle electrodes. When the Vc reaches up to 1000 V, the second discharge occurs in the same half cycle. It can be noticed that the discharge phenomenon happens only in the positive half cycles, and there is no microplasma discharge in the negative half cycle. That is because according to Paschen's curve, a microplasma discharge in air generally requires a threshold voltage of more than 1000 V. However, the maximum output voltage of TENG in negative cycle is around 500 V as shown in figure 4-11 (i), which is thereby incompetent to generate another microplasma discharge. The released energy for each microplasma discharge is an important parameter characterizing the micoplasma itself. It can be quantitatively analyzed by the voltage-charge-cyclogram, namely Lissajous figures. **Figure** 4-12 illustrates the Lissajous figures of the discharges process as mentioned. The released energy for each discharge (E_L) can be calculated as,

$$E_L = \int Q \cdot dV = A_{Lissajoous} \tag{6}$$

where Q is transferred charge during microplasma discharge, and V is the V_c during microplasma discharge, $A_{Lissajoous}$ is the area of the enclosed curve.

Wong Man Chung
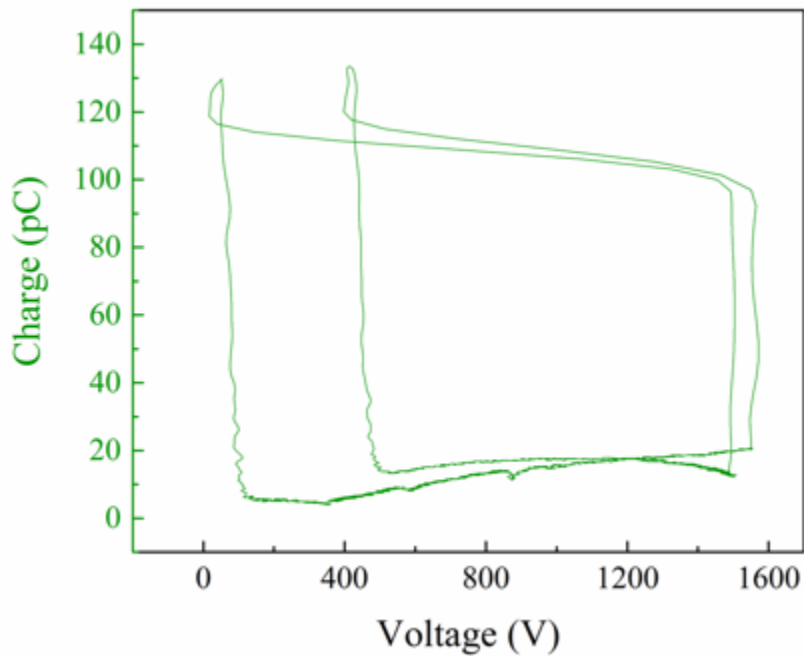
Figure 4-12 Lissajous figures of the microplasma discharge process with the gap distance of 0.2 mm.

The results show that for each microplasma discharge with a gap distance of 0.2 mm, the E_L is calculated as about 0.14 µJ. According to the statistical results in **Figure** 4-11, about 1.75 discharges are observed in per operation cycle of TENG. This means that the average released energy (E_{ave}) during discharge per cycle is about 0.26 µJ.

Wong Man Chung
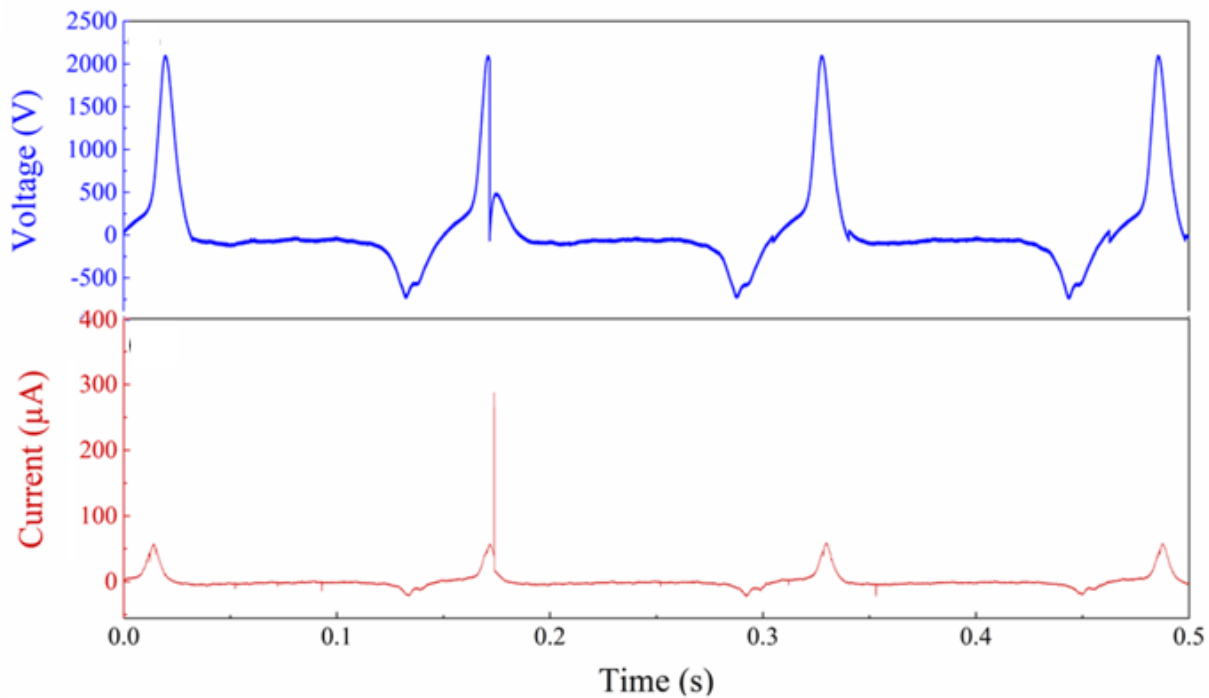
Figure 4-13 Change in voltage and current between needle electrodes during four operation cycle of TENG. Gap distance between needle electrodes is 0.6 mm.

The gap distance between needle electrodes plays an important role on the microplasma discharge process. **Figure** 4-13 shows the changes in Vc and Ic during the discharge process with the gap distance of 0.6 mm. The results show that compared with the microplasma discharge with the gap distance of 0.2 mm, the amount of microplasma discharges statistically decreases to about 0.3 times per operation cycle. Meanwhile, during the microplasma discharge, the discharge voltage increases to about 2 kV, while the discharge current decreases to 287 μA. That is because such a relatively wide gap distance (0.6 mm) would limit the ability of the formation of a conductive path

Wong Man Chung

Ultra-high voltage output triboelectric nanogenerator
powered mechano-nitrogenous fertilizer supplier
**THE HONG KONG POLYTECHNIC UNIVERSITY**

between needle electrodes via ionization of air molecules, leading to a higher threshold voltage, a smaller discharge current, and reduced number of discharges for each operation cycle. In addition, the released energy for each microplasma discharge E_L with the gap distance of 0.6 mm is also measured based on the Lissajous figures as shown in **Figure** 4-14.
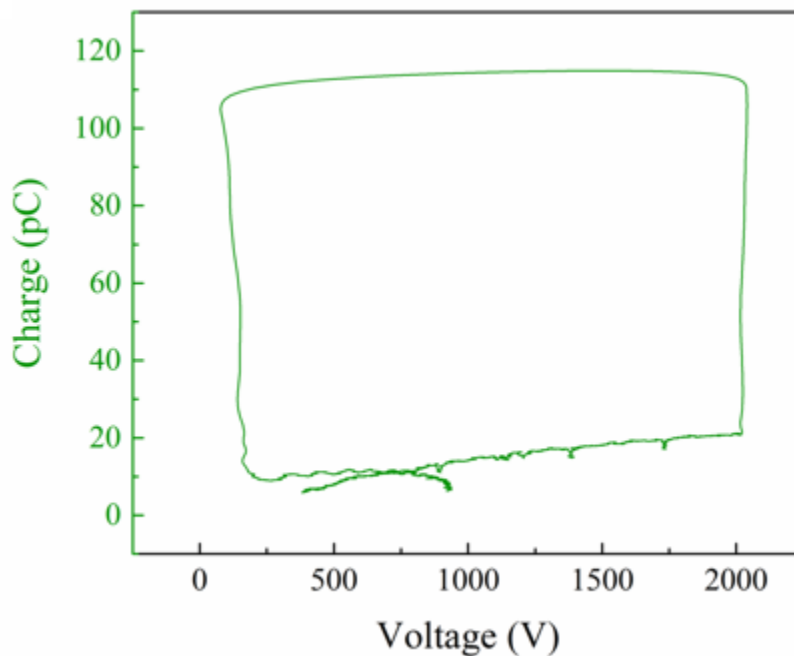
Figure 4-14 Lissajous figures of the microplasma discharge process with the gap distance of 0.6 mm.

The results reveal that the E_L from this discharge is about 0.19 µJ. Correspondingly, the average discharge energy per operation cycle E_{ave} is 0.16 µJ, which is comparatively lower than that of the discharge with the gap distance of 0.2 mm. In order to optimize the TENG-driven

microplasma discharge process, the dependence of discharge voltage, discharge current, E_L and E_{ave} on the gap distance is summarized in **Figure** 4-15 and **Figure** 4-16, respectively.
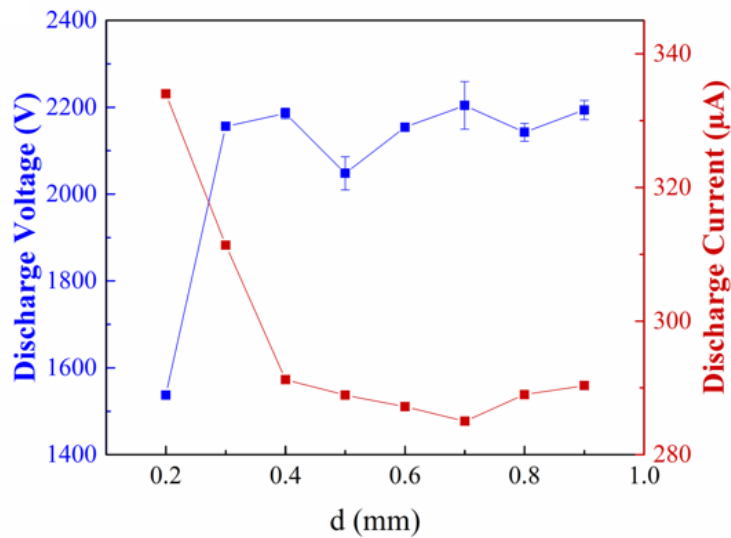
Figure 4-15 The discharge voltage and discharge current under different gap distance between needle electrodes.
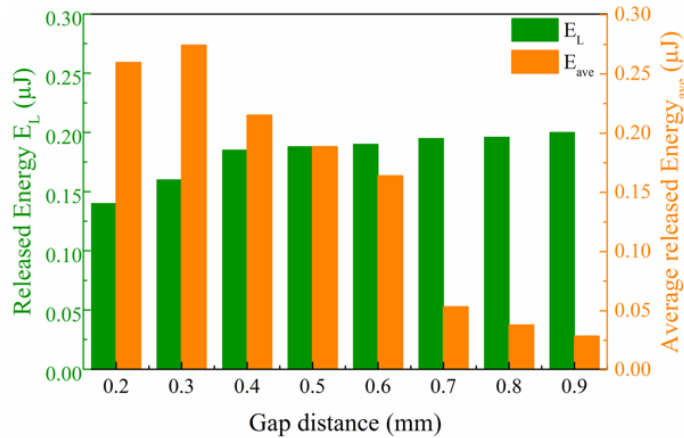
Figure 4-16 The released energy for each microplasma discharge and the average discharge energy in each TENG operation cycle under different gap distance.

It can be observed that the discharge voltage and E_L increase while the discharge current decreases with gap distance enhancement. Correspondingly, the average released energy E_{ave} arrives at maximum of 0.28 µJ when the discharge gap distance is about 0.3 mm, whereas more ionized gas is generated to benefit the microplasma discharge and nitrogen fixation.

4.4. Nitrogen fixation via triboelectric nanogenerator driven microplasma discharge system

Through the discharge driven by TENG, nitrogen in air will be converted into nitrogen compound for accomplishing nitrogen fixation. The related reactions were summarized in **Figure 4-17.**

Wong Man Chung
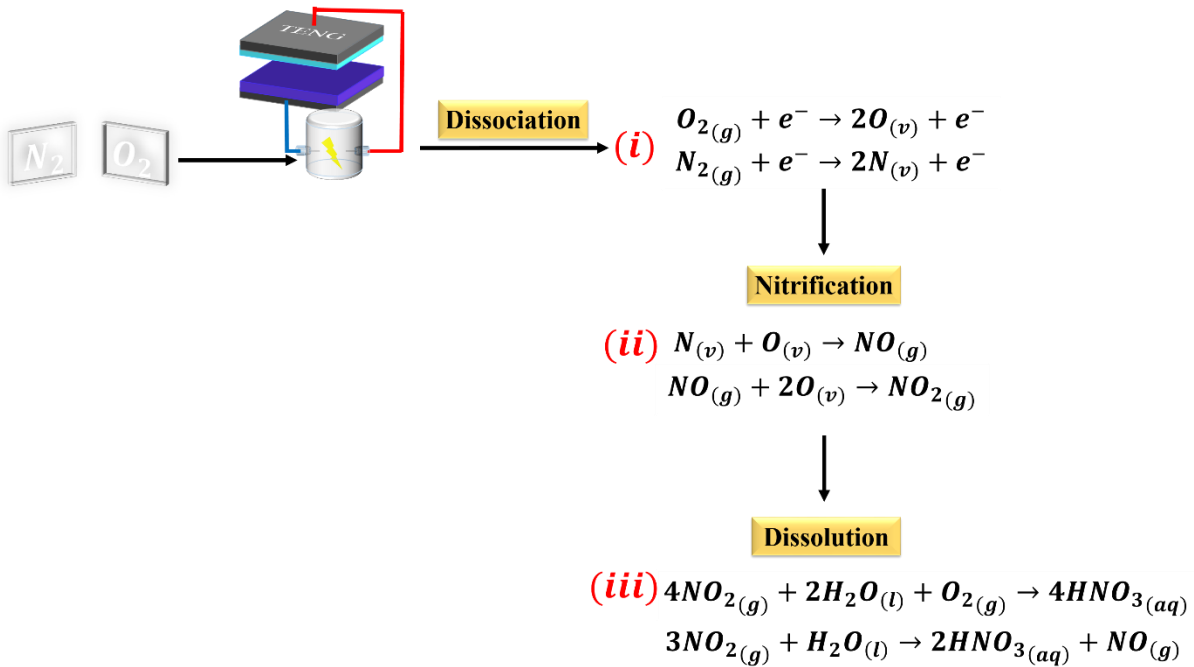
Figure 4-17 Schematic of the conversion from nitrogen and oxygen molecules to nitrogen dioxide and nitric acid in TENG-microplasma nitrogen fixation system.

Particularly, during the microplasma discharge process, the high electric field strength between needle electrodes excites these nitrogen and oxygen atoms in the air between needle electrodes. This excitation generates high energy electrons and causes molecular N_2 and O_2 to be dissociated into nitrogen and oxygen free radicals, as shown in the following equations:

$$O_{2(g)} + e^- \rightarrow 2O_{(v)} + e^- \tag{7}$$

$$N_{2(g)} + e^- \rightarrow 2N_{(v)} + e^- \tag{8}$$

These free radicals further lead to the generation of nitrogen oxides by different reaction routes. Among them, the essential reaction can be considered as:

$$N_{(v)} + O_{(v)} \rightarrow NO_{(g)} \tag{9}$$

$$N_{(v)} + 2O_{(v)} \rightarrow NO_{2(g)} \tag{10}$$
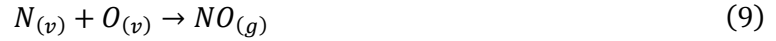
The synthesized nitrogen oxides are then collected via dissolving them into DI water placed in the discharge reactor, forming nitric acid and complete the nitrogen fixation, as shown below：

$$4NO_{2(g)} + 2H_2O_{(l)} + O_{2(g)} \rightarrow 4HNO_{3(aq)} \tag{11}$$

To provide more evidences concerning these reactions, the emission spectrum of the discharge microplasma is shown as in **Figure** 4-18. The emission spectrum of the microplasma discharge driven by the TENG is recorded by Ocean optics USB 4000 spectrometer. The characteristic emission peaks of the dinitrogen and nitrogen free radical are observed, indicating the dissociation of dinitrogen molecules.

Ultra-high voltage output triboelectric nanogenerator
powered mechano-nitrogenous fertilizer supplier
THE HONG KONG POLYTECHNIC UNIVERSITY
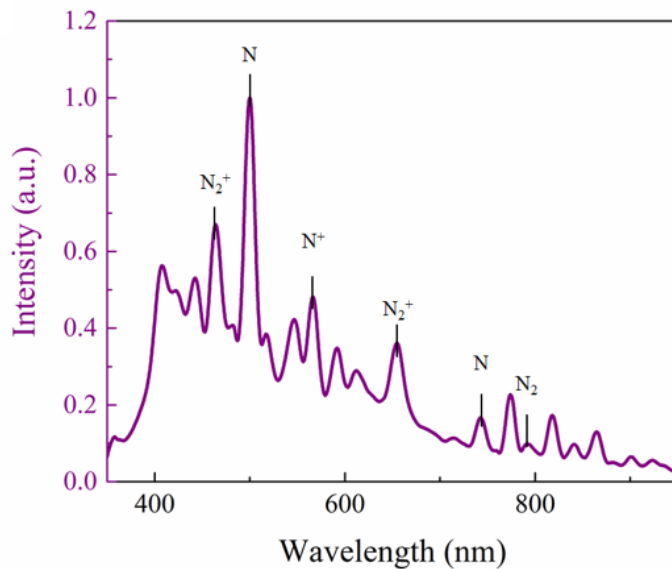
Figure 4-18 The emission spectrum of microplasma discharge.

To verify the subsequent generation of nitrogen oxides from the recombination of free radicals. Investigation were conducted to obtain the concentrations profile of nitrogen dioxide (NO_2) at different sampling distance. (**Figure** 4-19)

Ultra-high voltage output triboelectric nanogenerator
powered mechano-nitrogenous fertilizer supplier
THE HONG KONG POLYTECHNIC UNIVERSITY
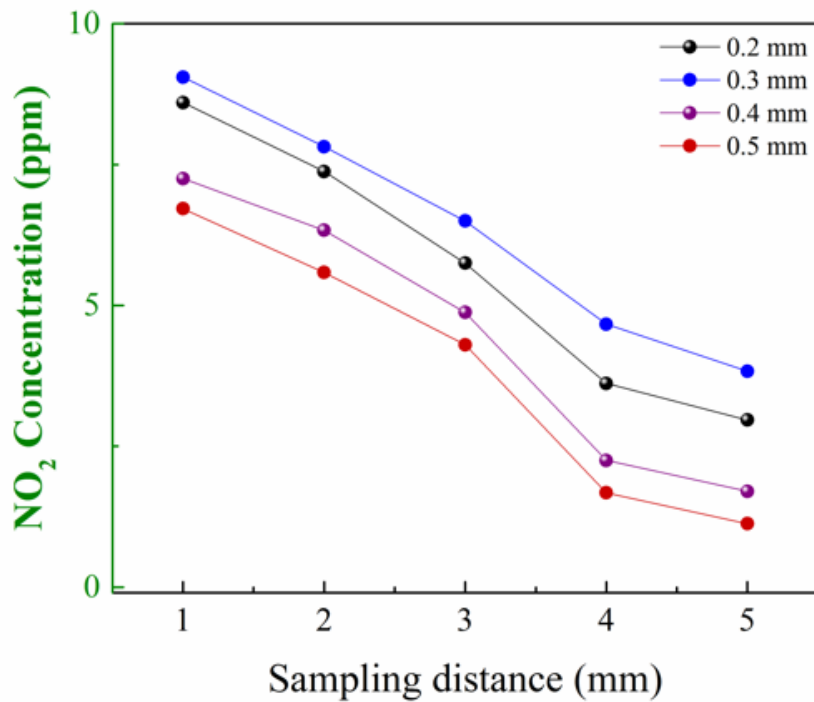
Figure 4-19 The concentration of nitrogen dioxide detected under different sampling distance.

Herein, the sampling distance was defined as the length between the discharge and the probe of a gas sensor (EDKORS ADKS-1) as shown in **Figure** 4-20. The results demonstrate that the NO_2 concentration increases with the decrement of sampling distance. This phenomenon confirms that NO_2 was generated during the microplasma discharge.

Ultra-high voltage output triboelectric nanogenerator
powered mechano-nitrogenous fertilizer supplier
## THE HONG KONG POLYTECHNIC UNIVERSITY
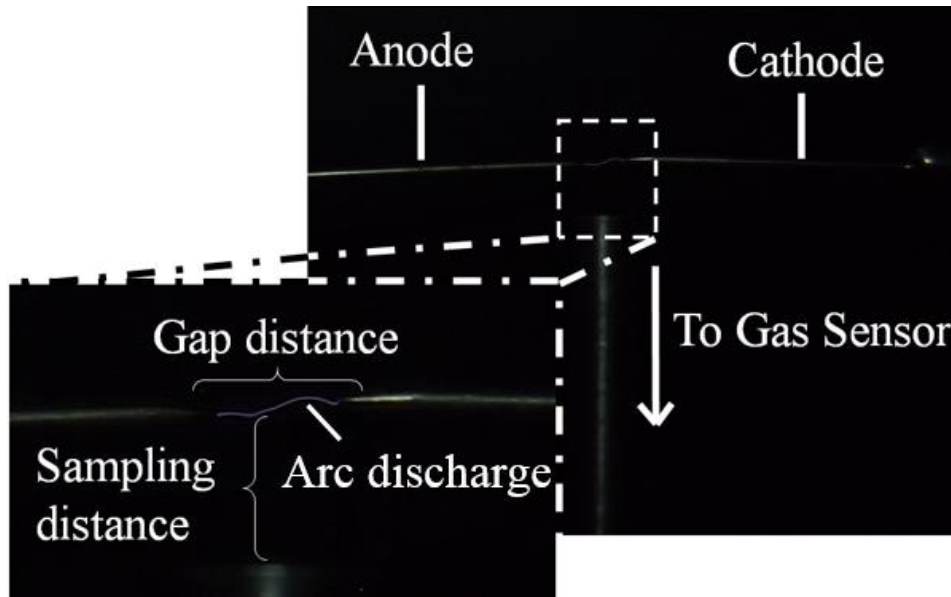
Figure 4-20 Schematic for nitrogen dioxide concentration measurement based on the EDKORS ADKS-1 gas detector.

In addition, the effect of gap distance between needle electrodes on the amount of produced NO_2 were also measured. As shown in **Figure** 4-19, it is interesting to notice that the concentration of NO_2 in microplasma discharge reactor reaches a maximum value when the gap distance is 0.3 mm. This is because the highest average discharge energy E_{ave} is arrived in this case as shown in figure 4-16, which means that more ionized gas is generated during this discharge process to obtain the maximum amount of NO_2.

The generated NO_2 is supposed to be dissolved into water to form the nitric acid solution, and its Raman spectrum after 12000 operation cycles is exhibited in **Figure** 4-22. Herein, shown in **Figure** 4-21 the strong emission bands at 1046 cm^{-1} and at 688 cm^{-1} are observed, which

correspond to the symmetric stretching ν_{1s} NO_3 vibration and the NO_2 bending δ O-N-O mode vibration, respectively. Moreover, a minor shoulder peak can be observed at 929 cm^{-1} and 1304 cm^{-1}, which are attributed to ν N-(OH) and ν_s NO_2 vibration modes, respectively. Therefore, it is reasonable to deduce that nitric acid has been successfully synthesized via TENG-driven microplasma discharge.
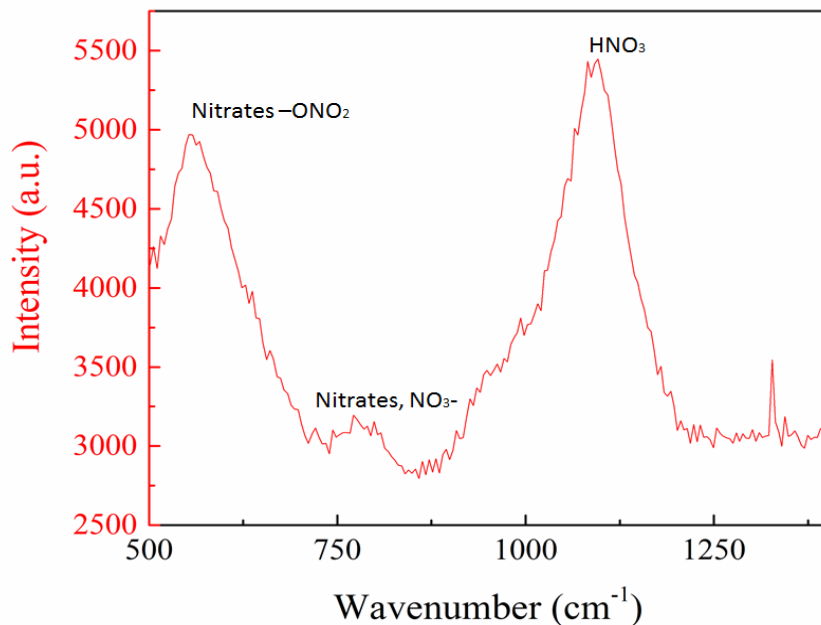
Figure 4-21 Raman spectrum of the prepared nitric acid solution in discharge reactor.

It is noticed that the nitrate concentration in nitric acid increases with the extended operation time of the nitrogen fixation system as illustrated in **Figure** 4-22. The nitrate concentration in the range of 0-2000 ppm was detected by a spectrograph (HORIBA,

Wong Man Chung

LAQUAtwin-NO3-11). The peak nitrate concentration of about 250 ppm is arrived when the operation time and gap distance are 400 min and 0.3 mm, respectively.

In this respective, the energy efficiency of the nitrogen dioxide can be calculated as following. The force acted onto the TENG is given as 70 N with a frequency of 7 Hz. The mechanical energy applied in one second will be 4.9 J. Secondly, the concentration of the nitrogen dioxide was measured to be 9 ppm. Since the sampling rate of the gas sensor is 4.167 ml/s, in one second, the volume of generated nitrogen dioxide is given by

$$4.167 \, ml \, \times \, (9 \times 10^{-6}) = \, 37.5 \, \times 10^{-6} \, ml \tag{12}$$

Correspondingly, in one second, the moles number of generated nitrogen dioxide is 1.53×10^{-9} mol. Therefore, the efficiency is calculated as

$$4.9 \, J \, \div \, (1.53 \, \times 10^{-9} \, mol) = \, 3197 MJ/mol \tag{13}$$

Even though the energy efficiency of the TENG-microplasma based nitrogen dioxide synthesis is lower than that of Haber Bosch process and gliding arc-based nitrogen oxide synthesis (37.1 MJ/mol), this novel strategy still processes unique advantages whereas other methods lacked. Especially, the TENG-microplasma nitrogen fixation can harvest ambient and ignored mechanical energy to realize in-situ nitrogen fixation, which benefits relieving energy shortage.

Wong Man Chung
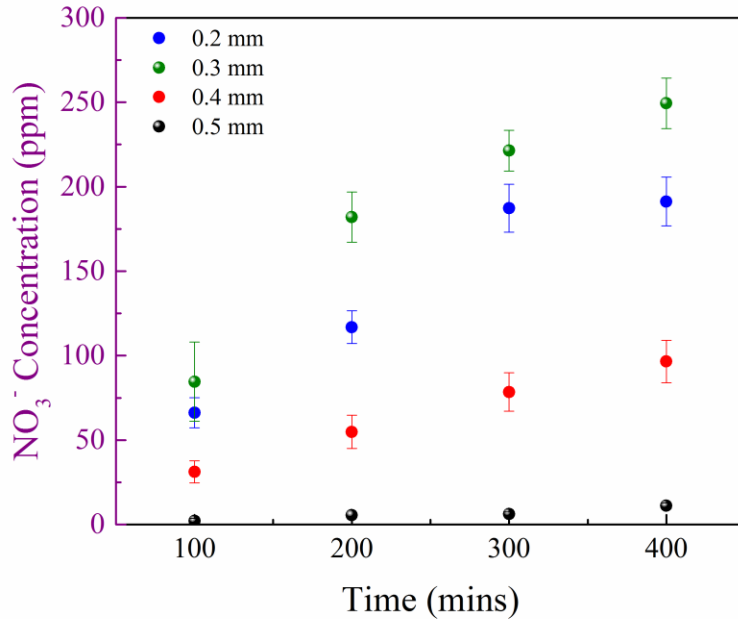
Figure 4-22 The nitrate concentration in nitric acid solution detected at the different operation time of TENG-microplasma nitrogen fixation system.

4.4.1. Preparation and characterization of the as-prepared nitrogen dioxide and nitrogenous fertilizer

The generated nitric acid can be utilized in various fields, and its primary consumption is for the synthesis of nitrogenous fertilizer, including $NaNO_3$, NH_4NO_3 and $CaNO_3$ etc. These synthetic nitrogenous fertilizers are essential for the agricultural development. **Figure** 4-23 demonstrate an application scenario of the TENG-microplasma nitrogen fixation system as the

sustainable, environmental-friendly and safe *in-situ* nitrogenous fertilizer supplier. Specifically, in the system, TENG with the size of 64 cm^2 is covered with artificial turf and then buried inside a pothole (highlighted with blue blanket in Figure 4-23).
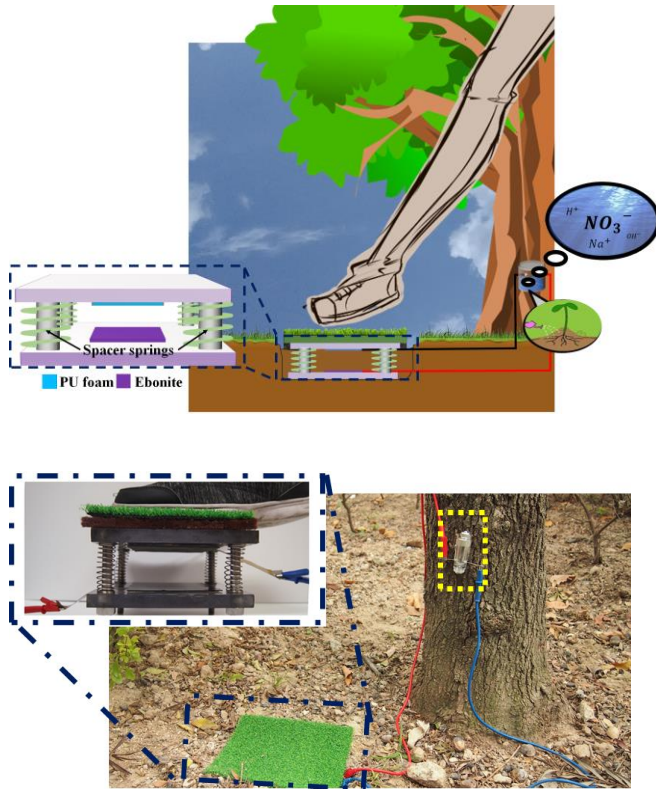
Figure 4-23 Schematic and Photograph demonstrating the setup of TENG-microplasma nitrogen fixation system as nitrogenous fertilizer supplier.

Ultra-high voltage output triboelectric nanogenerator
powered mechano-nitrogenous fertilizer supplier
**THE HONG KONG POLYTECHNIC UNIVERSITY**

Once the TENG is triggered by the ambient mechanical stimuli, such as human walking, the mechanical energy will be harvested and converted into electricity, and the output V_{oc} can reach up to above 1000 V as shown in **Figure** 4-24.
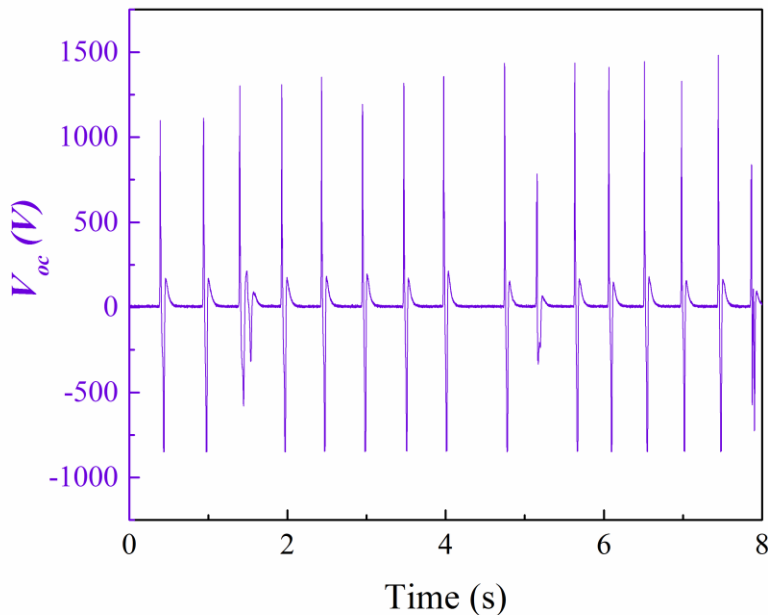
Figure 4-24 Open-circuit voltage generated by the buried TENG driven by human walking.

This output voltage is applied between two needle electrodes inside the microplasma discharge reactor (highlighted with yellow blanket in figure 4-23) for the microplasma discharge and the generation of NO_2. With regarding to safe direct *in-situ* nitrogenous fertilizer fabrication, weak sodium bicarbonate solution was placed inside the discharge reactor to absorb and react with

Ultra-high voltage output triboelectric nanogenerator
powered mechano-nitrogenous fertilizer supplier
**THE HONG KONG POLYTECHNIC UNIVERSITY**

the generated NO_2 for forming the sodium nitrate ($NaNO_3$) solution as fertilizer, instead of nitric acid.
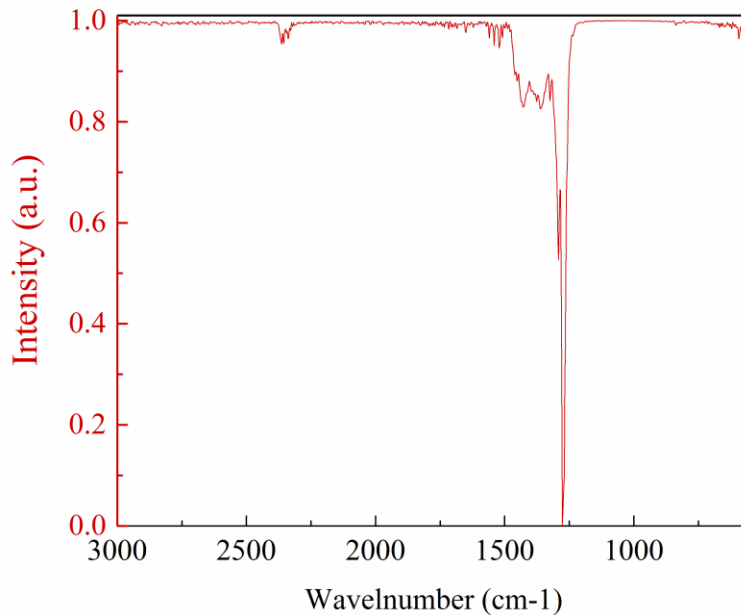
Figure 4-25 FTIR spectrum of the prepared NaNO3 solution.

Figure 4-25 illustrates the Fourier-transform infrared spectroscopy (FTIR) analysis of the solution, and the transmittance characteristic peak of N-O stretching vibration group is found in the wave numbers of 1290 cm^{-1}, 2431 cm^{-1}and 875 cm^{-1}, [227] [227] [227] which confirms the successful preparation of $NaNO_3$.

As a demonstration, these synthesized $NaNO_3$ are utilized as fertilizers to benefit the growth of green bean. A comparison between two green bean samples with and without addition

of NaNO₃ fertilizers generated by TENG-microplasma nitrogen fixation system was conducted. Green bean seeds were cultivated in Petri dishes at 28 °C in darkness for three days. Afterwards, uniform seedlings were transferred and placed in an incubator with DI water for growth with climate control. Continuous NaNO₃ solution was supplied to one sample, while only DI water was supplied to the reference sample. After growth for one week, the fresh weight of total biomass was measured for evaluating the growth rate of samples. The results reveal that after growth for one week, the fresh weight of total biomass (leaves, stems, and roots) of the sample with NaNO₃ addition is 1.4-fold heavier than that of the sample without NaNO₃, as shown in Figure 4-26.
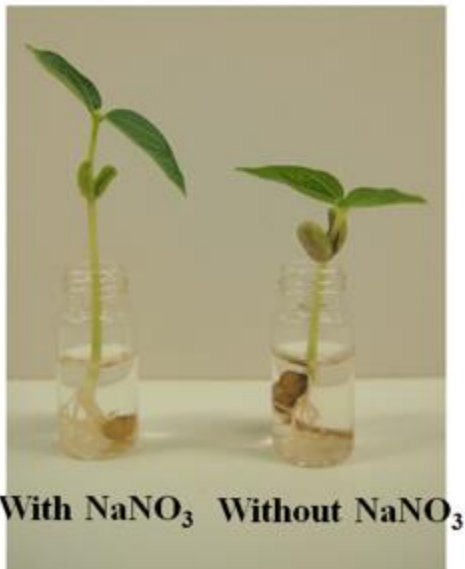
Figure 4-26 Comparison in growth rates between green bean samples with and without NaNO₃ addition.

This indicates the feasibility and application potential of the self-powered TENG-microplasma nitrogen fixation system as the mechano-nitrogenous fertilizer supplier. Compared to the other nitrogen fixation technologies, such as traditional Haber Bosch process, the TENG-microplasma nitrogen fixation system makes full use of the dissipated, ignored and wasted ambient mechanical energy for the synthesis of nitrogen compounds and therefore possesses the unique features of energy-saving and environmental-friendliness. Meanwhile, the TENG-microplasma nitrogen fixation system also avoids the operation environment of high temperature and high pressure in Haber Bosch process, leading to the improved system safety. Additionally, the simple structure and low cost of our system also contributes to an improved portability and usability for practical application. Therefore, the self-powered TENG-microplasma nitrogen fixation is considered as an attractive alternative to traditional nitrogen fixation technology. The detailed comparison between the TENG-microplasma nitrogen fixation and the other nitrogen fixation technologies is summarized in Table 2. Concerning the TENG driven nitrogen fixation system working in a harsh condition such as high temperature, and humid environment. Although the performance of the system hasn't been investigated quantitatively. However, it can be regarded that the performance of the fixation system is strictly depended on the efficiency of the mechano-electrical conversion of the TENG as the discharge electrode is isolated from the environment. Since the TENG is buried in a pothole covered with artificial turf which provides a partially isolated working environment from the ambient. Therefore, it is reasonable to assume that the performance of the system will remain the same.

Wong Man Chung

Ultra-high voltage output triboelectric nanogenerator
powered mechano-nitrogenous fertilizer supplier
**THE HONG KONG POLYTECHNIC UNIVERSITY**

Table 3 Comparison between traditional nitrogen fixation method with the TENG-microplamsa nitrogen fixation.

Methods	Energy source	Raw materials	Synthetization Condition	Site of Synthetization	Product	Emission
The Haber–Bosch process	Fossil fuel	Natural gas, air, K^+, Fe^{3+} catalyst etc.	High pressure, high temperature	Centralized	Ammonia	Carbon dioxide
Biological nitrogen Fixation	Adenosine triphosphate (ATP), sugar	Microbial organisms with nitrogenase enzymes	Ambient temperature and pressure	Depends	Ammonia	Adenosine diphosphate (ADP), Inorganic phosphate, etc.
Metallocomplex nitrogen fixation	Chemical energy	Strong metal reducing agents and transition metal complexes	Ambient temperature and pressure	Depends	Ammonia	Nil
Plasma based nitrogen fixation	Fossil fuel, renewable energy e.g. wind, solar, etc.	Air, water	Depends	Centralized	Nitric oxide	Nil
TENG-microplasma nitrogen fixation	Wasted or renewable mechanical energy	Air, water	Ambient environment	*In-situ*	Nitrogenous fertilizer	Nil

The proposed novel TENG-driven microplasma nitrogen fixation system paves the way to prepare the nitrogen compound from air in an energy-saving, environmental-friendly, flexible, and safe way.

Wong Man Chung

Ultra-high voltage output triboelectric nanogenerator
powered mechano-nitrogenous fertilizer supplier
**THE HONG KONG POLYTECHNIC UNIVERSITY**

4.5. Conclusion

In summary, a TENG-driven microplasma discharge-based nitrogen fixation system has been developed by integrating a high voltage output TENG with an microplasma-discharge reactor. Based on maximized electrons affinity difference between contact materials and optimized pore sizes of PU foam, the TENG can steady output a high voltage of about 1300 V driven by mechanical stimuli without any auxiliary. The generated voltage is directly applied between needle electrodes of the discharge reactor for atmospheric microplasma discharge, and the effect of gap distance on discharge process, including discharge voltage, discharge current and average discharge energy per TENG operation cycle, have been systematically investigated. It is observed that the nitrogen gas in air can be successfully converted into nitrogen compound, including nitrogenous oxide and nitric acid solution, via the TENG-driven discharge process to finally realize the nitrogen fixation. The NO_3^- concentration of 250 ppm can be achieved after continuously operating the TENG driven fixation system for 400 min. Furthermore, the TENG-microplasma nitrogen fixation system was employed as a mechano-nitrogenous fertilizer supplier. After driving the system by human walking stimuli, the $NaNO_3$ fertilizer is produced to benefit the green beans growth. This work provides a feasibility to develop an energy-saving, environmental-friendly, flexible, and safe nitrogen fixation route.

Chapter 5   Mechanical controlled AIE elastomer emission

5.1. Introduction

Fluorescent organic molecules have been vigorously investigated in the past two decades,[102, 124] due to the interesting photophysical properties accompanied by their intrinsic and lightness. For these applications, it is desirable for the fluorescent that in these applications to be tunable in terms of the luminescent intensity in a simple and reversible way.

Research on AIE emission tuning previously had been focused on changing AIE luminogen aggregation either by a temperature gradient, the polarity of solvent, grinding or surface group, etc.[124, 228] However, these changes are essentially a chemical method and required a different form of energy input. An *in situ* and mechanical excitation modulated the AIE luminescence intensity from a novel phosphor with a fixed composition is rarely reported. Since the pioneering work by Tang et al., numerous reports on AIE have been published. [116] Which include applications of AIE luminogens in such as fluorescent sensors, biological probes, and lighting devices. They based their operation on the restriction of intramolecular rotation of the luminogens. AIE dispersed state, when light energy excited an AIE molecule the phenyl rotors in an AIE molecule undergo dynamic intramolecular rotations against its silole stator which non-radiatively annihilates its excited state and renders its molecule non-luminescent. On the other hand, when AIE in aggregates state, since most AIE cannot adopted a stacking through a pi-pi interaction due to its non-planar structure. Thereby, these intramolecular rotations are physically restricted.[116]

Wong Man Chung

This restriction of intramolecular rotations opens the radiative pathway. As a result, the AIE molecules become emissive in the aggregate state. Based on these studies, the limited intramolecular rotation of the AIE luminogens is regarded as a significant factor that causes AIE phenomenon. On the contrary, this factor can also be satisfied by means of other method.

For instance, macromolecules attributed with AIE luminogens is regards as a promising composite owning to its enhanced emission state.[112] Generally, AIE incorporated macromolecules (AIE macromolecules) are a novel class of luminescent materials that incorporate typical AIE luminogen into the polymer structures. Since both of the polymers structures, topology, functionalities and morphology can be manipulated. Hence, it provides an enormous advantage to be applied in various circumstances because of their excellent processability, high emission efficiency in the aggregated states, etc. Therefore, it should be feasible to utilize this AIE macromolecules approach to realizes the tuning of emission from AIE luminogen solely based on mechanical stimuli.

5.2. Structure and working principle of mechanical stimulation responsive fluorescence AIE Elastomer

The AIE macromolecules generally imposes a steric restriction onto the rotation of these phenyl rotors of the AIE luminogen based on the polymer inherent long-chain length, such that the intensity of AIE macromolecules emission may be mechanically tunable.

AIE macromolecules of various structures such as linear, stat-shaped, crosslinked can be fabricated through numerous methods. These structures generally aimed either to integrate archetypical AIE luminogens into monomer or empowered these AIE luminogens as crosslinker and directly ultizaed as polymerization agent. Another method is the integration of archetypical AIE into monomer, typical methods include direct linkages of AIE into monomers or copolymerization AIE luminogens with other polymers. These two basic strategies can be further modified with an AIE luminogens act as a side chain of the polymer or as a terminator of individual polymer chains.

In this work, AIE luminogens was empowered to act as a crosslinker to the polymers. This is realized by the modification of AIE luminogen. Generally, an archetypical AIE luminogen Tetraphenylethene or Tetra(4-hydroxyphenyl)ethene(TPE) was first modified such that each four of the phenyl rotors are all 1-butene terminated. The location of the olefin of the AIE luminogen empowered it with the ability function as the crosslinker of elastomer as shown in **Figure** 5-1.
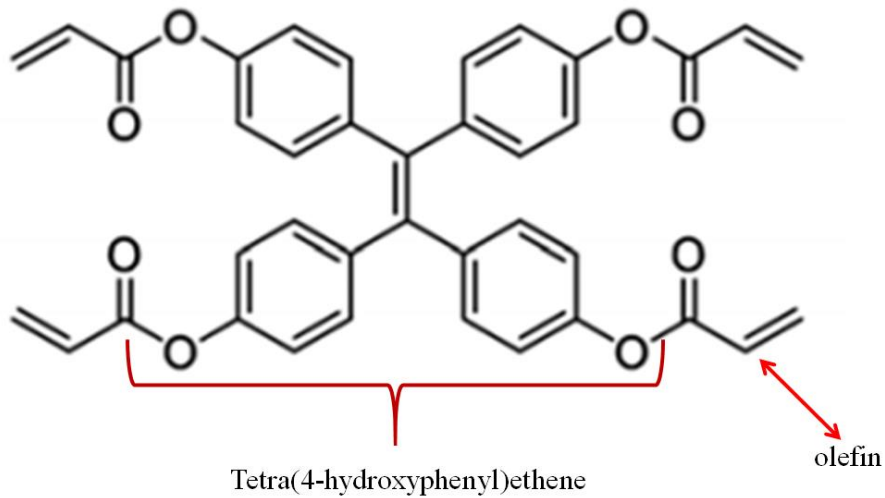
Figure 5-1 Schematic of AIE crosslinkers.

The elastomer fabricated for this work is hydrogen terminated polydimethylsiloxane, the structure of the elastomer fabricated adopted a topology of radical crosslinking that the phenyl rotor of an AIE luminogen is linked with the end of a siloxane polymer. As shown in the **Figure 5-2,**
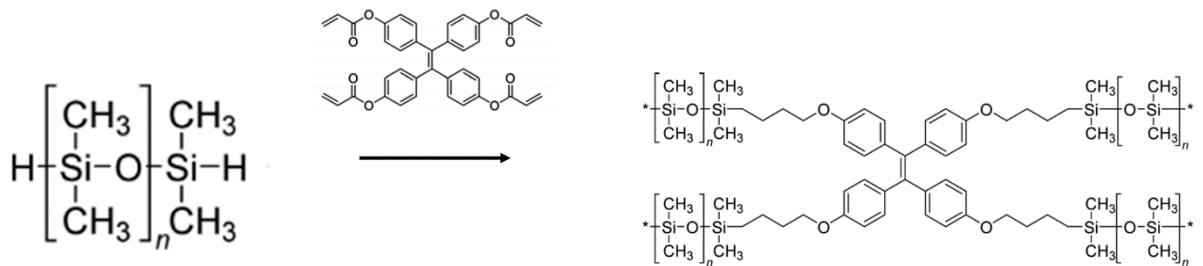
Figure 5-2 Preparation of elastomers PDMS-TPE

Wong Man Chung

By adapting this topological structure, the AIE luminogen inside the elastomer should be more receptive to motion restriction upon structural rigidification.

The working mechanism of the mechanical stimuli responsive fluorescence of AIE elastomer is proposed as the following. Firstly, after curing the TPE crosslinked elastomer, an AIE fluorescence from this elastomer upon UV illumination. This fluorescence is owning to the entanglement between these polymer chains prohibited the intramolecular motions of the phenyl rotors in the TPE luminogen. Once an organic solvent was dissolved into the AIE elastomer, the volume increases between each polymer chain would decreases the entanglement of the polymer chain. The elastomer becomes swollen, the phenyl rotors thereby have less restriction upon photon-excitation because the increases of void or free volume around the TPE luminogens restricts the molecular motions. As a result, a nonradiative decay occur inside the TPE luminogen, the AIE elastomer thereby become non emissive. Since the emission from the TPE luminogen in this case depended on the level of entanglement of the polymer chain and the void of volume around the TPE luminogens. By carefully modulating the degree of swelling of elastomer, and the free volume round the TPE luminogens, such that the free volume around the TPE elastomer reaches a critical value, results the emission of AIE elastomer can able to be modulated solely by mechanical energy stimuli. Therefore, the emission from AIE macromolecules may be mechanically tunable.

Wong Man Chung

5.3. Fabrication of the AIE elastomer

(1) The preparation of Tetra(4-((4-acryloxyphenyl) ethene crosslinker

The preparation process was carried out under a nitrogen atmosphere. Tertra(4-hydroxyphenyl)ethene were dissolved in anhydrous Dichloromethane in an ice bath for 20 mins. Then triethylamine was added into the mixture. Afterwards, acryloyl chloride dropwise added. The mixture was stirred for 24 hour and washed with aqueous sodium hydrocarbonate.

The precipitate was filtered off, and the filtrate was evaporated to dryness in vacuo. The residue was dissolved in Tetrahydrofuran, and the solution was washed by distilled water twice. The collected organic layer was dried by sodium sulfate, and the solvent was removed in vacuo.

(2) Preparation of AIE elastomer PDMS Gel.

PDMS polymer and the Tetra(4-(4-acryloxyphenyl)) ethene crosslinker were dissolved in dry toluene, and Karstedt's catalyst (90 mM xylene solution) was added to the mixture. The mixture was poured into a PTFE mold and heated to 70 degree Celsius for 12 hours. The set elastomer was immersed in THF for 24 h and dried in vacuo.

5.3.1. Emission characterization of AIE crosslinker

The optical characterization of the Tetra(4-((4-acryloxyphenyl) ethene crosslinker, fluorescence and UV-vis absorption were recorded.

In the UV-Vis measurement, the absorption spectra shown a maximum appeared at 300 nm where the crosslinker with high molar extinction, indicating $\pi \rightarrow \pi^*$ transition.
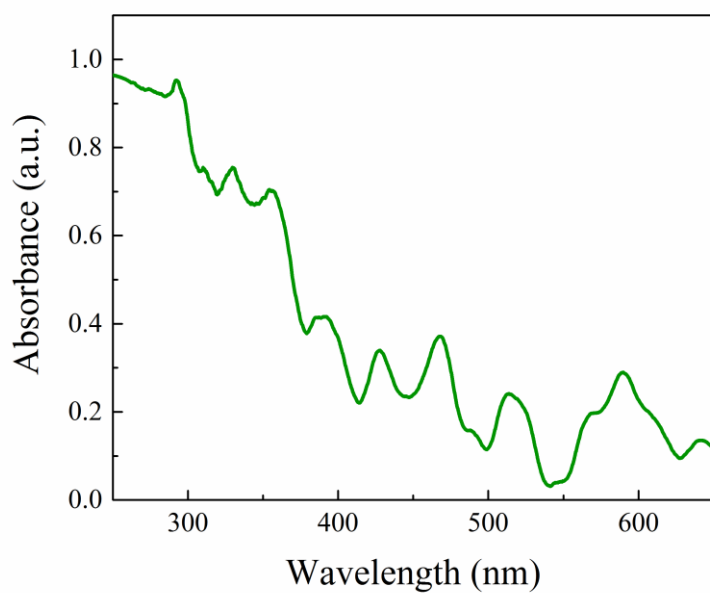
Figure 5-3 UV-vis spectra of AIE crosslinker
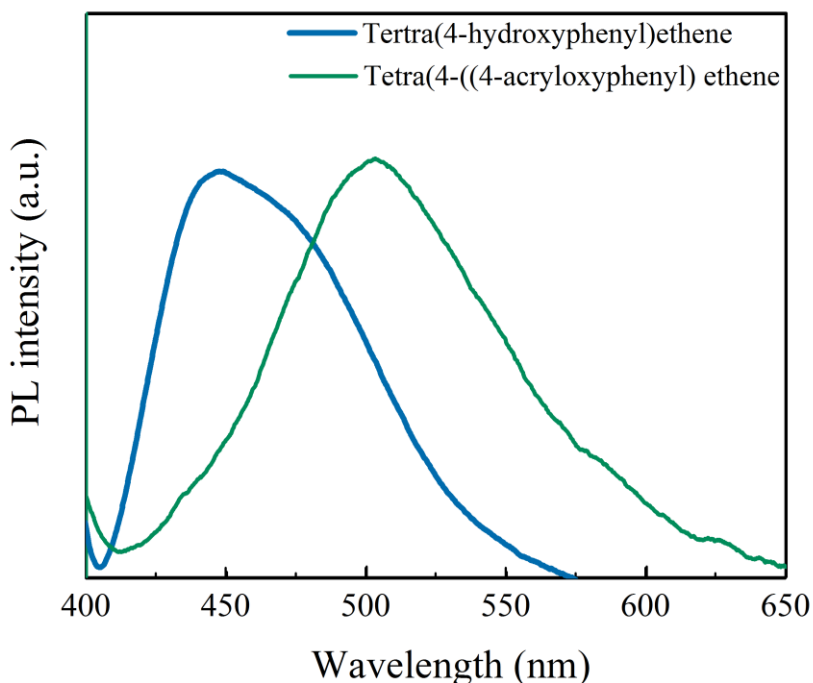
Figure 5-4 Emission spectrum of AIE luminogen and AIE crosslinker

The fluorescence measurement demonstrated inherent AIE characteristic in **Figure** 5-4. To be precise, the Tetra(4-((4-acryloxyphenyl) ethene crosslinker dissolve a good solvent will not exhibit fluorescence. On the other hand, fluorescence intensity increases significantly as the crosslinkers aggregated as it dissolved in water. The emission is around 473 nm. This phenomenon demonstrated that the crosslinker can acted as a conventional crosslinker for a radical polymerization and an AIE luminogen.

Wong Man Chung

5.4. Elucidation of AIE elastomer

5.4.1. Mechanical response of AIE elastomer

The curing of H-terminated PDMS through the Tetra(4-((4-acryloxyphenyl) ethene crosslinking agent was realized with evaluated temperature of 60 degree Celsius. The mechanical properties of the elastomer were investigated by a tension experiment at ambient environment. During the experiment, a dog bone specimen was prepared with the H terminated PDMS of molecular mass of 10,000. The obtained stress strain curve is shown in **Figure** 5-5.
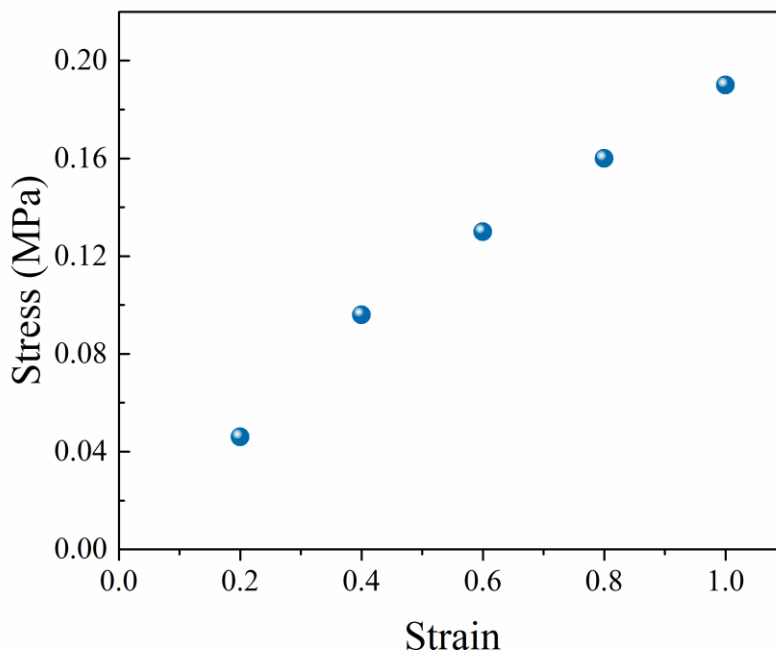
Figure 5-5 Stress-strain curves measured at room temperature for the AIE elastomer

Wong Man Chung

This result demonstrated the Tetra(4-((4-acryloxyphenyl) ethene crosslinked PDMS shown a comparable mechanical property of these reported PDMS elastomers.

5.4.2. Optical property of the Tetra(4-((4-acryloxyphenyl) ethene crosslinked PDMS

To realizes a mechanically tuning of AIE, a study of the emission properties of the Tetra(4-((4-acryloxyphenyl) ethene crosslinked PDMS was conducted to examine the elastomer process the ability of AIE. Precisely, the study was based on the assumption that the free volume around the Tetra(4-((4-acryloxyphenyl) ethene change as the elastomer in different swelling level. Such that this level can be modulated results the AIE of the Tetra(4-((4-acryloxyphenyl) ethene can be directly controlled by mechanical stimuli.
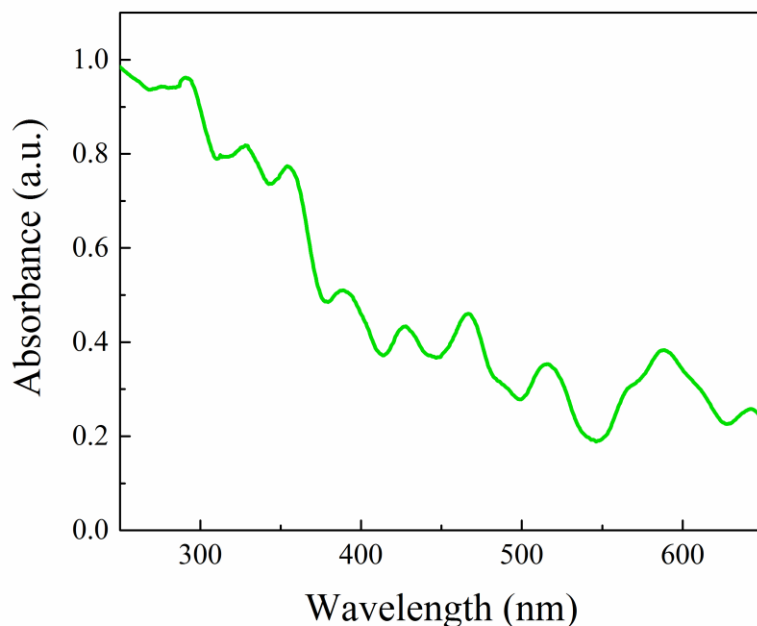
Figure 5-6 UV-Vis spectran of AIE elastomer.

Firstly, the spectra of UV-vis of the elastomer is shown in **Figure** 5-6, which is similar to that of AIE crosslinker.

Next, fluorescent study on the AIE elastomer was conducted. The emission wavelength of the elastomer is red shifted as the AIE elastomer has been swelled, compared with the Tetra(4-((4-acryloxyphenyl) ethene crosslinker before the elastomer crosslinked or the AIE elastomer in its ridged state. It can be suspected that the radical polymerization of the H-terminated PDMS and the Tetra(4-((4-acryloxyphenyl) ethene crosslinker cause a constrict of the rotation of the phenyl rotor

in the Tetra(4-((4-acryloxyphenyl) ethene, the fluorescent emission intensity will therefore decreased .

As a demonsstration, the AIE elastomer was immersed under various organic solvents. In the experiment, The AIE elastomer was immersed in Tetrahydrofuran, fluorescence response from AIE elastomer is measured upon the swelling of the elastomer reaches a quasi-stable state. Tetrahydrofuran is chosen as it is a one of the good solvents for PDMS elastomer. Once the AIE elastomer was well immersed in the Tetrahydrofuran. The fluorescence intensity of the AIE elastomer had significantly decreases to nearly zero. On the other hand, as the AIE elastomer was taken out of the Tetrahydrofuran and placed in an ambient environment, the fluorescence intensity raised back once the Tetrahydrofuran begin to evaporate and the swelling of the AIE elastomer decreased, the result is shown in **Figure** 5-7.
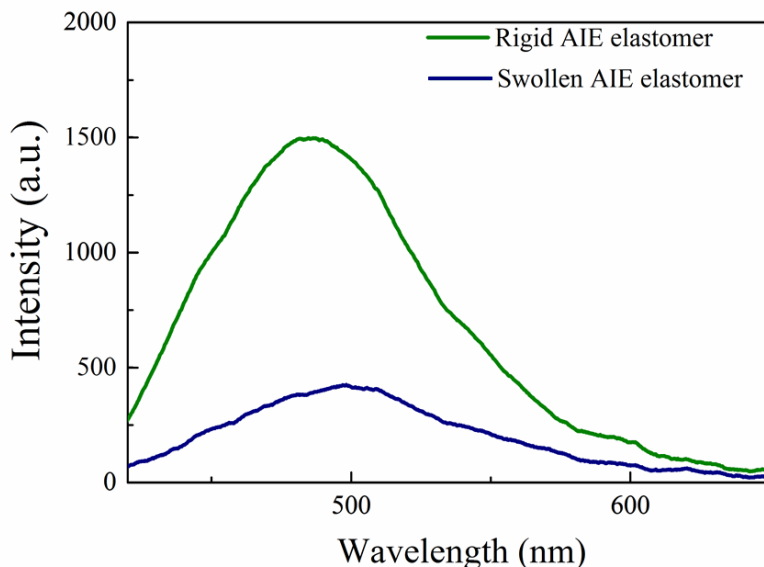
Figure 5-7 Fluorescence emission of AIE elastomer in different states.

To visualizes the changes in Fluorescence intensity, **Figure** 5-8 shown AIE elastomer fluorescence intensity as it washed with different solvent. During the swollen state of the AIE elastomer, if Tetrahydrofuran was washed and diluted with poor solvent such as methanol or ethanol. Since these poor solvents not only posed a weak or no swelling ability upon the AIE elastomer, but also have the capability to dilute the Tetrahydrofuran. Therefore, the free volume around the phenyl rotor of the Tetra(4-((4-acryloxyphenyl) ethene decreases, results the restriction of intramolecular rotation of these phenyl rotors. The fluorescence response thereby increased again.

Wong Man Chung
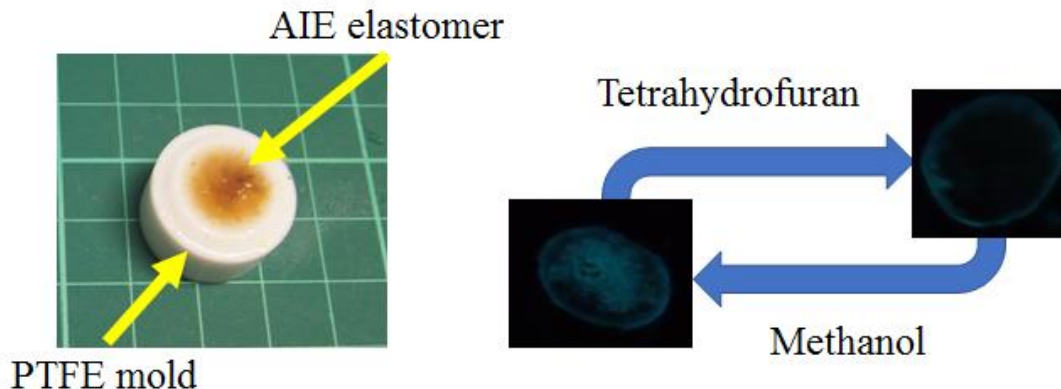
Figure 5-8 Modulation of AIE elastomer emission intensity via solvent exchange method.

5.4.3.　Mechanical modulation of AIE intensity

Based on controlling sizes of the free volume surrounding the phenyl rotors Tetra(4-((4-acryloxyphenyl) ethene through swelling level of AIE elastomer. The direct mechanical tuning fluorescence of AIE can be realized. Prior to the results in the previous section and according to the swelling ratio of various solvent. The organic solvent that posed the highest possibility is chlorobenzene, or Tetrahydrofuran. However, in this stage, since the swelling causes the stress unable to restrict the motion of the AIE luminogen rotor. Thereby, radiative path cannot be established.

5.5. Conclusion

In this section, a mechanical tuning of AIE luminogen based on tetraphenylethene (TPE-CL) and following hydrosilylation reaction of TPE-CL and H-terminated PDMS was proposed.

Wong Man Chung

examined to construct AIE elastomers. Facile progress of the preparative reaction was confirmed by spectroscopy studies. A tensile test of the obtained sample strips showed archetypal elastomeric behavior, while the chain length of employed PDMS substantially affected on their mechanical properties such as Young's modulus and maximum strain. UV−vis absorption measurement upon increase of TPE content in the elastomeric samples represented the homogeneous distribution of TPE- in them. Fluorescence of the elastomers was found to be stimuli-sensitive against employed organic solvents, and reversibility of these responsiveness was also confirmed. The AIE characteristics are clearly responsible for these features, which is susceptible for intramolecular rotation. The combination of elastomeric polymer network and AIE luminogen will open a new horizon for material chemistry, such as sensing materials for volatile organic compounds.

Wong Man Chung

Chapter 6   Conclusion

In this thesis, three strategies have been developed and realized mechanical energy harvesting and converting utilizing luminescence materials and triboelectric nanogenerator. Firstly, a tuning of piezophotonic-effect induced luminescence and color gamut via modulating mechanical excitation is realized. Secondly, a triboelectric nanogenerator capable of powering microplasma discharge-based nitrogen fixation driven by harvesting ambient mechanical energy is fabricated. Thirdly, a mechanical energy tuning AIE emission tuning based on AIE elastomer was discussed. The main conclusions can be briefly described as follows:

A convenient physical approach of temporal and remote tuning of light-emitting wavelength and color is piezophosphors demonstrated. By means of temporal tuning, it is an unconventional method that by modulating the frequency of the mechanical excitation, emission wavelength from a ZnS:Al, Cu piezophosphors induced by can be tuned in an *in-situ* manner. Furthermore, a mechanistic investigation was conducted for the temporal tuning. It suggests that the observed tunable piezophotonic emission is ascribed to the steepened tilting of the energy band structure in the piezophosphors under a high frequency of mechanical excitation. Subsequently, different charge traps are thereby activated or saturated. Experimentally, evidences are provided to proof this intriguing tuning emission peak wavelength and color of ZnS: Al, Cu piezophosphors by modulating the frequency of the mechanical excitation in the form of a magnetic field. Moreover, RGB full-color and white light with tunable color temperature are achieved via photon energy coupling with YAG:Ce and $(Ca_{1-x}Sr_x)S$:Eu persistence phosphor. These results offer new

insight and understanding of the piezophotonic emission mechanism. These novels finding of the luminescent materials with the ability to be accessed and modulated remotely will offer opportunities for applications in the fields of mechanical optical sensing, piezophotonic, energy harvester, nondestructive environmental surveillance, novel light sources, and displays.

A novel triboelectric nanogenerator -driven microplasma discharge-based nitrogen fixation system (TENG-microplasma nitrogen fixation system) reactor was demonstrated. The application of traditional microplasma discharge-based nitrogen fixation technology is severely limited because this route generally requires a high-voltage input, leading to the large power consumption, complicated apparatus fabrication, high cost, and safety risk etc. Herein, A TENG-driven microplasma discharge-based nitrogen fixation system is conceived by integrating a TENG and a discharge reactor. The novel high voltage output TENG with simple structure was designed based on evaluating contact electrification ability of different materials and was prepared using polyurethane foam and ebonite sheet as contact materials. It could provide a high voltage output of about 1300 V and a low current output of about 60 μA driven by an unpretentious mechanical energy input, capable of instantaneously converts a basic human–TENG interactions into a large voltage directly without the requisition of neither supplementary nor magnification entity. TENG performance characterization was conducted, demonstrated the robustness and durability of the TENG. Furthermore, the generated voltage is directly applied on electrodes of the discharge reactor for atmospheric microplasma discharge, where the nitrogen gas in the air is successfully converted into nitrogenous compound, including nitrogen dioxide and nitric acid solution. Characterization and optimization of the TENG-microplasma nitrogen fixation system was also

Wong Man Chung

conducted, such that the highest amount of nitric acid produces had been achieved. The TENG-microplasma nitrogen fixation system can serve as a nitrogenous fertilizer supplier, and correspondingly, $NaNO_3$ fertilizer was produced via driving the system by human walking stimuli for crop cultivation. This study offers a promising atmospheric nitrogen fixation strategy with energy-saving, environmental friendliness, flexible operation and high safety. work is particularly timely given the recent surge of interest in TENGs high voltage applications, and such findings can motivate the exploration of coupling and implementation of TENG based on TENG critical behaviors.

Fluorescent organic molecules have been vigorously investigated in the past two decades due to the interesting photophysical properties accompanied by their intrinsic and lightness. For these applications, it is desirable for the fluorescent that in these applications to be tunable in terms of the luminescent intensity in a simple and reversible way. Therefore, a strategy is purposed based on utilizing AIE macromolecules approach to realizes the tuning of emission from AIE luminogen solely based on mechanical stimuli. However, the intramolecular motion of rotor rotation restriction in the aggregated state is suspected to be not a necessary condition for AIE to occur, an alternative strategy may exist for the tuning of AIE. Therefore, a method is proposed in term of applying mechanical stress to the AIE macromolecules composite to control the free volume or void around the AIE luminogen, such that restricting the molecular motion of AIE luminogen and these nonradiative decay. Thereby, the emission intensity can be enhanced.

6.1. Future prospect

This thesis has proposed some strategies and concepts based on utilizing luminescence materials and triboelectric generator to realized harvesting and conversion of mechanical energy. Based on the current results, some issues deserve further investigation.

Specifically, for the frequency tuning the piezoluminescence emission wavelength in chapter 3, there are few aspects that deserved in-depth investigations, they are the emission duration of piezoluminescence and the ranges of *in situ* tunable emission wavelength from a piezophosphor, also the responsiveness of a piezophosphor also required further investigation, either the resultant emission intensity from the phosphor and the turnability under a more moderated temporal of mechanic excitation. For TENG nitrogen fixation system illustrated in chapter 4, the efficiency of nitrogen fixation needed to improve since the rates of conversion from nitrogen gas to nitric acid should be further enhanced. This enhancement may be arising from catalytic implement inside the discharge reactor or advancing the output power of the current triboelectric nanogenerator by different types of smart material. The AIE tuning based on mechanical energy stimuli, the AIE macromolecules or AIE elastomer is recommended for the realization of the tinning. The deformation of the AIE elastomer when it in its swollen state hinders the interaction between the mechanical energy input and the AIE luminogen. Thereby, an optimized elastomer host with sufficient elasticity to minimized deformation during swollen state and a free void that enable the rotation of these phenyl rotor.

Wong Man Chung

THE HONG KONG POLYTECHNIC UNIVERSITY

Mechanical energy has existed in an ambient environment and recognized as a promising renewable energy source. Generally, the ability to fully utilize the energy and the effect upon different materials based on the mechanical energy properties gives rises to important issues such as promoting the practical application of the energy harvesting devices and expanding the understanding of the conversion of mechanical energy with different material.

The energy converting efficiency can be improved by designing the materials energy band gap structures, optimizing the interaction between the dopant and host material, and controlling the interaction between the interface of these dopants and host based on their mechanical properties. Meanwhile, the management and storage of the generated or converted energy are also important for various applications. Although persistence phosphors and nitrogen-based energy storage have been used as examples in this work for realizing such an endeavor, it is vital if more system as such can be developed and diversified the mechanical energy harvesting and its subsequent conversion.

References

1. Priya, S. and D.J. Inman, *Energy harvesting technologies*. Vol. 21. 2009: New York

    Springer.

2. Chen, X., et al., 1.6 V Nanogenerator for Mechanical Energy Harvesting Using PZT

    Nanofibers. *Nano Letters*, 2010. 10(6): p. 2133-2137.

3. Elvin, N. and A. Erturk, Advances in energy harvesting methods. 2013: *Springer Science

    & Business Media*.

4. Fang, J., et al., Enhanced mechanical energy harvesting using needleless electrospun poly

    (vinylidene fluoride) nanofibre webs. *Energy & Environmental Science*, 2013. 6(7): p.

    2196-2202.

5. Zi, Y., et al., Harvesting low-frequency (< 5 Hz) irregular mechanical energy: a possible

    killer application of triboelectric nanogenerator. *Acs Nano*, 2016. 10(4): p. 4797-4805.

6. Wang, Z.L. and J. Song, Piezoelectric Nanogenerators Based on Zinc Oxide Nanowire

    Arrays. *Science*, 2006. 312(5771): p. 242-246.

7. Zi, Y., et al., Harvesting Low-Frequency (<5 Hz) Irregular Mechanical Energy: A

    Possible Killer Application of Triboelectric Nanogenerator. *ACS Nano*, 2016. 10(4): p.

    4797-4805.

8. Wang, Z.L., J. Chen, and L. Lin, Progress in triboelectric nanogenerators as a new energy

    technology and self-powered sensors. *Energy & Environmental Science*, 2015. 8(8): p.

    2250-2282.

Wong Man Chung

9.   Niu, S. and Z.L. Wang, Theoretical systems of triboelectric nanogenerators. *Nano Energy*, 2015. 14: p. 161-192.

10.   *Mechanical Energy Harvesting*, in *Energy Autonomous Micro and Nano Systems*. p. 115-151.

11.   Zhou, M., et al., A review on heat and mechanical energy harvesting from human – Principles, prototypes and perspectives. *Renewable and Sustainable Energy Reviews*, 2018. 82: p. 3582-3609.

12.   Wang, X., Piezoelectric nanogenerators—Harvesting ambient mechanical energy at the nanometer scale. *Nano Energy*, 2012. 1(1): p. 13-24.

13.   Sun, C., J. Shi, and X. Wang, Fundamental study of mechanical energy harvesting using piezoelectric nanostructures. *Journal of Applied Physics*, 2010. 108(3): p. 034309.

14.   Zhang, C., et al., Theoretical Comparison, Equivalent Transformation, and Conjunction Operations of Electromagnetic Induction Generator and Triboelectric Nanogenerator for Harvesting Mechanical Energy. *Advanced Materials*, 2014. 26(22): p. 3580-3591.

15.   Hu, Y., et al., Hybridizing Triboelectrification and Electromagnetic Induction Effects for High-Efficient Mechanical Energy Harvesting. *ACS Nano*, 2014. 8(7): p. 7442-7450.

16.   Harne, R.L. and K.W. Wang, A review of the recent research on vibration energy harvesting via bistable systems. *Smart Materials and Structures*, 2013. 22(2): p. 023001.

17.   Wang, Z.L., Progress in Piezotronics and Piezo-Phototronics. *Advanced Materials*, 2012. 24(34): p. 4632-4646.

18.   Wang, Z.L., W. Wu, and C. Falconi, Piezotronics and piezo-phototronics with third-generation semiconductors. *MRS Bulletin*, 2018. 43(12): p. 922-927.

19.   Wang, Z.L., On Maxwell's displacement current for energy and sensors: the origin of nanogenerators. *Materials Today*, 2017. 20(2): p. 74-82.

20.   Wang, P., et al., An Ultra-Low-Friction Triboelectric–Electromagnetic Hybrid Nanogenerator for Rotation Energy Harvesting and Self-Powered Wind Speed Sensor. *ACS nano*, 2018. 12(9): p. 9433-9440.

21.   Liu, F., et al., Electrical analysis of triboelectric nanogenerator for high voltage applications exampled by DBD microplasma. *Nano Energy*, 2019. 56: p. 482-493.

22.   Zi, Y., et al., Effective energy storage from a triboelectric nanogenerator. *Nature Communications*, 2016. 7: p. 10987.

23.   Liu, W., et al., Integrated charge excitation triboelectric nanogenerator. *Nature Communications*, 2019. 10(1): p. 1426.

24.   Zhang, K., et al., Hybridized Electromagnetic–Triboelectric Nanogenerator for Scavenging Biomechanical Energy for Sustainably Powering Wearable Electronics. *ACS Nano*, 2015. 9(4): p. 3521-3529.

25.   Levi, E., Multiphase electric machines for variable-speed applications. *IEEE Transactions on industrial electronics*, 2008. 55(5): p. 1893-1909.

26.   Wang, J., et al., Sustainably powering wearable electronics solely by biomechanical energy. *Nature communications*, 2016. 7: p. 12744.

Wong Man Chung

27.   Xi, F., et al., Universal power management strategy for triboelectric nanogenerator. *Nano Energy*, 2017. 37: p. 168-176.

28.   Cheng, X., et al., High efficiency power management and charge boosting strategy for a triboelectric nanogenerator. *Nano Energy*, 2017. 38: p. 438-446.

29.   Zhao, X., et al., Ultralight, self-powered and self-adaptive motion sensor based on triboelectric nanogenerator for perceptual layer application in Internet of things. *Nano Energy*, 2018. 48: p. 312-319.

30.   Wang, Z.L., et al., Lateral nanowire/nanobelt based nanogenerators, piezotronics and piezo-phototronics. *Materials Science and Engineering: R: Reports*, 2010. 70(3-6): p. 320-329.

31.   Ezechina, M., K. Okwara, and C. Ugboaja, The internet of things (Iot): a scalable approach to connecting everything. *The International Journal of Engineering and Science*, 2015. 4(1): p. 09-12.

32.   Wu, W., et al., Lead zirconate titanate nanowire textile nanogenerator for wearable energy-harvesting and self-powered devices. *ACS nano*, 2012. 6(7): p. 6231-6235.

33.   Xu, S., et al., Flexible piezoelectric PMN–PT nanowire-based nanocomposite and device. *Nano letters*, 2013. 13(6): p. 2393-2398.

34.   Kwon, J., et al., A high performance PZT ribbon-based nanogenerator using graphene transparent electrodes. *Energy & Environmental Science*, 2012. 5(10): p. 8970-8975.

35.   Lee, J.H., et al., Highly stretchable piezoelectric-pyroelectric hybrid nanogenerator. *Advanced Materials*, 2014. 26(5): p. 765-769.

Wong Man Chung

36.   Lee, J.-H., et al., Highly sensitive stretchable transparent piezoelectric nanogenerators. *Energy & Environmental Science*, 2013. 6(1): p. 169-175.

37.   Kim, K.N., et al., Highly stretchable 2D fabrics for wearable triboelectric nanogenerator under harsh environments. *ACS nano*, 2015. 9(6): p. 6394-6400.

38.   Lin, L., et al., Transparent flexible nanogenerator as self-powered sensor for transportation monitoring. *Nano Energy*, 2013. 2(1): p. 75-81.

39.   Lee, M., et al., Self-powered environmental sensor system driven by nanogenerators. *Energy & Environmental Science*, 2011. 4(9): p. 3359-3363.

40.   Fan, F.R., W. Tang, and Z.L. Wang, Flexible nanogenerators for energy harvesting and self-powered electronics. *Advanced Materials*, 2016. 28(22): p. 4283-4305.

41.   Otsuka, K. and C.M. Wayman, *Shape memory materials*. 1999: Cambridge university press.

42.   Shahinpoor, M., et al., Ionic polymer-metal composites (IPMCs) as biomimetic sensors, actuators and artificial muscles-a review. *Smart materials and structures*, 1998. 7(6): p. R15.

43.   Wang, S., et al., Efficient scavenging of solar and wind energies in a smart city. *ACS nano*, 2016. 10(6): p. 5696-5700.

44.   Nie, J., X. Chen, and Z.L. Wang, Electrically responsive materials and devices directly driven by the high voltage of triboelectric nanogenerators. *Advanced Functional Materials*, 2018: p. 1806351.

45.   Bai, G., M.-K. Tsang, and J. Hao, Tuning the Luminescence of Phosphors: Beyond

         Conventional Chemical Method. *Advanced Optical Materials*, 2015. 3(4): p. 431-462.

46.   Kabe, R. and C. Adachi, Organic long persistent luminescence. *Nature*, 2017. 550(7676):

         p. 384.

47.   Hirata, S., Recent advances in materials with room-temperature phosphorescence:

         photophysics for triplet exciton stabilization. *Advanced Optical Materials*, 2017. 5(17):

         p. 1700116.

48.   Zhao, W., et al., Rational molecular design for achieving persistent and efficient pure

         organic room-temperature phosphorescence. *Chem*, 2016. 1(4): p. 592-602.

49.   De Araújo, C.B., et al., Photoluminescence and nonlinear optical phenomena in

         plasmonic random media—A review of recent works. *Journal of Luminescence*, 2016.

         169: p. 492-496.

50.   Signorello, G., et al., Tuning the Light Emission from GaAs Nanowires over 290 meV

         with Uniaxial Strain. *Nano Letters*, 2013. 13(3): p. 917-924.

51.   Sutherland, B.R. and E.H. Sargent, Perovskite photonic sources. *Nat Photon*, 2016.

         10(5): p. 295-302.

52.   Ziemelis, K., Glowing developments. *Nature*, 1999. 399(6735): p. 409-411.

53.   Li, F., et al., Blue-light-emitting organic electroluminescence via exciplex emission based

         on a fluorene derivative. *Journal of Physics D: Applied Physics*, 2004. 37(12): p. 1613-

         1616.

54.   Dong, Z.C., et al., Generation of molecular hot electroluminescence by resonant nanocavity plasmons. *Nature Photonics*, 2009. 4: p. 50.

55.   Pust, P., et al., Narrow-band red-emitting Sr[LiAl3N4]:Eu2+ as a next-generation LED-phosphor material. *Nature Materials*, 2014. 13: p. 891.

56.   Schmiechen, S., et al., Toward New Phosphors for Application in Illumination-Grade White pc-LEDs: The Nitridomagnesosilicates Ca[Mg3SiN4]:Ce3+, Sr[Mg3SiN4]:Eu2+, and Eu[Mg3SiN4]. *Chemistry of Materials*, 2014. 26(8): p. 2712-2719.

57.   Bai, G., M.-K. Tsang, and J. Hao, Luminescent Ions in Advanced Composite Materials for Multifunctional Applications. *Advanced Functional Materials*, 2016. 26(35): p. 6330-6350.

58.   Wong, M.C., et al., Magnetic-Induced Luminescence from Flexible Composite Laminates by Coupling Magnetic Field to Piezophotonic Effect. *Advanced Materials*, 2015. 27(30): p. 4488-4495.

59.   Tu, D., et al., LiNbO3:Pr3+: A Multipiezo Material with Simultaneous Piezoelectricity and Sensitive Piezoluminescence. *Advanced Materials*, 2017. 29(22): p. 1606914.

60.   Tu, D., et al., Mechanism of mechanical quenching and mechanoluminescence in phosphorescent CaZnOS:Cu. *Light: Science &Amp; Applications*, 2015. 4: p. e356.

61.   Tu, D., et al., Photoluminescent properties of LiSrxBa1−xPO4:RE3+ (RE=Sm3+, Eu3+) f–f transition phosphors. *Journal of Alloys and Compounds*, 2011. 509(18): p. 5596-5599.

62.   Erwin, S.C., et al., Doping semiconductor nanocrystals. *Nature*, 2005. 436(7047): p. 91-94.

63.   Peng, X., et al., Shape control of CdSe nanocrystals. *Nature*, 2000. 404(6773): p. 59-61.

64.   Nguyen, T.-D., C.-T. Dinh, and T.-O. Do, Shape- and Size-Controlled Synthesis of Monoclinic ErOOH and Cubic Er2O3 from Micro- to Nanostructures and Their Upconversion Luminescence. *ACS Nano*, 2010. 4(4): p. 2263-2273.

65.   Teng, X., et al., Lanthanide-Doped NaxScF3+x Nanocrystals: Crystal Structure Evolution and Multicolor Tuning. *Journal of the American Chemical Society*, 2012. 134(20): p. 8340-8343.

66.   Sagara, Y. and T. Kato, Mechanically induced luminescence changes in molecular assemblies. *Nature Chemistry*, 2009. 1: p. 605.

67.   Sagara, Y. and T. Kato, Stimuli-Responsive Luminescent Liquid Crystals: Change of Photoluminescent Colors Triggered by a Shear-Induced Phase Transition. *Angewandte Chemie International Edition*, 2008. 47(28): p. 5175-5178.

68.   Atari, N.A., Piezoluminescence phenomenon. *Physics Letters A*, 1982. 90(1): p. 93-96.

69.   Kamimura, S., H. Yamada, and C.-N. Xu, Development of new elasticoluminescent material SrMg2(PO4)2:Eu. *Journal of Luminescence*, 2012. 132(2): p. 526-530.

70.   Zhang, C., et al., Luminescence Modulation of Ordered Upconversion Nanopatterns by a Photochromic Diarylethene: Rewritable Optical Storage with Nondestructive Readout. *Advanced Materials*, 2010. 22(5): p. 633-637.

Wong Man Chung

71. Boyer, J.-C., et al., Photomodulation of Fluorescent Upconverting Nanoparticle Markers in Live Organisms by Using Molecular Switches. *Chemistry – A European Journal*, 2012. 18(11): p. 3122-3126.

72. Gorris, H.H., et al., Tuning the Dual Emission of Photon-Upconverting Nanoparticles for Ratiometric Multiplexed Encoding. *Advanced Materials*, 2011. 23(14): p. 1652-1655.

73. Eddingsaas, N.C. and K.S. Suslick, Mechanoluminescence: Light from sonication of crystal slurries. *Nature*, 2006. 444(7116): p. 163-163.

74. Chandra, B.P., Mechanoluminescence of Nanoparticles. *The Open Nanoscience Journal*, 2011, . 5: p. 45-58.

75. Terasaki, N., H. Yamada, and C.-N. Xu, Ultrasonic wave induced mechanoluminescence and its application for photocatalysis as ubiquitous light source. *Catalysis Today*, 2013. 201(Supplement C): p. 203-208.

76. Xu, C.N., et al., Artificial skin to sense mechanical stress by visible light emission. *Applied Physics Letters*, 1999. 74(9): p. 1236-1238.

77. Chandra, B.P., et al., Transient behaviour of the mechanoluminescence induced by impulsive deformation of fluorescent and phosphorescent crystals. *Journal of Luminescence*, 2008. 128(12): p. 2038-2047.

78. Jeong, S.M., et al., Color manipulation of mechanoluminescence from stress-activated composite films. *Advanced Materials*, 2013. 25(43): p. 6194-200.

79. Hurt, C.R., et al., High Intensity Triboluminescence in Europium Tetrakis (Dibenzoylmethide)-triethylammonium. *Nature*, 1966. 212(5058): p. 179-180.

80. Chandra, B.P., V.K. Chandra, and P. Jha, Elastico-mechanoluminescence and crystal-structure relationships in persistent luminescent materials and II–VI semiconductor phosphors. *Physica B: Condensed Matter*, 2015. 463: p. 62-67.

81. Chandra, B.P., V.K. Chandra, and P. Jha, Piezoelectrically-induced trap-depth reduction model of elastico-mechanoluminescent materials. *Physica B: Condensed Matter*, 2015. 461: p. 38-48.

82. Rao, N.M., et al., Structural, optical and electrical properties of luminescent (ZnS)1−x(MnTe)x powders. *Journal of Alloys and Compounds*, 2009. 468(1): p. 360-364.

83. Xu, C.-N., et al., Direct view of stress distribution in solid by mechanoluminescence. *Applied Physics Letters*, 1999. 74(17): p. 2414-2416.

84. Zhang, H., et al., Mechanoluminescence of Europium-Doped SrAMgSi2O7(A=Ca, Sr, Ba). *Japanese Journal of Applied Physics*, 2009. 48(4): p. 04C109.

85. Wang, X., et al., Dynamic pressure mapping of personalized handwriting by a flexible sensor matrix based on the mechanoluminescence process. *Advanced Materials*, 2015. 27(14): p. 2324-31.

86. Tu, D., et al., Mechanism of mechanical quenching and mechanoluminescence in phosphorescent CaZnOS:Cu. *Light Sci Appl.*, 2015. 4(11): p. e356.

87. Gan, J., et al., Enhanced piezoluminescence in non-stoichiometric ZnS:Cu microparticle based light emitting elastomers. *Journal of Materials Chemistry C*, 2017. 5(22): p. 5387-5394.

Wong Man Chung

88.   Fan, X.-H., et al., Piezoluminescence from ferroelectric Ca3Ti2O7:Pr3+ long-persistent phosphor. *Optics Express*, 2017. 25(13): p. 14238-14246.

89.   Chen, L., et al., White and green light emissions of flexible polymer composites under electric field and multiple strains. *Nano Energy*, 2015. 14: p. 372 - 381.

90.   Jeong, S.M., et al., Bright, wind-driven white mechanoluminescence from zinc sulphide microparticles embedded in a polydimethylsiloxane elastomer. *Energy Environ Sci.*, 2014. 7(10): p. 3338-3346.

91.   Jeong, S.M., et al., Mechanically driven light-generator with high durability. *Applied Physics Letters*, 2013. 102(5): p. 051110.

92.   Yang, Z., et al., Recent advances in mechano-responsive luminescence of tetraphenylethylene derivatives with aggregation-induced emission properties. *Materials Chemistry Frontiers*, 2018. 2(5): p. 861-890.

93.   Zhao, J., et al., Recent progress in the mechanofluorochromism of cyanoethylene derivatives with aggregation-induced emission. *Journal of Materials Chemistry C*, 2018. 6(24): p. 6327-6353.

94.   Gong, Y.-B., et al., The Influence of Molecular Packing on the Emissive Behavior of Pyrene Derivatives: Mechanoluminescence and Mechanochromism. *Advanced Optical Materials*, 2018. 6(16): p. 1800198.

95.   Li, Y., G. Vamvounis, and S. Holdcroft, Tuning Optical Properties and Enhancing Solid-State Emission of Poly(thiophene)s by Molecular Control: A Postfunctionalization Approach. *Macromolecules*, 2002. 35(18): p. 6900-6906.

Wong Man Chung

96.   Moth-Poulsen, K. and T. Bjørnholm, Molecular electronics with single molecules in solid-state devices. *Nature Nanotechnology*, 2009. 4: p. 551.

97.   Xie, Y. and Z. Li, Triboluminescence: Recalling Interest and New Aspects. *Chem*, 2018. 4(5): p. 943-971.

98.   Li, J.-A., et al., Transient and Persistent Room-Temperature Mechanoluminescence from a White-Light-Emitting AIEgen with Tricolor Emission Switching Triggered by Light. *Angewandte Chemie*, 2018. 130(22): p. 6559-6563.

99.   Nan, G., et al., Influences of molecular packing on the charge mobility of organic semiconductors: from quantum charge transfer rate theory beyond the first-order perturbation. *Physical Chemistry Chemical Physics*, 2011. 13(20): p. 9736-9746.

100.   Qiu, Z., et al., Dynamic Visualization of Stress/Strain Distribution and Fatigue Crack Propagation by an Organic Mechanoresponsive AIE Luminogen. *Advanced Materials*, 2018. 30(44): p. 1803924.

101.   Zhao, W., et al., Highly sensitive switching of solid-state luminescence by controlling intersystem crossing. *Nature communications*, 2018. 9(1): p. 3044.

102.   Hu, R., Y. Kang, and B.Z. Tang, Recent advances in AIE polymers. *Polymer Journal*, 2016. 48: p. 359.

103.   Wang, H., et al., AIE luminogens: emission brightened by aggregation. *Materials Today*, 2015. 18(7): p. 365-377.

104.   Luo, J., et al., Aggregation-induced emission of 1-methyl-1,2,3,4,5-pentaphenylsilole. *Chemical Communications*, 2001(18): p. 1740-1741.

Wong Man Chung

105. Tang, B.Z., et al., Efficient blue emission from siloles. *Journal of Materials Chemistry*, 2001. 11(12): p. 2974-2978.

106. Martínez-Abadía, M., R. Giménez, and M.B. Ros, Self-Assembled α-Cyanostilbenes for Advanced Functional Materials. *Advanced Materials*, 2018. 30(5): p. 1704161.

107. Sun, J., et al., Fabrication of Nano/Microstructure of Cyano Substituted Oligo(para-phenylenevinylene) with Aggregation-Induced Emission and Morphology Dependent Luminescence. *Integrated Ferroelectrics*, 2014. 153(1): p. 42-47.

108. Shi, B., et al., Nanoparticles with Near-Infrared Emission Enhanced by Pillararene-Based Molecular Recognition in Water. *Journal of the American Chemical Society*, 2016. 138(1): p. 80-83.

109. Palakollu, V. and S. Kanvah, α-Cyanostilbene based fluorophores: aggregation-induced enhanced emission, solvatochromism and the pH effect. *New Journal of Chemistry*, 2014. 38(12): p. 5736-5746.

110. Kokado, K., R. Taniguchi, and K. Sada, Rigidity-induced emission enhancement of network polymers crosslinked by tetraphenylethene derivatives. *Journal of Materials Chemistry C*, 2015. 3(33): p. 8504-8509.

111. Li, W., et al., A novel stimuli-responsive fluorescent elastomer based on an AIE mechanism. *Polymer Chemistry*, 2015. 6(47): p. 8194-8202.

112. Taniguchi, R., et al., Stimuli-Responsive Fluorescence of AIE Elastomer Based on PDMS and Tetraphenylethene. *Macromolecules*, 2014. 47(18): p. 6382-6388.

113. Mei, J., et al., Aggregation-Induced Emission: Together We Shine, United We Soar! *Chemical Reviews*, 2015. 115(21): p. 11718-11940.

114. Zhao, Z., B. He, and B.Z. Tang, Aggregation-induced emission of siloles. *Chemical Science*, 2015. 6(10): p. 5347-5365.

115. Hong, Y., J.W.Y. Lam, and B.Z. Tang, Aggregation-induced emission. *Chemical Society Reviews*, 2011. 40(11): p. 5361-5388.

116. Hong, Y., J.W.Y. Lam, and B.Z. Tang, Aggregation-induced emission: phenomenon, mechanism and applications. *Chemical Communications*, 2009(29): p. 4332-4353.

117. Zhang, X., et al., Aggregation induced emission-based fluorescent nanoparticles: fabrication methodologies and biomedical applications. *Journal of Materials Chemistry B*, 2014. 2(28): p. 4398-4414.

118. Zhao, Z., J.W.Y. Lam, and B.Z. Tang, Tetraphenylethene: a versatile AIE building block for the construction of efficient luminescent materials for organic light-emitting diodes. *Journal of Materials Chemistry*, 2012. 22(45): p. 23726-23740.

119. Yen, H.-J., C.-J. Chen, and G.-S. Liou, Novel high-efficiency PL polyimide nanofiber containing aggregation-induced emission (AIE)-active cyanotriphenylamine luminogen. *Chemical Communications*, 2013. 49(6): p. 630-632.

120. Zhang, C., et al., A smart pH-switchable luminescent hydrogel. *Chemical Communications*, 2015. 51(20): p. 4168-4171.

121. Gu, Y., et al., Pressure-Induced Emission Enhancement of Carbazole: The Restriction of Intramolecular Vibration. *The Journal of Physical Chemistry Letters*, 2017. 8(17): p. 4191-4196.

122. Kokado, K., A. Nagai, and Y. Chujo, Poly(γ-glutamic acid) Hydrogels with Water-Sensitive Luminescence Derived from Aggregation-Induced Emission of o-Carborane. *Macromolecules*, 2010. 43(15): p. 6463-6468.

123. Wang, X., et al., Phase transition triggered aggregation-induced emission in a photoluminescent uranyl–organic framework. *Chemical Communications*, 2018. 54(6): p. 627-630.

124. Hu, R., N.L.C. Leung, and B.Z. Tang, AIE macromolecules: syntheses, structures and functionalities. *Chemical Society Reviews*, 2014. 43(13): p. 4494-4562.

125. Zhan, R., et al., AIE Polymers: Synthesis, Properties, and Biological Applications. *Macromolecular Bioscience*, 2017. 17(5): p. 1600433.

126. Wang, L., G. Fang, and D. Cao, Recent Advances of AIE-Active Conjugated Polymers: Synthesis and Application. *Journal of Macromolecular Science, Part A*, 2014. 51(8): p. 668-681.

127. Zhang, X., et al., Polymeric AIE-based nanoprobes for biomedical applications: recent advances and perspectives. *Nanoscale*, 2015. 7(27): p. 11486-11508.

128. Mitchell, J.F.B., et al., Climate response to increasing levels of greenhouse gases and sulphate aerosols. *Nature*, 1995. 376(6540): p. 501-504.

129. Rodhe, H., A Comparison of the Contribution of Various Gases to the Greenhouse Effect. *Science*, 1990. 248(4960): p. 1217-1219.

130. Dresselhaus, M.S. and I.L. Thomas, Alternative energy technologies. *Nature*, 2001. 414(6861): p. 332-337.

131. Searchinger, T., et al., Use of U.S. Croplands for Biofuels Increases Greenhouse Gases Through Emissions from Land-Use Change. *Science*, 2008. 319(5867): p. 1238-1240.

132. Fan, F.R., W. Tang, and Z.L. Wang, Flexible Nanogenerators for Energy Harvesting and Self-Powered Electronics. *Advanced Materials*, 2016. 28(22): p. 4283-4305.

133. Urry, J., Sociology and Climate Change. *The Sociological Review*, 2009. 57(2_suppl): p. 84-100.

134. Urry, J., *Climate Change and Society*, in *Why the Social Sciences Matter*, J. Michie and C.L. Cooper, Editors. 2015, Palgrave Macmillan UK: London. p. 45-59.

135. Beck, U., Climate for Change, or How to Create a Green Modernity? *Theory, Culture & Society*, 2010. 27(2-3): p. 254-266.

136. Pu, X., et al., A Self-Charging Power Unit by Integration of a Textile Triboelectric Nanogenerator and a Flexible Lithium-Ion Battery for Wearable Electronics. *Advanced Materials*, 2015. 27(15): p. 2472-2478.

137. Wen, Z., et al., Self-powered textile for wearable electronics by hybridizing fiber-shaped nanogenerators, solar cells, and supercapacitors. *Science Advances*, 2016. 2(10): p. e1600097.

Wong Man Chung

138. Wang, Z.L., Triboelectric nanogenerators as new energy technology and self-powered sensors–Principles, problems and perspectives. *Faraday discussions*, 2015. 176: p. 447-458.

139. Xia, F., et al., Internet of Things. *International Journal of Communication Systems*, 2012. 25(9): p. 1101-1102.

140. Kopetz, H., *Internet of Things*, in *Real-Time Systems: Design Principles for Distributed Embedded Applications*. 2011, Springer US: Boston, MA. p. 307-323.

141. Kim, J., et al., Research Update: Hybrid energy devices combining nanogenerators and energy storage systems for self-charging capability. *APL Materials*, 2017. 5(7): p. 073804.

142. Lee, J.-H., et al., All-in-one energy harvesting and storage devices. *Journal of Materials Chemistry A*, 2016. 4(21): p. 7983-7999.

143. Wang, S., L. Lin, and Z.L. Wang, Nanoscale Triboelectric-Effect-Enabled Energy Conversion for Sustainably Powering Portable Electronics. *Nano Letters*, 2012. 12(12): p. 6339-6346.

144. Annapureddy, V., et al., Magnetic energy harvesting with magnetoelectrics: an emerging technology for self-powered autonomous systems. *Sustainable Energy & Fuels*, 2017. 1(10): p. 2039-2052.

145. Wang, J., et al., Achieving ultrahigh triboelectric charge density for efficient energy harvesting. *Nature Communications*, 2017. 8(1): p. 88.

Wong Man Chung

146.   Wang, Z.L., Triboelectric nanogenerators as new energy technology for self-powered systems and as active mechanical and chemical sensors. *ACS nano*, 2013. 7(11): p. 9533-9557.

147.   Wu, C., et al., Triboelectric nanogenerator: A foundation of the energy for the new era. *Advanced Energy Materials*, 2019. 9(1): p. 1802906.

148.   Tang, W., B. Meng, and H.X. Zhang, Investigation of power generation based on stacked triboelectric nanogenerator. *Nano Energy*, 2013. 2(6): p. 1164-1171.

149.   Feng, Y., et al., A new protocol toward high output TENG with polyimide as charge storage layer. *Nano Energy*, 2017. 38(Supplement C): p. 467-476.

150.   Naik, S., R. Mukherjee, and B. Chaudhuri, Triboelectrification: A review of experimental and mechanistic modeling approaches with a special focus on pharmaceutical powders. *International Journal of Pharmaceutics*, 2016. 510(1): p. 375-385.

151.   Khan, U. and S.-W. Kim, Triboelectric Nanogenerators for Blue Energy Harvesting. *ACS Nano*, 2016. 10(7): p. 6429-6432.

152.   Jiang, T., et al., Structural Optimization of Triboelectric Nanogenerator for Harvesting Water Wave Energy. *ACS Nano*, 2015. 9(12): p. 12562-12572.

153.   Wang, Y., Y. Yang, and Z.L. Wang, Triboelectric nanogenerators as flexible power sources. *npj Flexible Electronics*, 2017. 1(1): p. 10.

154.   Wang, Z.L., et al., *Triboelectric Nanogenerator: Vertical Contact-Separation Mode*, in *Triboelectric Nanogenerators*. 2016, Springer International Publishing: Cham. p. 23-47.

155.   Zhu, G., et al., Triboelectric-Generator-Driven Pulse Electrodeposition for Micropatterning. *Nano Letters*, 2012. 12(9): p. 4960-4965.

156.   Fan, F.-R., et al., Transparent Triboelectric Nanogenerators and Self-Powered Pressure Sensors Based on Micropatterned Plastic Films. *Nano Letters*, 2012. 12(6): p. 3109-3114.

157.   Yang, Y., et al., Self-Powered Magnetic Sensor Based on a Triboelectric Nanogenerator. *ACS Nano*, 2012. 6(11): p. 10378-10383.

158.   Lin, Z.-H., et al., A Self-Powered Triboelectric Nanosensor for Mercury Ion Detection. *Angewandte Chemie International Edition*, 2013. 52(19): p. 5065-5069.

159.   Zhu, Y., et al., A flexible and biocompatible triboelectric nanogenerator with tunable internal resistance for powering wearable devices. *Scientific Reports*, 2016. 6: p. 22233.

160.   Wang, S., et al., Sliding-Triboelectric Nanogenerators Based on In-Plane Charge-Separation Mechanism. *Nano Letters*, 2013. 13(5): p. 2226-2233.

161.   Zhu, G., et al., Linear-Grating Triboelectric Generator Based on Sliding Electrification. *Nano Letters*, 2013. 13(5): p. 2282-2289.

162.   Lin, L., et al., Segmentally Structured Disk Triboelectric Nanogenerator for Harvesting Rotational Mechanical Energy. *Nano Letters*, 2013. 13(6): p. 2916-2923.

163.   Niu, S., et al., Theory of Sliding-Mode Triboelectric Nanogenerators. *Advanced Materials*, 2013. 25(43): p. 6184-6193.

164.   Wang, Z.L., et al., Triboelectric Nanogenerator: Lateral Sliding Mode, *Triboelectric Nanogenerators*. 2016, Springer International Publishing: Cham. p. 49-90.

Wong Man Chung

165.   Niu, S., et al., Theoretical Investigation and Structural Optimization of Single-Electrode Triboelectric Nanogenerators. *Advanced Functional Materials*, 2014. 24(22): p. 3332-3340.

166.   Yang, Y., et al., A Single-Electrode Based Triboelectric Nanogenerator as Self-Powered Tracking System. *Advanced Materials*, 2013. 25(45): p. 6594-6601.

167.   Yang, Y., et al., Single-Electrode-Based Sliding Triboelectric Nanogenerator for Self-Powered Displacement Vector Sensor System. *ACS Nano*, 2013. 7(8): p. 7342-7351.

168.   Yang, W., et al., Harvesting Energy from the Natural Vibration of Human Walking. *ACS Nano*, 2013. 7(12): p. 11317-11324.

169.   Pu, X., et al., Eye motion triggered self-powered mechnosensational communication system using triboelectric nanogenerator. *Science Advances*, 2017. 3(7): p. e1700694.

170.   Kim, W., et al., A self-powered triboelectric microfluidic system for liquid sensing. *Journal of Materials Chemistry A*, 2018. 6(29): p. 14069-14076.

171.   Meng, B., et al., A transparent single-friction-surface triboelectric generator and self-powered touch sensor. *Energy & Environmental Science*, 2013. 6(11): p. 3235-3240.

172.   Wang, S., et al., Freestanding Triboelectric-Layer-Based Nanogenerators for Harvesting Energy from a Moving Object or Human Motion in Contact and Non-contact Modes. *Advanced Materials*, 2014. 26(18): p. 2818-2824.

173.   Niu, S., et al., Theory of freestanding triboelectric-layer-based nanogenerators. *Nano Energy*, 2015. 12: p. 760-774.

Wong Man Chung

174. Wang, Z.L., et al., Triboelectric Nanogenerator: Freestanding Triboelectric-Layer Mode, in *Triboelectric Nanogenerators*. 2016, Springer International Publishing: Cham. p. 109-153.

175. *Tribocharging and the Triboelectric Series*, in *Encyclopedia of Inorganic and Bioinorganic Chemistry*.

176. Diaz, A.F. and R.M. Felix-Navarro, A semi-quantitative tribo-electric series for polymeric materials: the influence of chemical structure and properties. *Journal of Electrostatics*, 2004. 62(4): p. 277-290.

177. Park, C.H., et al., Triboelectric series and charging properties of plastics using the designed vertical-reciprocation charger. *Journal of Electrostatics*, 2008. 66(11): p. 578-583.

178. Shin, S.-H., et al., Formation of Triboelectric Series via Atomic-Level Surface Functionalization for Triboelectric Energy Harvesting. *ACS Nano*, 2017. 11(6): p. 6131-6138.

179. Xu, W., et al., Environmentally Friendly Hydrogel-Based Triboelectric Nanogenerators for Versatile Energy Harvesting and Self-Powered Sensors. *Advanced Energy Materials*, 2017. 7(1): p. 1601529.

180. Pu, X., et al., Ultrastretchable, transparent triboelectric nanogenerator as electronic skin for biomechanical energy harvesting and tactile sensing. *Science Advances*, 2017. 3(5): p. e1700015.

Wong Man Chung

181. Wang, J., et al., A Flexible Fiber-Based Supercapacitor–Triboelectric-Nanogenerator Power System for Wearable Electronics. *Advanced Materials*, 2015. 27(33): p. 4830-4836.

182. Chun, J., et al., Boosted output performance of triboelectric nanogenerator via electric double layer effect. *Nature Communications*, 2016. 7: p. 12985.

183. Li, A., et al., Triboelectric nanogenerators for sensitive nano-coulomb molecular mass spectrometry. *Nat Nano*, 2017. 12(5): p. 481-487.

184. Chen, X., et al., Tunable Optical Modulator by Coupling a Triboelectric Nanogenerator and a Dielectric Elastomer. *Advanced Functional Materials*, 2017. 27(1): p. 1603788.

185. Šutka, A., et al., Inversely polarised ferroelectric polymer contact electrodes for triboelectric-like generators from identical materials. *Energy & Environmental Science*, 2018. 11(6): p. 1437-1443.

186. Zi, Y., et al., Field Emission of Electrons Powered by a Triboelectric Nanogenerator. *Advanced Functional Materials*, 2018. 28(21): p. 1800610.

187. Li, C., et al., Self-Powered Electrospinning System Driven by a Triboelectric Nanogenerator. *ACS Nano*, 2017. 11(10): p. 10439-10445.

188. Yang, Y., et al., Triboelectric Nanogenerator for Harvesting Wind Energy and as Self-Powered Wind Vector Sensor System. *ACS Nano*, 2013. 7(10): p. 9461-9468.

189. Wang, S., L. Lin, and Z.L. Wang, Triboelectric nanogenerators as self-powered active sensors. *Nano Energy*, 2015. 11: p. 436-462.

190.   Zhang, H., et al., Triboelectric Nanogenerator for Harvesting Vibration Energy in Full
        Space and as Self-Powered Acceleration Sensor. *Advanced Functional Materials*, 2014.
        24(10): p. 1401-1407.

191.   Lee, K.Y., et al., Hydrophobic Sponge Structure-Based Triboelectric Nanogenerator.
        Advanced Materials, 2014. 26(29): p. 5037-5042.

192.   Ding, W., et al., Self-powered wireless optical transmission of mechanical agitation
        signals. *Nano Energy*, 2018. 47: p. 566-572.

193.   Dai, K., et al., Triboelectric nanogenerators as self-powered acceleration sensor under
        high-g impact. *Nano Energy*, 2018. 45: p. 84-93.

194.   Zi, Y., et al., An inductor-free auto-power-management design built-in triboelectric
        nanogenerators. *Nano Energy*, 2017. 31: p. 302-310.

195.   Pu, X., W. Hu, and Z.L. Wang, Toward Wearable Self-Charging Power Systems: The
        Integration of Energy-Harvesting and Storage Devices. *Small*, 2018. 14(1): p. 1702817.

196.   Güven, O., *Crosslinking and scission in polymers*. Vol. 292. 2012: Springer Science &
        Business Media.

197.   Tyona, M., A theoritical study on spin coating technique. *Advances in materials
        Research*, 2013. 2(4): p. 195-208.

198.   Vaezi, M., H. Seitz, and S. Yang, A review on 3D micro-additive manufacturing
        technologies. *The International Journal of Advanced Manufacturing Technology*,
        2013. 67(5-8): p. 1721-1754.

Wong Man Chung

199.   Chia, H.N. and B.M. Wu, Recent advances in 3D printing of biomaterials. *Journal of biological engineering*, 2015. 9(1): p. 4.

200.   Joshi, S.C. and A.A. Sheikh, 3D printing in aerospace and its long-term sustainability. *Virtual and Physical Prototyping*, 2015. 10(4): p. 175-185.

201.   Zhang, Y., et al., Piezo-phototronic effect-induced dual-mode light and ultrasound emissions from ZnS:Mn/PMN-PT thin-film structures. *Advanced Materials*, 2012. 24(13): p. 1729-35.

202.   Lee, J., et al., Universal process-inert encoding architecture for polymer microparticles. *Nat. Mater*, 2014. 13(5): p. 524-529.

203.   Fang, H., et al., A Stretchable Nanogenerator with Electric/Light Dual-Mode Energy Conversion. *Advanced Energy Materials*, 2016. 6(18): p. 1600829-n/a.

204.   Tu, D., et al., LiNbO3:Pr3+: A Multipiezo Material with Simultaneous Piezoelectricity and Sensitive Piezoluminescence. *Advanced Materials*, 2017. 29(22): p. 1606914-n/a.

205.   Pan, C., et al., Progress in Piezo-Phototronic-Effect-Enhanced Light-Emitting Diodes and Pressure Imaging. *Advanced Materials*, 2016. 28(8): p. 1535-1552.

206.   Peng, D.F., B. Chen, and F. Wang, Recent Advances in Doped Mechanoluminescent Phosphors. *Chempluschem*, 2015. 80(8): p. 1209-1215.

207.   Feldmann, C., et al., Inorganic luminescent materials: 100 years of research and application. *Advanced Functional Materials*, 2003. 13(7): p. 511-516.

208.   Li, H., et al., Piezotronic and piezo-phototronic logic computations using Au decorated ZnO microwires. *Nano Energy*, 2016. 27: p. 587-594.

Wong Man Chung

209.   Deng, R., et al., Temporal full-colour tuning through non-steady-state upconversion. *Nat. Nanotechnol.*, 2015. 10(3): p. 237-42.

210.   Edgar, A., *Luminescent materials*, in *Springer Handbook of Electronic and Photonic Materials*. 2017, Springer. p. 1-1.

211.   Ibañez, J., et al., Frequency-dependent light emission and extinction of electroluminescent ZnS:Cu phosphor. *Displays*, 2007. 28(3): p. 112-117.

212.   Wood, V., et al., Alternating current driven electroluminescence from ZnSe/ZnS: Mn/ZnS nanocrystals. *Nano letters*, 2009. 9(6): p. 2367-2371.

213.   Stanley, J., et al., Degradation and rejuvenation studies of AC electroluminescent ZnS:Cu,Cl phosphors. *J. Phys. Condens. Matter*, 2010. 22(5): p. 055301.

214.   Qiu, W., et al., High-performance artificial nitrogen fixation at ambient conditions using a metal-free electrocatalyst. *Nature Communications*, 2018. 9(1): p. 3485.

215.   Glock, N., et al., Coupling of oceanic carbon and nitrogen facilitates spatially resolved quantitative reconstruction of nitrate inventories. *Nature Communications*, 2018. 9(1): p. 1217.

216.   Wang, W., et al., Nitrogen Fixation by Gliding Arc Plasma: Better Insight by Chemical Kinetics Modelling. *ChemSusChem*, 2017. 10(10): p. 2145-2157.

217.   Yang, J., et al., Nitrogen fixation in water using air phase gliding arc plasma. *Journal of The Electrochemical Society*, 2016. 163(10): p. E288-E292.

218.   Peng, P., et al., In situ plasma-assisted atmospheric nitrogen fixation using water and spray-type jet plasma. *Chemical Communications*, 2018. 54(23): p. 2886-2889.

219.   Xu, W., M.-C. Wong, and J. Hao, Strategies and progress on improving robustness and reliability of triboelectric nanogenerators. *Nano Energy*, 2019. 55: p. 203-215.

220.   Huang, L.B., et al., Magnetic-Assisted Noncontact Triboelectric Nanogenerator Converting Mechanical Energy into Electricity and Light Emissions. *Advanced Materials*, 2016. 28(14): p. 2744-2751.

221.   Cheng, G., et al., Managing and maximizing the output power of a triboelectric nanogenerator by controlled tip–electrode air-discharging and application for UV sensing. *Nano Energy*, 2018. 44: p. 208-216.

222.   Kim, M., et al., Remarkable Output Power Density Enhancement of Triboelectric Nanogenerators via Polarized Ferroelectric Polymers and Bulk MoS2 Composites. *ACS Nano*, 2019. 13(4): p. 4640-4646.

223.   Kim, D., et al., Triboelectric nanogenerator based on the internal motion of powder with a package structure design. *ACS nano*, 2015. 10(1): p. 1017-1024.

224.   Cui, N., et al., Dynamic Behavior of the Triboelectric Charges and Structural Optimization of the Friction Layer for a Triboelectric Nanogenerator. *ACS Nano*, 2016. 10(6): p. 6131-6138.

225.   Wang, S., et al., Maximum Surface Charge Density for Triboelectric Nanogenerators Achieved by Ionized-Air Injection: Methodology and Theoretical Understanding. *Advanced Materials*, 2014. 26(39): p. 6720-6728.

THE HONG KONG POLYTECHNIC UNIVERSITY

226. Zhang, S.L., et al., Auxetic Foam-Based Contact-Mode Triboelectric Nanogenerator with Highly Sensitive Self-Powered Strain Sensing Capabilities to Monitor Human Body Movement. *Advanced Functional Materials*, 2017. 27(25): p. 1606695-n/a.

227. Trivedi, M., et al., Spectroscopic characterization of disodium hydrogen orthophosphate and sodium nitrate after biofield treatment. *Journal of Chromatography & Separation Techniques*, 2015. 6(5).

228. Hong, Y., J.W. Lam, and B.Z. Tang, Aggregation-induced emission. *Chemical Society Reviews*, 2011. 40(11): p. 5361-5388.